

Siberian Branch of Russian Academy of Science
BUDKER INSTITUTE OF NUCLEAR PHYSICS

V.N. Baier and V.M. Katkov

CONCEPT OF FORMATION LENGTH
IN RADIATION THEORY

Budker INP 2003-58

Novosibirsk
2003

Concept of formation length in radiation theory

V.N. Baier and V.M. Katkov

Budker Institute for Nuclear Physics
630090 Novosibirsk, Russia

Abstract

The features of electromagnetic processes are considered which connected with finite size of space region in which final particles (photon, electron-positron pair) are formed. The longitudinal dimension of the region is known as the formation length. If some external agent is acting on an electron while traveling this distance the emission process can be disrupted. There are different agents: multiple scattering of projectile, polarization of a medium, action of external fields, etc. The theory of radiation under influence of the multiple scattering, the Landau-Pomeranchuk-Migdal (LPM) effect, is presented. The probability of radiation is calculated with an accuracy up to "next to leading logarithm" and with the Coulomb corrections taken into account. The integral characteristics of bremsstrahlung are given. The LPM effect for pair creation is also presented. The multiple scattering influences also on radiative corrections in a medium (and an external field too) including the anomalous magnetic moment of an electron and the polarization tensor as well as coherent scattering of a photon in a Coulomb field. The polarization of a medium alters the radiation probability in soft part of spectrum. Specific features of radiation from a target of finite thickness include: the boundary photon emission, interference effects for a thin target, the multi-photon radiation. The experimental study of LPM effect is described. For electron-positron colliding beams following items are discussed: the mechanisms of radiation, the beam-size effect in bremsstrahlung, the coherent radiation and mechanisms of electron-positron creation.

Contents

1	Introduction	5
1.1	General outlook	5
1.2	Processes in a medium	7
1.3	Radiation in the presence of an external field	10
2	The effect of a medium in an infinitely thick target	13
2.1	The LPM effect for radiation	13
2.2	Integral characteristics of bremsstrahlung	23
2.3	The LPM effect for pair creation	25
2.4	Anomalous magnetic moment of the electron in a medium	30
2.5	Propagation of high-energy photon in a medium in presence of an external field	35
2.6	An influence of multiple scattering on coherent scattering of photon	41
2.7	The polarization of a medium and the bremsstrahlung process	47
3	Impact of a medium for a target of finite thickness	49
3.1	General consideration	49
3.2	Boundary effects for a thick target	51
3.3	A thin target	53
3.4	A target of intermediate thickness	57
3.5	Multiphoton effects in energy loss spectra	63
3.6	Radiation from structured target	71
3.7	Comparison of the results obtained in different papers	79
3.8	Qualitative behavior of the spectral intensity of radiation	81
3.9	Experimental investigation of the LPM effect	84
3.9.1	Early experiments	85
3.9.2	SLAC E-146	85
3.9.3	Data Analysis and Results	88
3.9.4	Backgrounds and Monte Carlo	88
3.9.5	Results	89
3.10	Discussion of theory and experiment	95

4	Effects in colliding electron-positron beams	103
4.1	Mechanisms of radiation	103
4.2	The beam-size effect in bremsstrahlung	108
4.3	The coherent radiation	112
4.4	Mechanisms of e^+e^- pair creation	119
A	Appendix	122

1 Introduction

1.1 General outlook

The electromagnetic interaction is of the local nature, e.g. the interaction Hamiltonian in quantum electrodynamics is

$$H_{int}(x) = e\bar{\psi}(x)\gamma_{\mu}\psi(x)A^{\mu}(x), \quad (1.1)$$

i.e. the current in a point x interacts with an electromagnetic field $A^{\mu}(x)$ in the same point. However the process of photon radiation takes place not in one point but in some domain of space-time, in which a photon (an emitted wave in the classical language) is originating. The longitudinal dimension of this domain is called *the formation (coherence) length*. It is evident that the minimal size of the formation length is the wave length of the emitted photon. One can estimate the formation length from the phase factor entering the expression for the probability of photon emission. In the quasiclassical operator method (see Eq.(A.1), Appendix A) this factor is (in this paper we employ units such that $\hbar = c = 1$)

$$\exp\left[-\frac{i\varepsilon}{\varepsilon'}(\omega t - \mathbf{k}\mathbf{r}(t))\right], \quad (1.2)$$

where $\varepsilon(\varepsilon')$ is the energy of the initial (final) electron, ω is the photon energy, $\varepsilon' = \varepsilon - \omega$, \mathbf{k} is the wave vector of the photon, $\mathbf{r}(t)$ is the particle location on a classical trajectory, t is the time. The main contribution into the integral over time in the general expression for the probability of radiation Eq.(A.1) gives the region

$$\frac{\varepsilon}{\varepsilon'}(\omega t - \mathbf{k}\mathbf{r}(t)) \sim 1, \quad (1.3)$$

Taking into account that

$$\mathbf{k} = \sqrt{\mathcal{E}(\omega)}\omega\mathbf{n}, \quad \mathbf{r}(t) = \mathbf{v}t, \quad \mathcal{E}(\omega) = 1 - \frac{\omega_0^2}{\omega^2}, \quad \omega_0^2 = \frac{4\pi\alpha n_e}{m}, \quad \mathbf{n}\mathbf{v} = v \cos\vartheta, \quad (1.4)$$

where $\mathcal{E}(\omega)$ is the dielectric constant, ω_0 is the plasma frequency, n_e is the electron density, we have from Eq.(1.3) for $\vartheta \ll 1$

$$t \sim t_f = l_f(\omega) = \frac{2\varepsilon\varepsilon'}{\omega m^2 \left(1 + \gamma^2 \vartheta^2 + \frac{\omega_p^2}{\omega^2}\right)}, \quad \omega_p = \omega_0 \gamma. \quad (1.5)$$

In this paper we consider the processes at high energies, i.e. the Lorentz factor $\gamma = \varepsilon/m \gg 1$. Then from Eq.(1.5) follows:

1. ultrarelativistic particle radiates into the narrow cone with the vertex angle $\vartheta \leq 1/\gamma$ along the momentum of the initial particle, the contribution of larger angles is suppressed because of shortening of the formation length;
2. the effect of the polarization of a medium described by the dielectric constant $\mathcal{E}(\omega)$ manifest itself for soft photons only when $\omega \leq \omega_b$, since on the Earth $\omega_0 < 100$ eV we have $\omega_b < \varepsilon\omega_0/m < 2 \cdot 10^{-4}\varepsilon$;
3. when $\vartheta \leq 1/\gamma$, $\omega_0\gamma/\omega \ll 1$ the formation length is of the order

$$l_f \simeq l_{f0}(\omega) = \frac{2\varepsilon\varepsilon'}{\omega m^2}. \quad (1.6)$$

In the classical case $\omega \ll \varepsilon$ one has $l_{f0} = 2\gamma^2/\omega$. So for ultrarelativistic particles the formation length extends substantially. For example for a $\varepsilon = 25$ GeV electron emitting a $\omega = 100$ MeV photon, $l_{f0} = 10\mu\text{m}$, i.e. $\sim 10^5$ interatomic distances.

The formation length is important in many electromagnetic processes including creation of electron-positron pair, magnetic bremsstrahlung, transition radiation, Čerenkov radiation. There is also a set of applications involving other forces.

There is a number of physical interpretation of the formation length.

- The momentum transfer \mathbf{q} to a nucleus in the process of the photon emission by the particle with the momentum \mathbf{p}

$$\mathbf{q} = \mathbf{p} - \mathbf{p}' - \mathbf{k}, \quad (1.7)$$

takes the minimal value when it is longitudinal $q_{\parallel} = q_{min} = p - p' - k$, and in this case $q_{min} = 1/l_{f0} = (\hbar/l_{f0})$, i.e. from the uncertainty principle follows that if the minimal momentum transfer is small, then the formation length is large.

- For creation of the electron-positron pair the formation length is the distance required for the final state particles to separate enough that they act as independent particles.
- This is the distance over which the amplitudes of several interactions can add coherently to the total probability.
- The transverse size of the region, where the radiation is formed ϱ_{\perp} is determined by the minimal transverse momentum transfer q_{\perp}^{min} : $\varrho_{\perp} = 1/q_{\perp}^{min} = (\hbar/q_{\perp}^{min})$. Although usually $q_{\perp} \gg q_{\parallel}$ and this dimension is much smaller, we consider below the situation when the constraint of q_{\perp} is the main effect.

The formation length concept is important because within it the amplitudes can add coherently if a charged particle is moving freely. In the opposite case, when some perturbation is acting on the particle within the formation length, breakdown of the coherence happens and radiation will be suppressed.

1.2 Processes in a medium

Landau and Pomeranchuk were the first to show that if the formation length of the bremsstrahlung becomes comparable to the distance over which the multiple scattering becomes important, the bremsstrahlung will be suppressed [1]. They considered radiation of soft photons. Migdal [2], [3] developed a quantitative theory of this phenomenon. Now the common name is the Landau- Pomeranchuk -Migdal (LPM) effect.

Let us estimate a disturbance of the emission process due to a multiple scattering. As it is known, the mean angle of the multiple scattering at some length l_{f0} is

$$\vartheta_s = \sqrt{\vartheta_s^2} = \frac{\varepsilon_s}{\varepsilon} \sqrt{\frac{l_{f0}}{2L_{rad}}}, \quad \varepsilon_s = m\sqrt{\frac{4\pi}{\alpha}} = 21.2 \text{ MeV}, \quad (1.8)$$

where $\alpha = e^2 = 1/137$, L_{rad} is the radiation length. Since we are interesting in influence of the multiple scattering on the radiation process we put here the formation length Eq.(1.6). One can expect that when $\vartheta_s \geq 1/\gamma$ this influence will be substantial. From this inequality we have

$$\frac{\varepsilon'}{\varepsilon_{LP}} \geq \frac{\omega}{\varepsilon}, \quad \varepsilon_{LP} = \frac{m^4 L_{rad}}{\varepsilon_s^2}, \quad (1.9)$$

here ε_{LP} is the characteristic energy scale, for which the multiple scattering will influence the radiation process for the whole spectrum. It was introduced

in [1] and denoted by $E_0 = \varepsilon_{LP}$. For tungsten we have $\varepsilon_{LP} = 2.7$ TeV, and similar values for all the heavy elements. For the light elements the energy ε_{LP} is much larger. When $\varepsilon \ll \varepsilon_{LP}$ the multiple scattering will influence the emission of soft photons only with energy

$$\omega \leq \omega_{LP} = \frac{\varepsilon^2}{\varepsilon_{LP}}, \quad (1.10)$$

e.g. for particles with energy $\varepsilon = 25$ GeV one has $\omega_{LP} \simeq 230$ MeV. Of course, we estimate here the criterion only. For description of the effect one has to calculate the probability of the bremsstrahlung taking into account multiple scattering.

Side by side with the multiple scattering of an emitting electron one has to take into account also the influence of the medium on the radiated electromagnetic field. As it was shown above Eq.(1.5), this effect leads also to suppression of the soft photon emission (the dielectric suppression, the Ter-Mikaelian effect, see in [4]).

A clear qualitative analysis of different mechanisms of suppression is presented in early papers [5],[6]. More simple derivation of the Migdal's results is given in [8].

The next step in a quantitative theory of the Landau-Pomeranchuk-Migdal (LPM) effect was made in [9]. This theory is based on the quasi-classical operator method in QED developed by the authors (see [7], [8], [10], [11]). One of the basic equations (obtained with the use of kinetic equations describing the motion of an electron in the medium in the presence of an external field) is the Schrödinger equation in an external field with imaginary potential (Eq.(3.3) of [9]; see (A.22) in Appendix A).

New activity with the theory of the LPM effect is connected with a very successful series of experiments [12] - [15] performed at SLAC recently. In these experiments the cross section of the bremsstrahlung of soft photons with energy from 200 keV to 500 MeV from electrons with energy 8 GeV and 25 GeV was measured for a variety in materials with an accuracy of the order of a few percent. Both the LPM and the dielectric suppression was observed and investigated. These experiments were the challenge for the theory since in all the published before papers calculations are performed to logarithmic accuracy which is not enough for a description of the new experiments. The contribution of the Coulomb corrections (at least for heavy elements) is larger than experimental errors and these corrections should be taken into account. In papers [17]-[25] the problem was investigated using different approaches.

Very recently the LPM was studied at CERN [16] using iridium target and electrons with energy 287, 207 and 149 GeV. For iridium according to

Eqs.(1.9) and (1.10) $\varepsilon_{LP} = 2.2$ TeV, $\omega_{LP} \simeq 37$ GeV for the highest energy and the LPM suppression of bremsstrahlung was observed in much wider interval of photon energies than at SLAC.

The crossing process for the bremsstrahlung is the pair creation by a photon. The created particles in a medium can undergo the multiple scattering. It should be emphasized that for the bremsstrahlung the formation length (1.6) increases strongly if $\omega \ll \varepsilon$. Just because of this the LPM effect was investigated at SLAC at a relatively low energy. For the pair creation the formation length

$$l_p = \frac{2\varepsilon(\omega - \varepsilon)}{m^2\omega} \quad (1.11)$$

attains maximum at $\varepsilon = \omega/2$ and this maximum is $l_{p,max} = (\omega/2m)\lambda_c$. Because of this even for heavy elements the effect of multiple scattering on pair creation becomes noticeable at photon energies $\omega \geq 10$ TeV [21]. Starting from these energies one has to take into account the influence of a medium on the pair creation and on the bremsstrahlung hard part of the spectrum in electromagnetic showers being created by the cosmic ray particles of the ultrahigh energies. These effects can be quite significant in the electromagnetic calorimeters operating in the detectors on the colliders in TeV range.

The nonlinear effects of QED are due to the interaction of a photon with electron-positron field. These processes are the photon-photon scattering, the coherent photon scattering, the photon splitting into two photons, and the coalescence of two photons into photon in the Coulomb field.

The process of creation of the electron-positron pair by a photon connected with the coherent photon scattering [26]. In the quasiclassical approximation the amplitude M of the coherent photon scattering is described by diagram where the electron-positron pair is created by the initial photon with 4-momentum k_1 (ω, \mathbf{k}_1) and then annihilate into the final photon with 4-momentum k_2 . For high energy photon $\omega \gg m$ this process occurs over a rather long distance, known as the time of life of the virtual state

$$l_f = \frac{\omega}{2q_c^2}, \quad (1.12)$$

where $q_c \geq m$ is the characteristic transverse momentum of the process. When the virtual electron (or positron) is moving in a medium it scatters on atoms. The mean square of momentum transfer to the electron from a medium on the distance l_f is

$$q_s^2 = 4\pi Z^2 \alpha^2 n_a L(q_c) l_f, \quad L(q_c) = \ln \frac{q_c^2}{q_{min}^2}, \quad q_{min}^2 = a_s^{-2} + \Delta^2 + \frac{m^4}{\omega^2}, \quad (1.13)$$

where Z is the charge of nucleus, n_a is the number density of atoms in the medium, Δ is the photon momentum transfer ($\Delta = |\mathbf{k}_2 - \mathbf{k}_1| \ll q_c$), a_s is the screening radius of atom.

The coherent photon scattering amplitude M can be obtained from general formulas for probabilities of electromagnetic processes in the frame of the quasiclassical operator method (see e.g. [10]). It can be estimated as

$$M \sim \frac{\alpha\omega}{2\pi l_f n_a} \frac{q_s^2}{q_c^2} = \frac{\alpha}{\pi n_a} q_s^2. \quad (1.14)$$

We use the normalization condition $\text{Im}M = \omega\sigma_p$ for the case $\Delta = 0$, where σ_p is the total cross section of pair creation by a photon.

In the case of small momentum transfer $q_s \equiv \sqrt{q_s^2} \ll m$ we have in the region of small $\Delta \ll m$

$$q_c^2 = m^2, \quad M \sim \frac{2Z^2\alpha^3\omega}{m^2} \ln \frac{m^2}{a_s^{-2} + \Delta^2 + \frac{m^4}{\omega^2}}. \quad (1.15)$$

At an ultrahigh energy it is possible that $q_s \gg m$. In this case the characteristic momentum transfer is q_c , the combination q_c^2/m^2 enters in the formation length l_f Eq.(1.5). The self-consistency condition is

$$q_c^2 = q_s^2 = \frac{2\pi\omega Z^2\alpha^2 n_a L(q_c)}{q_c^2}, \quad q_c^2 = \varepsilon^2 \vartheta_c^2 \quad (1.16)$$

where $L(q_c)$ is defined in Eq.(1.13). So using Eq.(1.14) one gets for the estimate of the coherent photon scattering amplitude M (the influence of the multiple scattering manifests itself at the high photon energies such that $m^2 a_s/\omega \ll 1$)

$$M \sim \frac{2Z^2\alpha^3\omega}{\Delta_s^2} \sqrt{\ln \frac{\Delta_s^2}{a_s^{-2} + \Delta^2}}, \quad \Delta_s^2 = \sqrt{2\pi\omega Z^2\alpha^2 n_a} \gg \Delta^2. \quad (1.17)$$

1.3 Radiation in the presence of an external field

The authors have shown [27] that an external electromagnetic field can also modify the bremsstrahlung process. We consider the effect of an external field on the photon emission in electron-electron(positron) collision. This effect is associated as well with a reduction of the formation length of a photon (either real or virtual) due to relatively large turn of particle velocity over this length, and the corresponding increase in the vertex angle of the radiation cone. If a

photon of energy Ω is emitted by an electron (positron) at an angle ϑ to its velocity, the formation length of such a photon will be according to Eq.(1.5) (we neglect the polarization of a medium)

$$l_f(\Omega) = \frac{2(\varepsilon - \Omega)}{\varepsilon\Omega\vartheta_c^2} = \frac{2}{\varepsilon u_\Omega \vartheta_c^2}, \quad (1.18)$$

where $u_\Omega \equiv \Omega/(\varepsilon - \Omega)$, ϑ_c is defined in Eq.(1.16). The characteristic emission angle in weak field is $\vartheta_c = 1/\gamma$, and we can neglect the influence of the external field if

$$|\dot{\mathbf{v}}|l_f(\Omega) = \frac{eHl_f(\Omega)}{\varepsilon} \ll \frac{1}{\gamma}. \quad (1.19)$$

Substituting Eq.(1.18) into Eq.(1.19), we have the criterion for a field to be weak

$$\gamma \frac{eH}{\varepsilon} \frac{2\gamma^2}{\varepsilon u_\Omega} = \frac{2\chi}{u_\Omega} \ll 1. \quad (1.20)$$

Here we introduced the important parameter χ , which characterizes the quantum effects in an external field. When $\chi \ll 1$ we are in the classical domain and with $\chi \geq 1$ we are already well inside the quantum domain

$$\boldsymbol{\chi} = \frac{\mathbf{F}\gamma}{F_0} \quad \chi = |\boldsymbol{\chi}|, \quad \mathbf{F} = \mathbf{E}_\perp + (\mathbf{v} \times \mathbf{H}), \quad (1.21)$$

where $\mathbf{E}(\mathbf{H})$ is an electric (magnetic) field. Equation (1.21) contains the component of fields transverse with respect to particle velocity \mathbf{v} , F_0 is one of

$$\begin{aligned} E_0 &= \frac{m^2}{e} = \left(\frac{m^2 c^3}{e\hbar} \right) = 1.32 \cdot 10^{16} \text{V/cm, or} \\ H_0 &= \frac{m^2}{e} = \left(\frac{m^2 c^3}{e\hbar} \right) = 4.41 \cdot 10^{13} \text{Oe.} \end{aligned} \quad (1.22)$$

In strong fields, where $\chi/u \gg 1$, with characteristic radiation angles $\vartheta \gg 1/\gamma$, the effective emission angle ϑ_{ef} is determined by a self-consistency argument: the deviation angle of the particle in the field over the formation length must not exceed ϑ_c , i.e.

$$\begin{aligned} |\dot{\mathbf{v}}|l_f(\Omega, \vartheta_c) = \vartheta_c, \quad \vartheta_c &= \frac{1}{\gamma} \left(\frac{\chi}{u_\Omega} \right)^{1/3} = \left(\frac{2eH}{\varepsilon^2 u_\Omega} \right)^{1/3} \\ l_f(\Omega, \vartheta_c) &= \frac{\gamma}{mu_\Omega} \left(\frac{u_\Omega}{2\chi} \right)^{2/3} = \left(\frac{\varepsilon}{4u_\Omega e^2 H^2} \right)^{1/3}. \end{aligned} \quad (1.23)$$

It can be seen from Eq.(1.23) that when $\chi/u \gg 1$, neither the characteristic emission angle nor the photon formation length depends on the mass of the radiating particle. A parameter characterizing the effect of an external field on the radiation process was derived in [9].

It follows from Eq.(1.23) that, for $\chi/u_\Omega \gg 1$, the characteristic photon formation length is reduced by factor $(\chi/u_\Omega)^{2/3}$, and the emission angle is increased by factor $(\chi/u_\Omega)^{1/3}$. Since the relevant parameter χ/u_Ω depends on the frequency Ω (via u_Ω), this effect is manifested earlier for soft photons. Because of this a specific situation arises in bremsstrahlung in a collision of an electron and a positron(an electron) in colliding-beam experiment. The point is that the external factors act differently on the radiating particle and on the recoil particle. For the radiating particle the criterion of influence of external factors is the same in scattering by a nucleus as in collision of particles. For the recoil particles the effect turns out to be enhanced by γ^2 times (in the laboratory frame). This is due to the fact that the main contribution to the bremsstrahlung cross section give the virtual photons emitted by recoil particle with very low energy

$$\Omega \simeq q_0 = \frac{\omega m^2}{4\varepsilon\varepsilon'}, \quad (1.24)$$

where ω is the frequency of the real photon. The formation length of the virtual photon is

$$l_v = l_f(q_0) = \frac{8\varepsilon^3(\varepsilon - \omega)}{m^4\omega}, \quad (1.25)$$

for example, for $\varepsilon = 2$ GeV and $\omega = 10$ MeV the formation length is enormous: $l_v \simeq 4 \cdot 10^3$ cm. This is the reason why the field has a significant effect on virtual photon emission in e^-e^+ collisions even for moderate field and at relatively low particle energies, when the parameter $\frac{\chi(\varepsilon - \omega)}{\omega} \equiv \frac{\chi}{u}$ is small while the value $\frac{\chi(\varepsilon - q_0)}{q_0} \simeq 4\gamma^2 \frac{\chi}{u}$ is large. In that event, the picture of emission of a bremsstrahlung photon (radiation vertex) does not change directly, but a significant change takes place in the virtual photon spectrum at momentum transfers $|q| \leq q_{min}(4\gamma^2\chi/u)^{1/3}$, increasing the lower bound of the effective momentum transfer and resulting in a corresponding decrease of the cross section. The bremsstrahlung cross section under these conditions was derived to logarithmic accuracy in [27] using the equivalent photon method. In [28] the problem was solved to relativistic accuracy (terms $O(1/\gamma)$ were neglected).

It follows from Eq.(1.20), and was demonstrated in [9] that in the case $\chi/u \geq 1$ there is a change of the radiation vertex describing absorption of a virtual photon and emission of a real one. Since for $\chi/u \gg 1$ the formation length of a real photon l_ω falls off as $(u/\chi)^{2/3}$ (see Eq.(1.23)), the bremsstrahlung cross section falls off in just the same extent.

2 The effect of a medium in an infinitely thick target

2.1 The LPM effect for radiation

We consider first the case where the formation length is much shorter than the thickness of a target ($l_f \ll l$). The derivation of basic formulas for probability of radiation under influence of multiple scattering is given in Appendix A. The spectral distribution of the probability of radiation per unit time in this case is given by Eq.(A.20) and functions $\varphi_\mu(\varphi_0, \boldsymbol{\varphi})$ satisfy the Eq.(A.22). Introducing new variables

$$t = \frac{a}{2}\tau, \quad \boldsymbol{\varrho} = \sqrt{\frac{a}{b}}\mathbf{x} = \frac{1}{\gamma}\mathbf{x}, \quad (2.1)$$

where the quantities a and b are defined in Eqs.(A.14),(A.15), we obtain for the spectral distribution of the probability of radiation per unit time

$$\frac{dW}{d\omega} = \frac{2\alpha}{\gamma^2} \text{Re} \int_0^\infty dt e^{-it} [R_1 \varphi_0(0, t) + R_2 \mathbf{p} \boldsymbol{\varphi}(0, t)], \quad (2.2)$$

where $R_1 = \frac{\omega^2}{\varepsilon \varepsilon'}$, $R_2 = \frac{\varepsilon}{\varepsilon'} + \frac{\varepsilon'}{\varepsilon}$, and the functions $\varphi_\mu = \varphi_\mu(\varphi_0, \boldsymbol{\varphi})$ now satisfy the equation

$$i \frac{\partial \varphi_\mu}{\partial t} = \mathcal{H} \varphi_\mu, \quad \mathcal{H} = \mathbf{p}^2 - iV(\boldsymbol{\varrho}), \quad \mathbf{p} = -i\nabla_{\boldsymbol{\varrho}}, \quad V(\boldsymbol{\varrho}) = -Q\boldsymbol{\varrho}^2 \left(\ln \gamma^2 \vartheta_1^2 + \ln \frac{\boldsymbol{\varrho}^2}{4} + 2C - 1 \right), \quad Q = \frac{2\pi n_a Z^2 \alpha^2 \varepsilon \varepsilon'}{m^4 \omega}, \quad C = 0.577216... \quad (2.3)$$

with the initial conditions $\varphi_0(\boldsymbol{\varrho}, 0) = \delta(\boldsymbol{\varrho})$, $\boldsymbol{\varphi}(\boldsymbol{\varrho}, 0) = \mathbf{p} \delta(\boldsymbol{\varrho})$. Here $\varepsilon, \varepsilon', \omega$ are defined in Eq.(1.2) and Z, n_a are defined in Eq.(1.13). The functions φ_0 and $\boldsymbol{\varphi}$ in Eq.(2.2) are rescaled according with the initial conditions (factors $1/\gamma^2$ and $1/\gamma^3$, correspondingly). Note, that it is implied that in formula (2.2) a subtraction at $V = 0$ is made.

The potential $V(\boldsymbol{\varrho})$ Eq.(2.3) corresponds to consideration of scattering in the Born approximation. The difference of exact (as a function of $Z\alpha$) potential $V(\boldsymbol{\varrho})$ and taken in the Born approximation is computed in Appendix A of [17]. The potential $V(\boldsymbol{\varrho})$ with the Coulomb corrections taken into account is

$$\begin{aligned} V(\boldsymbol{\varrho}) &= -Q\boldsymbol{\varrho}^2 \left(\ln \gamma^2 \vartheta_1^2 + \ln \frac{\boldsymbol{\varrho}^2}{4} + 2C - 1 + 2f(Z\alpha) \right) \\ &= -Q\boldsymbol{\varrho}^2 \left(\ln \gamma^2 \vartheta_2^2 + \ln \frac{\boldsymbol{\varrho}^2}{4} + 2C \right), \end{aligned} \quad (2.4)$$

where $\vartheta_2 = \vartheta_1 \exp(f - 1/2)$, the function $f = f(Z\alpha)$ is

$$f(\xi) = \text{Re} [\psi(1 + i\xi) - \psi(1)] = \xi^2 \sum_{n=1}^{\infty} \frac{1}{n(n^2 + \xi^2)}, \quad (2.5)$$

where $\psi(\xi)$ is the logarithmic derivative of the gamma function.

In above formulas $\boldsymbol{\varrho}$ is space of the impact parameters measured in the Compton wavelengths λ_c , which is conjugate to space of the transverse momentum transfers measured in the electron mass m .

An operator form of a solution of Eq. (2.3) is

$$\begin{aligned} \varphi_0(\boldsymbol{\varrho}, t) &= \exp(-i\mathcal{H}t)\varphi_0(\boldsymbol{\varrho}, 0) = \langle \boldsymbol{\varrho} | \exp(-i\mathcal{H}t) | 0 \rangle, \quad \mathcal{H} = \mathbf{p}^2 - iV(\boldsymbol{\varrho}), \\ \varphi(\boldsymbol{\varrho}, t) &= \exp(-i\mathcal{H}t)\mathbf{p}\varphi_0(\boldsymbol{\varrho}, 0) = \langle \boldsymbol{\varrho} | \exp(-i\mathcal{H}t)\mathbf{p} | 0 \rangle, \end{aligned} \quad (2.6)$$

where we introduce the following Dirac state vectors: $|\boldsymbol{\varrho}\rangle$ is the state vector of coordinate $\boldsymbol{\varrho}$, and $\langle \boldsymbol{\varrho} | 0 \rangle = \delta(\boldsymbol{\varrho})$. Substituting Eq.(2.6) into Eq.(2.2) and taking integral over t we obtain for the spectral distribution of the probability of radiation

$$\frac{dW}{d\omega} = \frac{2\alpha}{\gamma^2} \text{Im}T, \quad T = \langle 0 | R_1 (G^{-1} - G_0^{-1}) + R_2 \mathbf{p} (G^{-1} - G_0^{-1}) \mathbf{p} | 0 \rangle, \quad (2.7)$$

where

$$G = \mathbf{p}^2 + 1 - iV, \quad G_0 = \mathbf{p}^2 + 1. \quad (2.8)$$

Here and below we consider an expression $\langle 0 | \dots | 0 \rangle$ as a limit: $\lim \mathbf{x} \rightarrow 0$, $\lim \mathbf{x}' \rightarrow 0$ of $\langle \mathbf{x} | \dots | \mathbf{x}' \rangle$.

Let us estimate the effective impact parameters ϱ_c which give the main contribution into the radiation probability. Since the characteristic values of ϱ_c can be found straightforwardly by calculation of Eq.(2.7), we estimate characteristic angles ϑ_c connected with ϱ_c by an equality $\varrho_c = 1/(\gamma\vartheta_c)$. The

mean square scattering angle of a particle on the formation length of a photon l_f Eq.(1.5) has the form

$$\vartheta_s^2 = \frac{4\pi Z^2 \alpha^2}{\varepsilon^2} n_a l_f \ln \frac{\zeta}{\gamma^2 \vartheta_1^2} = \frac{4Q}{\gamma^2 \zeta} \ln \frac{\zeta}{\gamma^2 \vartheta_1^2}, \quad (2.9)$$

where $\zeta = 1 + \gamma^2 \vartheta^2$, we neglect here the polarization of a medium. When $\vartheta_s^2 \ll 1/\gamma^2$ the contribution to the probability of radiation gives a region where $\zeta \sim 1$ ($\vartheta_c = 1/\gamma$), in this case $\varrho_c = 1$. When $\vartheta_s \gg 1/\gamma$ the characteristic angle of radiation is determined by self-consistency arguments (compare with Eq.(1.23)):

$$\vartheta_s^2 \simeq \vartheta_c^2 \simeq \frac{\zeta_c}{\gamma^2} = \frac{4Q}{\zeta_c \gamma^2} \ln \frac{\zeta_c}{\gamma^2 \vartheta_1^2}, \quad \frac{4Q}{\zeta_c^2} \ln \frac{\zeta_c}{\gamma^2 \vartheta_1^2} = 1, \quad 4Q \varrho_c^4 \ln \frac{1}{\gamma^2 \vartheta_1^2 \varrho_c^2} = 1. \quad (2.10)$$

It should be noted that when the characteristic impact parameter ϱ_c becomes smaller than the radius of nucleus R_n , the potential $V(\boldsymbol{\varrho})$ acquires an oscillator form (see Appendix B, Eq.(B.3) in [17])

$$V(\boldsymbol{\varrho}) = Q \varrho^2 \left(\ln \frac{a_s^2}{R_n^2} - 0.041 \right), \quad a_s = 0.81 a_B Z^{-1/3}, \quad (2.11)$$

here a_s is the screening radius, a_B is the Bohr radius.

Allowing for the estimates Eq.(2.10) we present the potential $V(\boldsymbol{\varrho})$ Eq.(2.4) in the following form

$$V(\boldsymbol{\varrho}) = V_c(\boldsymbol{\varrho}) + v(\boldsymbol{\varrho}), \quad V_c(\boldsymbol{\varrho}) = q \varrho^2, \quad q = QL_c, \quad L_c \equiv L(\varrho_c) = \ln \frac{1}{\gamma^2 \vartheta_1^2 \varrho_c^2},$$

$$L_1 \equiv L(1) = \ln \frac{1}{\gamma^2 \vartheta_2^2} = \ln \frac{a_{s2}^2}{\lambda_c^2}, \quad v(\boldsymbol{\varrho}) = -\frac{q \varrho^2}{L_c} \left(2C + \ln \frac{\varrho^2}{4 \varrho_c^2} \right), \quad (2.12)$$

here $a_{s2} = a_s \exp(-f + 1/2)$. So, one can to redefine the parameters a_s and ϑ_1 to include the Coulomb corrections. The inclusion of the Coulomb corrections ($f(Z\alpha)$ and $-1/2$) into $\ln \vartheta_2^2$ diminishes effectively the correction $v(\boldsymbol{\varrho})$ to the potential $V_c(\boldsymbol{\varrho})$. In accordance with such division of the potential we present the propagators in Eq. (2.7) as

$$G^{-1} - G_0^{-1} = G^{-1} - G_c^{-1} + G_c^{-1} - G_0^{-1}, \quad (2.13)$$

where

$$G_c = \mathbf{p}^2 + 1 - iV_c, \quad G = \mathbf{p}^2 + 1 - iV_c - iv.$$

This representation of the propagator G^{-1} permits one to expand it over the "perturbation" v . Indeed, with an increase of q the relative value of the perturbation is diminished ($\frac{v}{V_c} \sim \frac{1}{L_c}$) since the effective impact parameters diminishes and, correspondingly, the value of logarithm L_c in Eq.(2.12) increases. The maximal value of L_c is determined by the size of a nucleus R_n

$$L_{max} = \ln \frac{a_{s2}^2}{R_n^2} \simeq 2 \ln \frac{a_{s2}^2}{\lambda_c^2} \equiv 2L_1, \quad L_1 = 2(\ln(183Z^{-1/3}) - f(Z\alpha)), \quad (2.14)$$

The value L_1 is the important parameter of the radiation theory.

The matrix elements of the operator G_c^{-1} can be calculated explicitly. The exponential parametrization of the propagator is

$$G_c^{-1} = i \int_0^\infty dt e^{-it} \exp(-i\mathcal{H}_c t), \quad \mathcal{H}_c = \mathbf{p}^2 - iq\boldsymbol{\rho}^2 \quad (2.15)$$

The matrix elements of the operator $\exp(-i\mathcal{H}_c t)$ has the form (details see in [17])

$$\langle \boldsymbol{\rho}_1 | \exp(-i\mathcal{H}_c t) | \boldsymbol{\rho}_2 \rangle \equiv K_c(\boldsymbol{\rho}_1, \boldsymbol{\rho}_2, t), \quad (2.16)$$

$$K_c(\boldsymbol{\rho}_1, \boldsymbol{\rho}_2, t) = \frac{\nu}{4\pi i \sinh \nu t} \exp \left\{ \frac{i\nu}{4} \left[(\boldsymbol{\rho}_1^2 + \boldsymbol{\rho}_2^2) \coth \nu t - \frac{2}{\sinh \nu t} \boldsymbol{\rho}_1 \boldsymbol{\rho}_2 \right] \right\},$$

where $\nu = 2\sqrt{iq}$ (see Eq.(2.12)).

Substituting formulas (2.15) and (2.17) in the expression for the spectral distribution of the probability of radiation (2.7) we have

$$\begin{aligned} \frac{dW_c}{d\omega} &= \frac{\alpha}{2\pi\gamma^2} \text{Im} \Phi(\nu), \\ \Phi(\nu) &= \nu \int_0^\infty dt e^{-it} \left[R_1 \left(\frac{1}{\sinh z} - \frac{1}{z} \right) - i\nu R_2 \left(\frac{1}{\sinh^2 z} - \frac{1}{z^2} \right) \right] \\ &= R_1 \left(\ln p - \psi \left(p + \frac{1}{2} \right) \right) + R_2 \left(\psi(p) - \ln p + \frac{1}{2p} \right), \end{aligned} \quad (2.17)$$

where $z = \nu t$, $p = i/(2\nu)$, let us remind that $\psi(x)$ is the logarithmic derivative of the gamma function (see Eq.(2.5)). If we substitute in Eq.(2.17) $t \rightarrow t \exp(-i\pi/4)$ the probability will be transformed into the form containing the real functions only. Then it can be written as

$$\frac{dW_c}{d\omega} = \frac{\alpha|\nu|^2}{12\gamma^2} [R_1 G(s) + 2R_2 \phi(s)], \quad (2.18)$$

where

$$G(s) = 12s^2 \left[\frac{\pi}{4} - \int_0^\infty \exp(-sx) \frac{\sin(sx)}{\sinh x} dx \right],$$

$$\phi(s) = 6s^2 \left[\int_0^\infty \exp(-sx) \sin(sx) \coth x dx - \frac{\pi}{4} \right], \quad (2.19)$$

are the functions introduced by Migdal (see Eqs.(46), (47) in [2]). Note that parameter $s = \frac{1}{\sqrt{2}|\nu|}$ in Eq.(2.19) is two times larger than that used by Migdal. If one omits the Coulomb correction in Eqs.(2.18), (2.19), then the probability (2.18) coincides formally with the probability calculated by Migdal (see Eq.(49) in [2]).

Expanding the expression $G^{-1} - G_c^{-1}$ over powers of v we have

$$G^{-1} - G_c^{-1} = G_c^{-1}(iv)G_c^{-1} + G_c^{-1}(iv)G_c^{-1}(iv)G_c^{-1} + \dots \quad (2.20)$$

In accordance with Eqs.(2.13) and (2.20) we present the probability of radiation in the form

$$\frac{dW}{d\omega} = \frac{dW_c}{d\omega} + \frac{dW_1}{d\omega} + \frac{dW_2}{d\omega} + \dots \quad (2.21)$$

At $Q \geq 1$ the expansion (2.20) is a series over powers of $\frac{1}{L}$. It is important that variation of the parameter ϱ_c by a factor order of 1 has an influence on the dropped terms in (2.20) only. The probability of radiation $\frac{dW_c}{d\omega}$ is defined by Eq.(2.17).

The term $\frac{dW_1}{d\omega}$ in Eq.(2.21) corresponds to the term linear in v in Eq.(2.20). The explicit formula for the first correction to the probability of radiation [17] is

$$\frac{dW_1}{d\omega} = -\frac{\alpha}{4\pi\gamma^2 L_c} \text{Im } F(\nu);$$

$$-\text{Im } F(\nu) = D_1(\nu_0)R_1 + \frac{1}{s}D_2(\nu_0)R_2; \quad s = \frac{1}{\sqrt{2}\nu_0},$$

$$D_1(\nu_0) = \int_0^\infty \frac{dze^{-sz}}{\sinh^2 z} \left[d(z) \sin sz + \frac{\pi}{4}g(z) \cos sz \right], \quad D_2(\nu_0) = \int_0^\infty \frac{dze^{-sz}}{\sinh^3 z}$$

$$\times \left\{ \left[d(z) - \frac{1}{2}g(z) \right] (\sin sz + \cos sz) + \frac{\pi}{4}g(z) (\cos sz - \sin sz) \right\},$$

$$d(z) = (\ln \nu_0 \vartheta(1 - \nu_0) - \ln \sinh z - C)g(z) - 2G(z) \cosh z, \quad (2.22)$$

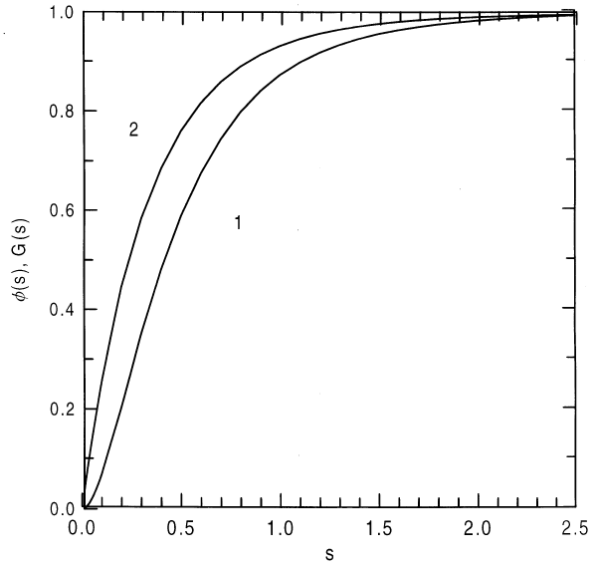


Figure 1: The functions $G(s)$ (curve 1) and $\phi(s)$ (curve 2) in Eq.(2.19).

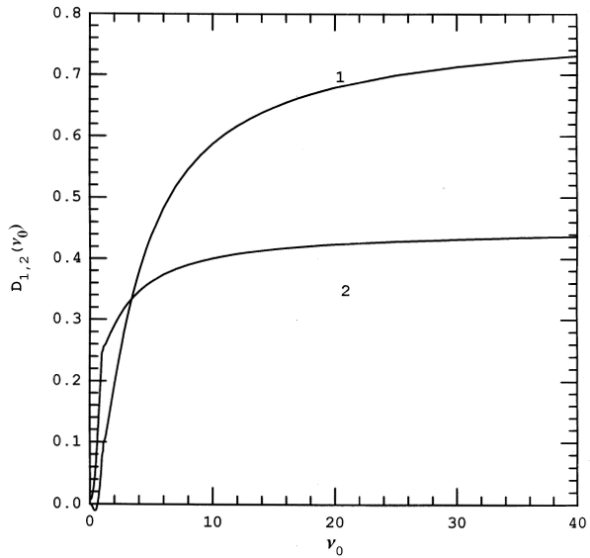


Figure 2: The functions $D_1(\nu_0)$ (curve 1) and $D_2(\nu_0)$ (curve 2) in Eq.(2.22).

where

$$\begin{aligned}
g(z) &= z \cosh z - \sinh z, \quad G(z) = \int_0^z (1 - y \coth y) dy \\
&= z - \frac{z^2}{2} - \frac{\pi^2}{12} - z \ln(1 - e^{-2z}) + \frac{1}{2} \text{Li}_2(e^{-2z}), \quad (2.23)
\end{aligned}$$

here $\text{Li}_2(x)$ is the Euler dilogarithm; and

$$\nu_0^2 \equiv |\nu|^2 = 4q = 4QL(\varrho_c) = \frac{8\pi n_a Z^2 \alpha^2 \varepsilon \varepsilon'}{m^4 \omega} L(\varrho_c), \quad (2.24)$$

The functions $G(s)$ and $\phi(s)$ are given in Fig.1 and the functions $D_1(\nu_0)$ and $D_2(\nu_0)$ are shown in Fig.2.

As it was said above (see Eqs.(2.10), (2.14)), $\varrho_c = 1$ at

$$|\nu^2| = \nu_1^2 = 4QL_1 \leq 1. \quad (2.25)$$

The logarithmic functions $L_c \equiv L(\varrho_c)$ and L_1 are defined in Eqs.(2.12) and (2.14). If the parameter $|\nu| > 1$, the value of ϱ_c is defined from the Eq.(2.10), where $\vartheta_1 \rightarrow \vartheta_2$, up to $\varrho_c = R_n/\lambda_c$. So, we have two representation of $|\nu|$ depending on ϱ_c : at $\varrho_c = 1$ it is $|\nu| = \nu_1$ and at $\varrho_c \leq 1$ it is $|\nu| = \nu_0$. The mentioned parameters can be presented in the following form

$$\begin{aligned}
\nu^2 &= i\nu_0^2, \quad \nu_0^2 = |\nu|^2 \simeq \nu_1^2 \left(1 + \frac{\ln \nu_1}{L_1} \vartheta(\nu_1 - 1) \right), \quad \nu_1^2 = \frac{\varepsilon}{\varepsilon_e} \frac{1-x}{x}, \quad x = \frac{\omega}{\varepsilon}, \\
\varepsilon_e &= m (8\pi Z^2 \alpha^2 n_a \lambda_c^3 L_1)^{-1}, \quad L_c \simeq L_1 \left(1 + \frac{\ln \nu_1}{L_1} \vartheta(\nu_1 - 1) \right). \quad (2.26)
\end{aligned}$$

It should be noted that in the logarithmic approximation the parameter ϱ_c entering into the parameter ν is defined up to the factor ~ 1 . However, we calculated the next term of the decomposition over $v(\boldsymbol{\rho})$ (an accuracy up to the "next to leading logarithm") and this permitted to obtain the result which is independent of the parameter ϱ_c (in terms $\propto 1/L$). Our definition of the parameter ϱ_c minimizes corrections to Eq.(2.17) practically for all values of the parameter ϱ_c .

The approximate solution of Eq.(2.10) given in Eq.(2.26) has quite good numerical accuracy: it is $\sim 2\%$ at $\nu_1 = 100$ and $\sim 4.5\%$ at $\nu_1 = 1000$. The LPM effect manifests itself when

$$\nu_1(x_c) = 1, \quad x_c = \frac{\omega_c}{\varepsilon} = \frac{\varepsilon}{\varepsilon_e + \varepsilon}. \quad (2.27)$$

So, the characteristic energy ε_e is the energy starting from which the multiple scattering distorts the whole spectrum of radiation including its hard part. If the radiation length L_{rad} is taken within the logarithmic approximation the value ε_e coincides with ε_{LP} Eq.(1.9). The difference between these values is

$$\frac{\varepsilon_e - \varepsilon_{LP}}{\varepsilon_e} = \frac{1}{9L_1} < 2\% .$$

The formulas derived in [17],[21] and written down above are valid for any energy. In Fig.3 the spectral radiation intensity in gold ($\varepsilon_e = 2.6$ TeV) is shown for different energies of the initial electron. In the case when $\varepsilon \ll \varepsilon_e$ ($\varepsilon = 25$ GeV and $\varepsilon = 250$ GeV) the LPM suppression is seen in the soft part of the spectrum only for $x \leq x_c \simeq \varepsilon/\varepsilon_e \ll 1$ while in the region $\varepsilon \geq \varepsilon_e$ ($\varepsilon = 2.5$ TeV and $\varepsilon = 25$ TeV) where $x_c \sim 1$ the LPM effect is significant for any x . For relatively low energies $\varepsilon = 25$ GeV and $\varepsilon = 8$ GeV used in famous SLAC experiment [14], [15] we have analyzed the soft part of spectrum, including all the accompanying effects: the boundary photon emission, the multiphoton radiation and influence of the polarization of the medium (see below). The perfect agreement of the theory and data was achieved in the whole interval of measured photon energies ($200 \text{ keV} \leq \omega \leq 500 \text{ MeV}$), see below and the corresponding figures in [17],[18],[19]. It should be pointed out that both the correction term with $F(\nu)$ and the Coulomb corrections have to be taken into account for this agreement.

When a scattering is weak ($\nu_1 \ll 1$), the main contribution in Eq.(2.22) gives a region where $z \ll 1$. Then

$$\begin{aligned} -\text{Im } F(\nu) &= \frac{1}{9} \text{Im } \nu^2 (R_2 - R_1), \quad L_c \rightarrow L_1, \\ \Phi(\nu) &\simeq \frac{\nu^2}{6} (R_1 + 2R_2), \quad (|\nu| \ll 1). \end{aligned} \quad (2.28)$$

Combining the results obtained in Eq.(2.28) we obtain the spectral distribution of the probability of radiation in the case when scattering is weak

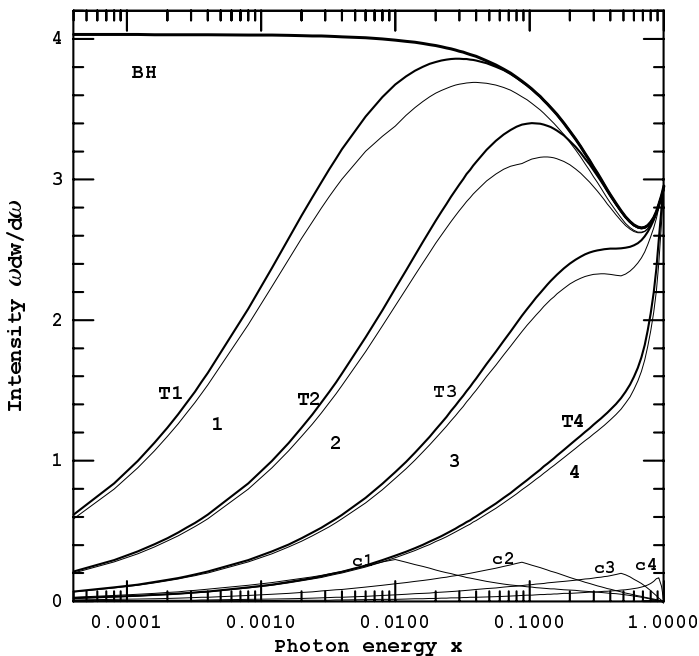


Figure 3: The spectral intensity of radiation $\omega \frac{dW}{d\omega} = x \frac{dW}{dx}$, $x = \frac{\omega}{\varepsilon}$ in gold in terms of $3L_{rad}$ taken with the Coulomb corrections (see Eq.(2.36)): *curve BH* is the Bethe-Maximon spectral intensity (see Eq.(2.29)); *curve 1* is the logarithmic approximation $\omega dW_c/d\omega$ Eq.(2.17), *curve c1* is the first correction to the spectral intensity $\omega dW_1/d\omega$ Eq.(2.22) and *curve T1* is the sum of the previous contributions for the electron energy $\varepsilon = 25$ GeV; *curve 2* is the logarithmic approximation $\omega dW_c/d\omega$ Eq.(2.17), *curve c2* is the first correction to the spectral intensity $\omega dW_1/d\omega$ Eq.(2.22) and *curve T2* is the sum of the previous contributions for the electron energy $\varepsilon = 250$ GeV; *curves 3, c3, T3* are the same for the electron energy $\varepsilon = 2.5$ TeV; *curves 4, c4, T4* are the same for the electron energy $\varepsilon = 25$ TeV.

($|\nu| \ll 1$)

$$\begin{aligned}
\frac{dW}{d\omega} &= \frac{dW_c}{d\omega} + \frac{dW_1}{d\omega} = \frac{\alpha}{2\pi\gamma^2} \text{Im} \left[\Phi(\nu) - \frac{1}{2L_1} F(\nu) \right] \\
&= \frac{\alpha}{2\pi\gamma^2} \frac{2Q}{3} \left[R_1 \left(L_1 - \frac{1}{3} \right) + 2R_2 \left(L_1 + \frac{1}{6} \right) \right] \\
&= \frac{4Z^2\alpha^3 n_a}{3m^2\omega} \left[\frac{\omega^2}{\varepsilon^2} \left(\ln \left(183Z^{-1/3} \right) - \frac{1}{6} - f(Z\alpha) \right) \right. \\
&\quad \left. + 2 \left(1 + \frac{\varepsilon'^2}{\varepsilon^2} \right) \left(\ln \left(183Z^{-1/3} \right) + \frac{1}{12} - f(Z\alpha) \right) \right], \quad (2.29)
\end{aligned}$$

where L_1 is defined in Eq.(2.14). This expression coincide with the known Bethe-Maximon formula for the probability of bremsstrahlung from high-energy electrons in the case of complete screening (if one neglects the contribution of atomic electrons) written down within power accuracy (omitted terms are of the order of powers of $\frac{1}{\gamma}$) with the Coulomb corrections, see e.g. Eq.(18.30) in [8], or Eq.(3.83) in [47].

At $\nu_0 \gg 1$ the function $\text{Im} F(\nu)$ Eq.(2.22) has the form

$$-\text{Im} F(\nu) = \frac{\pi}{4} R_1 + \frac{\nu_0}{\sqrt{2}} \left(\ln 2 - C + \frac{\pi}{4} \right) R_2. \quad (2.30)$$

Under the same conditions ($\nu_0 \gg 1$) the function $\text{Im} \Phi(\nu)$ Eq.(2.17) is

$$\text{Im} \Phi(\nu) = \frac{\pi}{4} R_1 + \frac{\nu_0}{\sqrt{2}} R_2 \rightarrow \frac{\nu_0}{\sqrt{2}} R_2. \quad (2.31)$$

So, in the region where the LPM effect is strong the probability Eq.(2.17) can written as

$$\frac{dW_c}{d\omega} = \frac{\alpha R_2}{\varepsilon^2} \left(\frac{Z^2 \alpha^2 \varepsilon \varepsilon' n_a}{\pi \omega} L(\varrho_c) \right)^{1/2}. \quad (2.32)$$

This means that in this limit the emission probability is proportional to the square root of the density. This fact was pointed out by Migdal [2], the expression (2.32) coincides formally with the probability calculated by Migdal (see Eq.(52) in [2]) with the same remarks which were made after Eq.(2.19).

Thus, at $\nu_0 \gg 1$ the relative contribution of the first correction $\frac{dW_1}{d\omega}$ is defined by

$$r = \frac{dW_1}{dW_c} = \frac{1}{2L(\varrho_c)} \left(\ln 2 - C + \frac{\pi}{4} \right) \simeq \frac{0.451}{L(\varrho_c)}, \quad (2.33)$$

where $L(\varrho_c) = \ln \frac{a_s^2}{\lambda_c^2 \varrho_c^2}$. In this expression the value r with the accuracy up to terms $\sim 1/L_c^2$ doesn't depend on the photon energy: $L_c \simeq L_1 + \ln(\varepsilon/\varepsilon_e)/2$. Hence we can find the correction to the total probability at $\varepsilon \gg \varepsilon_e$. The maximal value of the correction is attained at $\varepsilon \sim 10\varepsilon_e$, it is $\sim 6\%$ for heavy elements.

In the above analysis we did not consider an inelastic scattering of a projectile on atomic electrons. The potential $V_e(\boldsymbol{\varrho})$ connected with this process can be found from formula (2.4) by substitution $Z^2 \rightarrow Z, \vartheta_1 \rightarrow \vartheta_e = 0.153\vartheta_1$ (an analysis of an inelastic scattering on atomic electrons as well as the parameter ϑ_e can be found in [47]). The summary potential including both an elastic and an inelastic scattering is

$$\begin{aligned} V(\boldsymbol{\varrho}) + V_e(\boldsymbol{\varrho}) &= -Q\left(1 + \frac{1}{Z}\right)\boldsymbol{\varrho}^2 \left[\ln \gamma^2 \vartheta_2^2 + \ln \frac{\boldsymbol{\varrho}^2}{4} + 2C + \frac{1}{Z+1} \left(\ln \frac{\vartheta_e^2}{\vartheta_1^2} - 2f \right) \right] \\ &= -Q_{ef}\boldsymbol{\varrho}^2 \left(\ln \gamma^2 \vartheta_{ef}^2 + \ln \frac{\boldsymbol{\varrho}^2}{4} + 2C \right), \end{aligned} \quad (2.34)$$

where

$$Q_{ef} = Q\left(1 + \frac{1}{Z}\right), \quad \vartheta_{ef} = \vartheta_1 \exp \left[\frac{1}{1+Z} (Zf(\alpha Z) - 1.88) - \frac{1}{2} \right].$$

2.2 Integral characteristics of bremsstrahlung

Integrating Eq.(2.17) over $x = \omega/\varepsilon$ we obtain the total intensity of radiation in the logarithmic approximation

$$\begin{aligned} \frac{I}{\varepsilon} L_{rad}^0 &= 2 \frac{\varepsilon_e}{\varepsilon} \text{Im} \left[- \int_0^1 \frac{dx}{g} \sqrt{\frac{x}{1-x}} (2(1-x) + x^2) \right. \\ &\quad \left. + \int_0^1 \frac{x^3 dx}{1-x} \left(\psi(p+1) - \psi\left(p + \frac{1}{2}\right) \right) + 2 \int_0^1 x dx (\psi(p+1) - \ln p) \right], \end{aligned} \quad (2.35)$$

where

$$p = \frac{g\eta}{2}, \quad \eta = \sqrt{\frac{x}{1-x}}, \quad g = \exp\left(i\frac{\pi}{4}\right) \sqrt{\frac{L_1 \varepsilon_e}{L_c \varepsilon}},$$

L_{rad}^0 is the radiation length in the logarithmic approximation. The relative energy losses of electron per unit time in terms of the Bethe-Maximon radiation length L_{rad}^0 : $\frac{I}{\varepsilon} L_{rad}^0$ in gold is given in Fig.4 (curve 1), it reduces by 10%

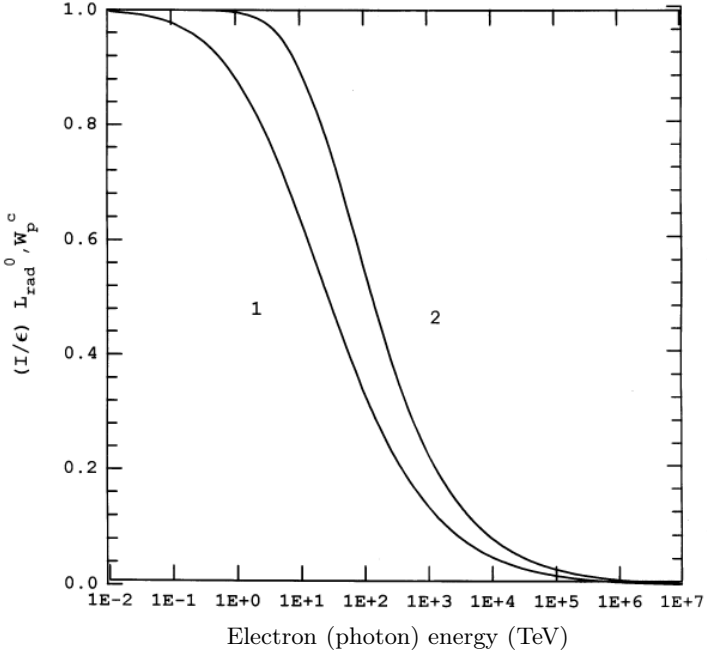


Figure 4: The relative energy losses of electron per unit time in terms of the Bethe-Maximon radiation length L_{rad}^0 : $\frac{I}{\epsilon}L_{rad}^0$ in gold vs the initial energy of electron (curve 1) and the total pair creation probability per unit time W_p^c (see Eq.(2.49)) in terms of the Bethe-Maximon total probability of pair creation W_{p0}^{BM} (see Eq.(2.47)) in gold vs the initial energy of photon (curve 2).

(15% and 25%) at $\epsilon \simeq 700$ GeV ($\epsilon \simeq 1.4$ TeV and $\epsilon \simeq 3.8$ TeV) respectively, and it cuts in half at $\epsilon \simeq 26$ TeV. This increase of effective radiation length can be important in electromagnetic calorimeters operating in detectors on colliders in TeV range as well as in analysis of high-energy cosmic rays. The influence of the correction terms was discussed after Eq.(2.33).

The spectral distribution of bremsstrahlung intensity and the spectral distribution over energy of created electron (positron) as well as the reduction of energy loss and the photon conversion cross section was calculated by Klein [15] using the Migdal [2] formulas. As will be explained below (see Sec. 3.7) we use more accurate procedure of fine tuning and because of this our calculation in logarithmic approximation differs from Migdal one. We

calculated also the correction term and include the Coulomb corrections. For this reason the results shown here in Figs.3-4 are more precise than given in [15].

In the case $\varepsilon \ll \varepsilon_e$ the correction term to the total intensity of radiation (or to the radiation length) can be written as [21]

$$\begin{aligned} \frac{I}{\varepsilon} &= \frac{\alpha m^2}{4\pi\varepsilon_e} \left(1 + \frac{1}{9L_1} - \frac{4\pi}{15} \frac{\varepsilon}{\varepsilon_e} \right) \simeq L_{rad}^{-1} \left(1 - \frac{4\pi}{15} \frac{\varepsilon}{\varepsilon_e} \right), \\ \frac{1}{L_{rad}} &= \frac{2Z^2\alpha^3 n_a L_1}{m^2} \left(1 + \frac{1}{9L_1} \right) \end{aligned} \quad (2.36)$$

In the opposite case $\varepsilon \gg \varepsilon_e$ we have [21]

$$\frac{I}{\varepsilon L_{rad}} \simeq \frac{5}{2} \sqrt{\frac{\varepsilon_e}{\varepsilon}} \left[1 - 2.37 \sqrt{\frac{\varepsilon_e}{\varepsilon}} + 4.57 \frac{\varepsilon_e}{\varepsilon} + \frac{1}{4L_1} \left(\ln \frac{\varepsilon}{\varepsilon_e} - 0.3455 \right) \right] \quad (2.37)$$

Although the coefficients in the last expression are rather large at two first terms of the decomposition over $\sqrt{\varepsilon_e/\varepsilon}$ this formula has the accuracy of the order of 10% at $\varepsilon \sim 10\varepsilon_e$.

Analogous expression for the integral probability of radiation has the form

$$W = \frac{11\pi Z^2 \alpha^3 n_a}{2\sqrt{2}m^2} \sqrt{\frac{\varepsilon_e}{\varepsilon}} L_1 \left[1 - 1.23 \sqrt{\frac{\varepsilon_e}{\varepsilon}} + 1.645 \frac{\varepsilon_e}{\varepsilon} + \frac{1}{4L_1} \left(\ln \frac{\varepsilon}{\varepsilon_e} + 2.53 \right) \right]. \quad (2.38)$$

Ratio of the main terms of Eqs.(2.37) and (2.38) gives the mean energy of radiated photon

$$\bar{\omega} = \frac{9}{22} \varepsilon \simeq 0.409\varepsilon. \quad (2.39)$$

2.3 The LPM effect for pair creation

The probability of the pair creation by a photon can be obtained from the probability of the bremsstrahlung with help of the substitution law:

$$\omega^2 d\omega \rightarrow \varepsilon^2 d\varepsilon, \quad \omega \rightarrow -\omega, \quad \varepsilon \rightarrow -\varepsilon, \quad (2.40)$$

where ω is the photon energy, ε is the energy of the particle. Making this substitution in Eq.(2.7) we obtain the spectral distribution of the pair creation probability [21] (over the energy of the created electron ε)

$$\frac{dW_p}{d\varepsilon} = \frac{2\alpha m^2}{\varepsilon \varepsilon'} \text{Im} \langle 0 | s_1 (G^{-1} - G_0^{-1}) + s_2 \mathbf{p} (G^{-1} - G_0^{-1}) \mathbf{p} | 0 \rangle, \quad (2.41)$$

where

$$s_1 = 1, \quad s_2 = \frac{\varepsilon^2 + \varepsilon'^2}{\omega^2}, \quad \varepsilon' = \omega - \varepsilon, \quad (2.42)$$

the other notations are given in Eqs.(2.8), (2.3), (2.4), (2.5).

Just as in the analysis of the LPM effect for radiation we present the potential Eq.(2.4) in the form $V(\boldsymbol{\rho}) = V_c(\boldsymbol{\rho}) + v(\boldsymbol{\rho})$ and will proceed as we did in Eqs.(2.12)- (2.17). Substituting the expression (2.17) in the formula for the spectral distribution of the pair creation probability (2.41) we have

$$\begin{aligned} \frac{dW_p^c}{d\varepsilon} &= \frac{\alpha m^2}{2\pi\varepsilon\varepsilon'} \text{Im} \Phi_p(\nu), \\ \Phi_p(\nu) &= \nu \int_0^\infty dt e^{-it} \left[s_1 \left(\frac{1}{\sinh z} - \frac{1}{z} \right) - i\nu s_2 \left(\frac{1}{\sinh^2 z} - \frac{1}{z^2} \right) \right] \\ &= s_1 \left(\ln p - \psi \left(p + \frac{1}{2} \right) \right) + s_2 \left(\psi(p) - \ln p + \frac{1}{2p} \right), \end{aligned} \quad (2.43)$$

where we used the same notations as in Eq.(2.17). This formula gives the spectral distribution of the pair creation probability in the logarithmic approximation which was used also by Migdal [3]. It should be noted that the parameter ϱ_c entering into the parameter ν (see Eqs.(2.17), (2.12) and (2.10)) is defined up to the factor ~ 1 , what is inherent in the logarithmic approximation. However, below we will calculate the next term of the decomposition over $v(\boldsymbol{\rho})$ (an accuracy up to the "next to leading logarithm") and this permits to obtain the result which is independent of the parameter ϱ_c . It will be shown that the definition of the parameter ϱ_c minimizes corrections to Eq.(2.43) practically for all values of the parameter ϱ_c . It should be emphasized also that here the Coulomb corrections are included into the parameter ν in contrast to [3].

Substituting the expansion (2.20) in Eq.(2.41) we obtain the decomposition of the probability of the pair creation:

$$\frac{dW_p}{d\varepsilon} = \frac{dW_p^c}{d\varepsilon} + \frac{dW_p^1}{d\varepsilon} + \frac{dW_p^2}{d\varepsilon} + \dots \quad (2.44)$$

The probability of pair creation $\frac{dW_p^c}{d\varepsilon}$ is defined by Eq.(2.43). The term $\frac{dW_p^1}{d\varepsilon}$ in Eq.(2.44) corresponds to the first term (linear in v) in Eq.(2.20). The explicit expression for the first correction to the pair creation probability is [21]

$$\begin{aligned}
\frac{dW_p^1}{d\varepsilon} &= -\frac{\alpha m^2}{4\pi\varepsilon\varepsilon' L_c} \text{Im } F_p(\nu); \quad F_p(\nu) = \int_0^\infty \frac{dz e^{-it}}{\sinh^2 z} [s_1 f_1(z) - 2i s_2 f_2(z)], \\
f_1(z) &= \left(\ln \varrho_c^2 + \ln \frac{\nu}{i} - \ln \sinh z - C \right) g(z) - 2 \cosh z G(z), \\
f_2(z) &= \frac{\nu}{\sinh z} \left(f_1(z) - \frac{g(z)}{2} \right), \quad t = t_1 + t_2,
\end{aligned} \tag{2.45}$$

where the functions $g(z)$ and $G(z)$ are defined in Eq.(2.23), L_c is defined in Eq.(2.12). Use of the last representation of function $G(z)$ simplifies the numerical calculation. As in radiation case the parameter ν has two representations: Eqs.(2.24) and (2.25).

When the scattering of created particles is weak ($\nu_1 \ll 1$), the main contribution in Eqs.(2.43) and (2.45) gives the region where $z \ll 1$ and one can expand the functions of z (compare with Eq.(2.28)). As result we obtain the spectral distribution of the pair creation probability for $|\nu| \ll 1$:

$$\begin{aligned}
\frac{dW_p}{d\varepsilon} &= \frac{dW_p^c}{d\varepsilon} + \frac{dW_p^1}{d\varepsilon} = \frac{\alpha m^2}{2\pi\varepsilon\varepsilon'} \text{Im} \left[\Phi_p(\nu) - \frac{1}{2L_c} F_p(\nu) \right] \\
&= \frac{4Z^2 \alpha^3 n_a}{3m^2 \omega} \left\{ \left(\ln(183Z^{-1/3}) - f(Z\alpha) \right) \left(1 - \frac{31\nu_1^4}{21} \right) - \frac{1}{6} \right. \\
&\quad \left. + 2 \frac{\varepsilon^2 + \varepsilon'^2}{\omega^2} \left[\left(\ln(183Z^{-1/3}) - f(Z\alpha) \right) \left(1 - \frac{16\nu_1^4}{21} \right) + \frac{1}{12} \right] \right\}, \tag{2.46}
\end{aligned}$$

where L_1 is defined in Eq.(2.12). Integrating Eq.(2.46) over ε we obtain

$$W_p = \frac{28Z^2 \alpha^3 n_a}{9m^2} \left[\left(\ln(183Z^{-1/3}) - f(Z\alpha) \right) \left(1 - \frac{3312}{2401} \frac{\omega^2}{\omega_e^2} \right) - \frac{1}{42} \right], \tag{2.47}$$

where

$$\omega_e = m \left(2\pi Z^2 \alpha^2 n_a \lambda_c^3 L_1 \right)^{-1} \tag{2.48}$$

Note that ω_e is four times larger than ε_e Eq.(2.26), in gold it is $\omega_e = 10.5$ TeV. This is just the value of photon energy starting with the LPM effect becomes essential for the pair creation process in heavy elements. If one omits here the terms $\propto \nu_1^4$ and $\propto (\omega/\omega_e)^2$ these expressions coincide with the known Bethe-Maximon formula for the probability of pair creation by a high-energy photon in the case of complete screening (if one neglects the contribution of atomic electrons) written down within power accuracy (omitted terms are of

the order of powers of $\frac{m}{\omega}$) with the Coulomb corrections, see e.g. Eqs.(19.4) and (19.17) in [8].

The pair creation spectral probability dW/dx vs $x = \varepsilon/\omega$ in gold is shown in Fig.5 for different energies. It is seen that for $\omega = 2.5$ TeV which below ω_e the difference with the Bethe-Maximon probability is rather small. When

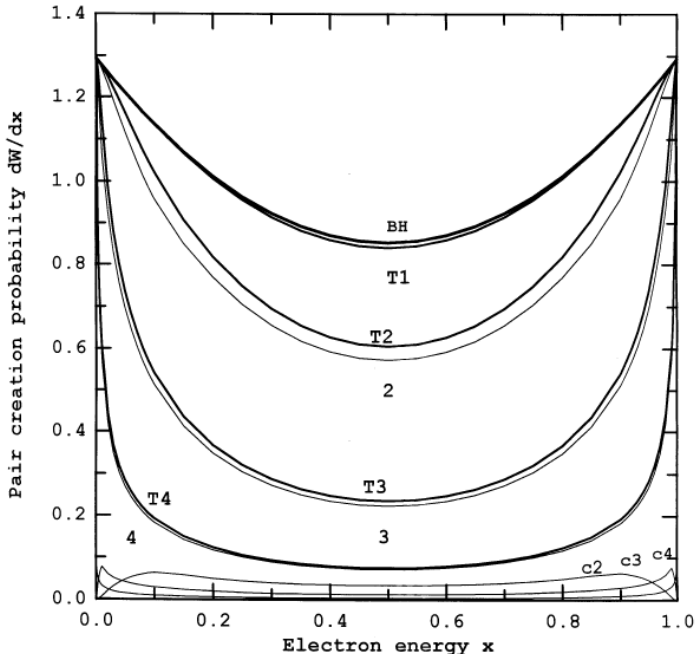


Figure 5: The pair creation spectral probability $\frac{dW_p}{dx}$, $x = \frac{\varepsilon}{\omega}$ in gold in terms of the exact total Bethe-Maximon probability taken with the Coulomb corrections (see Eq.(2.47)): *curve BH* is the Bethe-Maximon spectral probability (see Eq.(2.46)); *curve T1* is the total contribution (the sum of the logarithmic approximation $dW_p^c/d\varepsilon$ (2.43) and the first correction to the spectral probability $dW_p^1/d\varepsilon$ (2.45)) for the photon energy $\omega = 2.5$ TeV; *curve 2* is the logarithmic approximation $dW_p^c/d\varepsilon$ (2.43), *curve c2* is the first correction to the spectral probability $dW_p^1/d\varepsilon$ (2.45)) and *curve T2* is the sum of the previous contributions for the photon energy $\omega = 25$ TeV; *curves 3, c3, T3* are the same for the photon energy $\omega = 250$ TeV; *curves 4, c4, T4* are the same for the photon energy $\omega = 2500$ TeV.

$\omega > \omega_e$ there is significant difference with the Bethe-Maximon spectrum increasing with ω growth. In Fig.5 are shown the curves (thin lines 2,3,4) obtained in logarithmic approximation $dW_p^c/d\varepsilon$ Eq.(2.43), the first correction to the spectral probability $dW_p^1/d\varepsilon$ Eq.(2.45), curves $c2, c3, c4$ and the sum of these two contributions: curves $T1, T2, T3, T4$. It should be noted that for our definition of the parameter ϱ_c Eq.(2.10) the corrections are not exceed 6% of the main term. The corrections are maximal for $\nu_0 \sim 3$.

Integrating Eq.(2.43) over $y = \varepsilon/\omega$ we obtain the total probability of pair creation in the logarithmic approximation

$$\begin{aligned} \frac{W_p^c}{W_{p0}^{BM}} &= \frac{9}{14} \frac{\omega_e}{\omega} \text{Im} \int_0^1 \frac{dy}{y(1-y)} \left[\left(\ln p - \psi \left(p + \frac{1}{2} \right) \right) \right. \\ &+ \left. (1 - 2y + 2y^2) \left(\psi(p) - \ln p + \frac{1}{2p} \right) \right], \end{aligned} \quad (2.49)$$

where

$$p = \frac{bs}{4}, \quad s = \frac{1}{\sqrt{y(1-y)}}, \quad b = \exp\left(i\frac{\pi}{4}\right) \sqrt{\frac{L_1 \omega_e}{L_c \omega}},$$

W_{p0}^{BM} is the Bethe-Maximon probability of pair photoproduction in the logarithmic approximation. The total probability of pair creation W_p^c in gold is given in Fig.4 (curve 2), it reduced by 10% at $\omega \simeq 9$ TeV and it cuts in half at $\omega \simeq 130$ TeV.

At $\nu_0 \gg 1$ the function $F_p(\nu)$ (see Eq.(2.45)) has the form

$$-\text{Im} F_p(\nu) = \frac{\pi}{4}(s_1 - s_2) + \frac{\nu_0}{\sqrt{2}} \left(\ln 2 - C + \frac{\pi}{4} \right) s_2, \quad (2.50)$$

Under the same conditions ($\nu_0 \gg 1$) the function $\text{Im} \Phi_p(\nu)$ Eq.(2.43) is

$$\text{Im} \Phi_p(\nu) = \frac{\pi}{4}(s_1 - s_2) + \frac{\nu_0}{\sqrt{2}} s_2 \rightarrow \frac{\nu_0}{\sqrt{2}} s_2. \quad (2.51)$$

So, in the region where the LPM effect is strong the probability Eq.(2.43) can be written as

$$\frac{dW_p^c}{d\varepsilon} = \frac{\alpha(\varepsilon^2 + \varepsilon'^2)}{\omega^2} \left(\frac{Z^2 \alpha^2 n_a}{\pi \omega \varepsilon \varepsilon'} L(\varrho_c) \right)^{1/2}. \quad (2.52)$$

This means that in this limit the spectral probability of pair creation is proportional to the square root of the density just as the emission probability Eq.(2.32).

At $\nu_0 \gg 1$ the relative contribution of the first correction $\frac{dW_p^1}{d\varepsilon}$ is defined by

$$r = \frac{dW_p^1}{dW_p^c} = \frac{1}{2L_c} \left(\ln 2 - C + \frac{\pi}{4} \right) \simeq \frac{0.451}{L_c}. \quad (2.53)$$

In this expression the value r with the accuracy up to terms $\sim 1/L_c^2$ doesn't depend on the electron energy: $L_c \simeq L_1 + \ln(\omega/\omega_e)/2$. Hence we can find the correction to the total probability at $\omega \gg \omega_e$. The maximal value of the correction is attained at $\omega \sim 10\omega_e$, it is $\sim 6\%$ for heavy elements. In this region $\nu_0 \gg 1$ or $\omega \gg \omega_e$ the total probability of pair creation in terms of the Bethe-Maximon total probability can be presented as

$$\frac{W_p}{W_p^{BM}} \simeq 2.14 \sqrt{\frac{\omega_e}{\omega}} \left[1 - 0.836 \sqrt{\frac{\omega_e}{\omega}} - 0.548 \frac{\omega_e}{\omega} + \frac{1}{4L_1} \left(\ln \frac{\omega}{\omega_e} + 0.274 \right) \right]. \quad (2.54)$$

2.4 Anomalous magnetic moment of the electron in a medium

The contributions of higher orders of the perturbation theory over the interaction with an electromagnetic field give the electromagnetic radiative corrections to the electron mass and lead to appearance of the anomalous magnetic moment (AMM) of the electron [29]. It is known that under influence of an external electromagnetic field these effects in particular the AMM of electron are changed essentially [30], [8]. Here we consider how the mentioned effects modify in a medium [31].

The total probability of radiation W is connected with imaginary part of the radiative correction to the electron mass according to

$$m\Delta m = \varepsilon\Delta\varepsilon, \quad -2\text{Im}\Delta\varepsilon = W, \quad \text{Im} \Delta m = -\frac{\varepsilon}{2m}W. \quad (2.55)$$

Since T in Eq.(2.7) is the analytic function of the potential V we have that

$$\Delta m = -\alpha m \int_0^\varepsilon \frac{d\omega}{\varepsilon} T. \quad (2.56)$$

One can derive this formula considering the self-energy diagram and the corresponding amplitude of forward scattering of electron (see Eqs.(12.18) and (12.39) in [8]).

In the presence of a homogeneous external field the Hamiltonian \mathcal{H} (2.3),(2.6) acquires the linear over coordinate term. One can find the explicit form of this term using the Eqs.(A.18) and (A.22) of Appendix A and carrying out the scale transformation of variables according to Eq.(2.1):

$$\Delta\mathcal{H} = \frac{2}{u}\boldsymbol{\chi}\boldsymbol{\varrho}, \quad (2.57)$$

where $\boldsymbol{\chi}$ is the known parameter characterizing quantum effects in the radiation process (see Eq.(1.21)), $u = \omega/\varepsilon'$.

For polarized initial electron (see (A.4) in Appendix A) have for the addition to T in Eq.(2.7) depending on the spin vector $\boldsymbol{\zeta}$:

$$T \rightarrow T + T_{\boldsymbol{\zeta}}, \quad T_{\boldsymbol{\zeta}} = i\frac{\omega}{\varepsilon} \langle 0|(G^{-1}\mathbf{p} - \mathbf{p}G^{-1})|0 \rangle \times \mathbf{v} \boldsymbol{\zeta}. \quad (2.58)$$

For the radiative correction to the electron mass we have, respectively

$$\Delta m \rightarrow \Delta M = \Delta m + \Delta m_{\boldsymbol{\zeta}}. \quad (2.59)$$

It should be noted that expressions for T (2.7) and (2.58) have universal form while the specific of the particle motion is contained in the propagator G^{-1} through the effective potential

$$V_F(\boldsymbol{\varrho}) = -iV_c(\boldsymbol{\varrho}) + \frac{2}{u}\boldsymbol{\chi}\boldsymbol{\varrho}, \quad \mathcal{H}_F = \mathbf{p}^2 + V_F, \quad G_F = \mathcal{H}_F + 1, \quad (2.60)$$

where we restrict ourselves to the main term in the decomposition over v , see Eqs.(2.12), (2.20). This means that result has the logarithmic accuracy over the scattering (but not over an external field). With regard for an external field the parameter ϱ_c in Eq.(2.24) is defined by a set of equations:

$$\begin{aligned} \varrho_c &= 1 \quad \text{for} \quad 4\frac{\chi^2}{u^2} + 4QL_1 \leq 1; \\ \varrho_c^4 \left[4\frac{\chi^2}{u^2}\varrho_c^2 + |\nu(\varrho_c)|^2 \right] &= 1 \quad \text{for} \quad 4\frac{\chi^2}{u^2} + 4QL_1 \geq 1, \end{aligned} \quad (2.61)$$

where $\nu = 2\sqrt{iq}$, $q = QL_c$, L_1 , Q and L_c are defined in Eqs.(2.25) and (2.24). Substituting into the depending on the spin term in (2.58) we find

$$\begin{aligned} \langle 0|(G_F^{-1}\mathbf{p} - \mathbf{p}G_F^{-1})|0 \rangle &= \frac{\boldsymbol{\chi}}{2\pi u} \int_0^\infty \exp(-it) \frac{\varphi}{\cosh^2 \frac{\nu t}{2}} dt, \\ \varphi \equiv \varphi(\chi, \nu, t) &= \exp \left[-\frac{4i\chi^2 t}{\nu^2 u^2} \left(1 - \frac{2}{\nu t} \tanh \frac{\nu t}{2} \right) \right]. \end{aligned} \quad (2.62)$$

Thus, in the used approximation ($G = G_F$) we have for T_ζ Eq.(2.58)

$$T_\zeta = \frac{i}{2\pi u} \frac{\omega}{\varepsilon} \int_0^\infty \exp(-it) \frac{\varphi}{\cosh^2 \frac{\nu t}{2}} dt (\zeta \chi \mathbf{v}), \quad (2.63)$$

where $(\zeta \chi \mathbf{v}) = (\zeta \cdot (\chi \times \mathbf{v}))$. Within relativistic accuracy (up to terms of higher order over $1/\gamma$) the combination of vectors entering in Eq.(2.63) can be written as (see Eq.(12.19) in [8] and [33])

$$(\zeta \chi \mathbf{v}) = 2\mu_0 \frac{\zeta \mathbf{H}_R}{m}, \quad (2.64)$$

where $\mu_0 = e/2m = (e\hbar/2mc)$ is the Bohr magneton, $\mathbf{H}_R = \gamma(\mathbf{H}_\perp + \mathbf{E} \times \mathbf{v})$ is the magnetic field in the electron rest frame. Here we use that $\chi = \chi \mathbf{s}$, where \mathbf{s} is the unit vector in the direction of acceleration (this vector is used in [8]).

In the electron rest frame one can consider the value $\text{Re } \Delta m_\zeta$ depending on the electron spin as the energy of interaction of the AMM of electron μ' with the magnetic field \mathbf{H}_R (see Eq.(12.23) in [8] and [33])

$$\text{Re } \Delta m_\zeta = -\mu' \zeta \mathbf{H}_R, \quad (2.65)$$

Taking into account Eqs.(2.56), (2.58), (2.59), (2.63), (2.64), (2.65) we obtain the following general expression for the AMM of electron moving in a medium in the presence of an external electromagnetic field [31]:

$$\frac{\mu'}{\mu_0} = -\frac{\alpha}{\pi} \text{Im} \int_0^\infty \frac{du}{(1+u)^3} \int_0^\infty \exp(-it) \frac{\varphi}{\cosh^2 \frac{\nu t}{2}} dt \quad (2.66)$$

In the absence of scattering ($\nu \rightarrow 0$) the expression (2.66) gets over into the formula for the AMM of electron in external field (see Eq.(12.24) in [8] and [34], [33])

$$\frac{\mu'}{\mu_0} = -\frac{\alpha}{\pi} \text{Im} \int_0^\infty \frac{du}{(1+u)^3} \int_0^\infty \exp \left[-it \left(1 + \frac{\chi^2 t^2}{3u^2} \right) \right] dt \quad (2.67)$$

In the weak external field ($\chi \ll 1, \varphi \simeq 1$) we obtain the formula for the AMM of electron under influence of multiple scattering

$$\frac{\mu'}{\mu_0} = -\frac{\alpha}{\pi} \text{Im} \int_0^\infty \frac{du}{(1+u)^3} \int_0^\infty \exp(-it) \frac{1}{\cosh^2 \frac{\nu t}{2}} dt = \frac{\alpha}{2\pi} r, \quad (2.68)$$

where

$$\begin{aligned}
 r &= \text{Re}J, \quad J = 2i \int_0^\infty \frac{du}{(1+u)^3} \int_0^\infty \exp(-it) \frac{1}{\cosh^2 \frac{\nu t}{2}} dt \\
 &= 4i \int_0^\infty \frac{du}{(1+u)^3} \frac{1}{\nu} \left[\frac{2i}{\nu} \beta \left(\frac{i}{\nu} \right) - 1 \right], \\
 \beta &= \frac{1}{2} \left[\psi \left(\frac{1+x}{2} \right) - \psi \left(\frac{x}{2} \right) \right],
 \end{aligned} \tag{2.69}$$

where $\psi(x)$ is defined in Eq.(2.5).

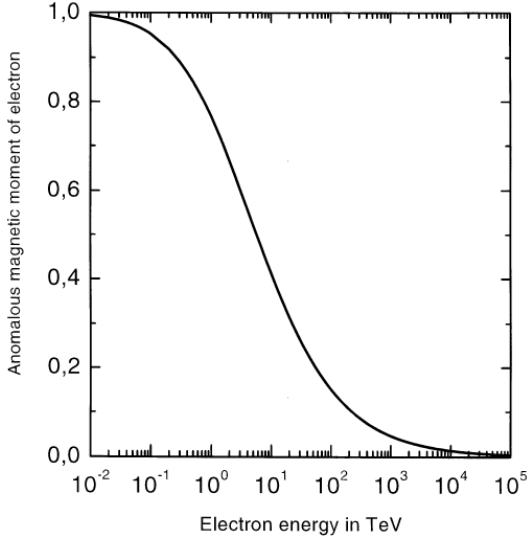


Figure 6: Anomalous magnetic moment(AMM) of electron in units $\alpha/2\pi$ (r in Eq.(2.69)) in gold vs electron energy in TeV.

The dependence of the AMM of electron on its energy ε in gold is shown in Fig.6. It is seen that at energy $\varepsilon = 500$ GeV value of AMM is 0.85 part of standard quantity (SQ) of AMM ($r = 1$), at energy $\varepsilon = 1$ TeV it is 0.77 part of SQ and at energy $\varepsilon = 5.5$ TeV it is 0.5 part of SQ. Actually in all heavy elements the behavior of AMM of electron will be quite similar, i.e. the scale of energy where the AMM of electron deviates from SQ is of order of TeV.

In the case of weak effect of multiple scattering when $\varepsilon \ll \varepsilon_e$, where ε_e is defined in Eq.(2.26) we obtain for AMM of electron

$$\frac{\mu'}{\mu_0} = \frac{\alpha}{2\pi} \left(1 - \frac{\pi}{2} \frac{\varepsilon}{\varepsilon_e} \right). \tag{2.70}$$

At very high energy $\varepsilon \gg \varepsilon_e$ the effect of multiple scattering becomes strong. In this case the asymptotic expression for AMM of electron is

$$r = \frac{2\pi}{\alpha} \frac{\mu'}{\mu_0} = \frac{\pi}{2\sqrt{2}} \sqrt{\frac{\varepsilon_c}{\varepsilon}} \left(1 - \frac{\pi^2}{2} \frac{\varepsilon_c}{\varepsilon} \right), \quad \varepsilon_c = \varepsilon_e \frac{L_1}{L_0}, \quad L_0 = L_1 + \frac{1}{2} \ln \frac{\varepsilon}{\varepsilon_e}. \quad (2.71)$$

Redefinition of the characteristic energy $\varepsilon_e \rightarrow \varepsilon_c$ is connected with enlargement of the radiation cone (in comparison with $1/\gamma$) or in another terms with increasing of the characteristic transverse momentum transfers due to the multiple scattering.

Let us discuss one of possibilities of experimental observation of influence of medium on the AMM of electron. At a very high energy where the observation becomes feasible the rotation angle φ of the spin vector ζ in the transverse to the particle velocity \mathbf{v} magnetic field \mathbf{H} depends only on the value of AMM and doesn't depend on the particle energy:

$$\varphi = \left(\frac{m}{\varepsilon} + \frac{\mu'}{\mu_0} \right) \frac{eH}{m} l \simeq r \frac{\alpha}{2\pi} \frac{H}{H_0} \frac{l}{\lambda_c}, \quad (2.72)$$

where l is the path of electron in the field, $H_0 = m^2/e = 4.41 \cdot 10^{13}$ Oe (see Eq.(1.22)). The dependence of r on energy ε is found above and shown in Fig.6.

Since at radiation of hard photons in a medium the picture is quite complicated: energy losses, cascade processes, spin flip and depolarization, it is desirable to measure the particles which don't radiate photons on the path l . The number of such particles N is determined by the total probability of radiation in a medium found in [21], Eqs.(3.12)-(3.14) (see Eqs.(2.38) and (2.39) in Sec.2.2 above):

$$N = N_0 \exp(-\psi(\varepsilon)), \quad \psi(\varepsilon) = W(\varepsilon)l = \frac{k(\varepsilon)\varphi_{SQ}}{2\chi(\varepsilon_e)}; \quad k(\varepsilon) = W(\varepsilon)L_{rad}^0, \\ (L_{rad}^0)^{-1} = \frac{\alpha}{4\pi} \frac{m^2}{\varepsilon_e}, \quad \chi(\varepsilon_e) = \frac{\varepsilon_e}{m} \frac{H}{H_0}, \quad (2.73)$$

where φ_{SQ} is the rotation angle for standard value of AMM in QED ($r = 1$), N_0 is the number of initial electrons. With energy increase the function $k(\varepsilon)$ decreases (see Eqs.(3.12), (3.13) in [21])

$$k(\varepsilon \ll \varepsilon_e) \simeq \frac{4}{3} \left(\ln \frac{\varepsilon_e}{\varepsilon} + 1.96 \right), \quad k(\varepsilon = \varepsilon_e) \simeq 3.56, \quad k(\varepsilon \gg \varepsilon_e) \simeq \frac{11\pi}{4\sqrt{2}} \sqrt{\frac{\varepsilon_e}{\varepsilon}}. \quad (2.74)$$

The crucial part of the experiment is an accuracy of measurement of electron polarization before target and after target. If one supposes that spin rotation angle can be measured with accuracy noticeably better than $1/10$ then we can put that $(1 - r)\varphi_{SQ} = 1/10$. In the gold we find for the energy $\varepsilon = \varepsilon_e = 2.61$ TeV and the magnetic field $H = 4 \cdot 10^5$ Oe that $1 - r = 0.371$, the path of electron in the target is $l \simeq 1$ cm and number of electron traversing the target without energy loss is $N \simeq 3.2 \cdot 10^{-5} N_0$. This estimates show that the measurement of the effect found in this paper will be feasible in the not very distant future.

2.5 Propagation of high-energy photon in a medium in presence of an external field

As known, the propagation of electromagnetic wave in a medium is defined by its dielectric tensor $\mathcal{E}_{ik}(\omega)$. For relatively low frequency ω (e.g. visible light) the dielectric tensor is defined by atomic phenomena. When the frequency of wave is much higher the atomic frequencies, the dielectric tensor has a form

$$\mathcal{E}_{ik}(\omega) = \delta_{ik}\mathcal{E}(\omega), \quad \mathcal{E}(\omega) = 1 - \frac{\omega_0^2}{\omega^2}, \quad \omega_0^2 = \frac{4\pi n_e e^2}{m}, \quad (2.75)$$

where ω_0 is the plasma frequency, in any medium $\omega_0 < 100$ eV. So that for $\omega \gg \omega_0$ an influence of atomic phenomena on propagation of electromagnetic wave in a medium becomes small.

At very high energy the nonlinear effects of QED enter into game. One of them is the polarization of the vacuum by a photon. In the presence of an external electromagnetic field the polarization of vacuum was considered first in the pioneer papers [35]. In the strong field this effect can be essential for propagation of high-energy photons [36], [8].

To evaluate the polarization tensor one has to consider the amplitude of photon scattering which included the polarization operator [32]. As above we use the quasiclassical operator method [7], [8], [10]. In this method the mentioned amplitude is described by diagram where the virtual electron-positron pair is first created by the initial photon with 4-momentum $k(\omega, \mathbf{k})$ and polarization \mathbf{e}_1 and then annihilate into final photon with 4-momentum k and polarization \mathbf{e}_2 . This corresponds to use of the non-covariant perturbation theory where at high energies ($\omega \gg m$) the contribution of this diagram survives only. For this energy of photon this process occurs in a rather long time (or at a rather long distance) known as the lifetime of the virtual state

$$l_f = \frac{\omega}{2q_c^2}, \quad (2.76)$$

where $q_c \geq m$ is the characteristic transverse momentum of the process. When the virtual electron (or positron) is moving in a medium it scatters by atoms and changes the velocity under influence of external electromagnetic field. The mean square of momentum transfer to the electron from a medium and an external field on the distance l_f is

$$\begin{aligned} q_f^2 &= q_s^2 + \mathbf{q}_F^2, & q_s^2 &= 4\pi Z^2 \alpha^2 n_a L l_f, & L &\equiv L(q_c^2) = \ln(q_c^2 a_s^2), \\ \mathbf{q}_F &= e\mathbf{F}l_f, & \mathbf{F} &= \mathbf{E}_\perp + \mathbf{v} \times \mathbf{H}, \end{aligned} \quad (2.77)$$

here the notations see Eqs.(1.13), (1.21).

In the case of small momentum transfer $q_f \equiv \sqrt{q_f^2} \ll m$ the influence of a medium and an external field is weak, in this case $q_c = m$. At high energy it is possible that $q_f \geq m$. In this case the characteristic value of the momentum transfer (giving the main contribution into the spectral probability) is defined by the value of q_f . The self-consistency condition is

$$\begin{aligned} q_c^2 = q_f^2 &= \frac{2\pi\omega Z^2 \alpha^2 n_a L(q_f)}{q_f^2} + \frac{m^6 \kappa^2}{4q_f^4} \geq m^2, & \kappa &= \frac{\omega}{m^3} e\mathbf{F}_\gamma, \\ \mathbf{F}_\gamma &= \mathbf{E} - \mathbf{n}(\mathbf{nE}) + \mathbf{n} \times \mathbf{H}, \end{aligned} \quad (2.78)$$

here $\kappa = |\kappa|$ is known parameter characterizing the pair production process in a homogeneous external field \mathbf{F}_γ . With q_c increase the lifetime of the virtual state Eq.(2.76) decreases.

We will use the following normalization condition for the amplitude under consideration

$$M = 2\omega\Delta\omega. \quad (2.79)$$

The amplitude M is the contraction of the tensor $e_j^{(i)*} e_k^{(f)}$ ($\mathbf{e}^{(i)}$ and $\mathbf{e}^{(f)}$ are the polarization vectors of the initial and the final photons) and the polarization tensor M_{jk} . We select the basic vectors as

$$\mathbf{e}_1 = \frac{\mathbf{F}_\gamma}{|\mathbf{F}_\gamma|}, \quad \mathbf{e}_2 = \mathbf{n} \times \mathbf{e}_1. \quad (2.80)$$

Since the tensor M_{jk} is invariant under the space inversion then in the selected basic vectors it has the diagonal form

$$M_{jk} = \frac{1}{2} [\delta_{jk}(M_{11} + M_{22}) + (e_{1j}e_{1k} - e_{2j}e_{2k})(M_{11} - M_{22})] \quad (2.81)$$

In absence of external field it is convenient to describe the process of photon scattering using the helicity polarization vector \mathbf{e}_λ ($\lambda = \pm 1$) connected with

momentum transfer Δ (see Eq.(2.97) in the next subsection). In presence of external field and for $\Delta = 0$ we choose the polarization vectors in the following way:

$$\mathbf{e}_\lambda = \frac{1}{\sqrt{2}}(\mathbf{e}_1 + i\lambda\mathbf{e}_2), \quad (\mathbf{e}_\lambda \mathbf{e}_\lambda^*) = 1, \quad (\mathbf{e}_\lambda \mathbf{e}_{-\lambda}^*) = 0, \quad \mathbf{e}_\lambda \times \mathbf{n} = i\lambda\mathbf{e}_\lambda. \quad (2.82)$$

In terms of helicity amplitudes M_{++} and M_{+-} the tensor M_{jk} and the corresponding dielectric tensor \mathcal{E}_{jk} has a form

$$\begin{aligned} M_{jk} &= \delta_{jk}k_{++}^2 + (e_{1j}e_{1k} - e_{2j}e_{2k})k_{+-}^2, \\ \mathcal{E}_{jk} &= \delta_{jk} - \frac{1}{\omega^2}M_{jk}, \quad k_{++}^2 \equiv M_{++}, \quad k_{+-}^2 \equiv M_{+-} \end{aligned} \quad (2.83)$$

The polarization tensor k_{jk}^2 is diagonal in the basic vectors \mathbf{e}_1 and \mathbf{e}_2 Eq.(2.80). The corresponding mass squared are

$$k_1^2 \equiv k_{11}^2 = k_{++}^2 + k_{+-}^2, \quad k_2^2 \equiv k_{22}^2 = k_{++}^2 - k_{+-}^2 \quad (2.84)$$

The probability of pair creation by a photon with polarization \mathbf{e} is

$$W_p^F(\mathbf{e}) = -\frac{1}{\omega} \text{Im} [(\mathbf{e}\mathbf{e}_1)^2 k_1^2 + (\mathbf{e}\mathbf{e}_2)^2 k_2^2] = -\frac{1}{\omega} \text{Im} [k_{++}^2 + \xi_3 k_{+-}^2], \quad (2.85)$$

where ξ_3 is the Stokes' parameter. For unpolarized photon one has

$$W_p^F = -\frac{1}{\omega} \text{Im} k_{++}^2. \quad (2.86)$$

The method of calculation of the functions k_{++}^2 and k_{+-}^2 which define the tensor M_{jk} is similar to used in previous subsection (see details in [32]). The general expressions for photon masses squared under simultaneous influence of multiple scattering in a medium and an external electromagnetic field has a form

$$\begin{aligned} k_{++}^2 &= \frac{\alpha m^2}{2\pi} \int_0^\omega \frac{\omega d\varepsilon}{\varepsilon \varepsilon'} \int_0^\infty e^{-it} \\ &\times \left[s_2 \nu \varphi_p \tanh \frac{\nu t}{2} \left(\frac{4\kappa'^2}{\nu^2} + 1 \right) - s_3 \left(\frac{\nu}{\sinh \nu t} \varphi_p - \frac{1}{t} \right) \right] dt. \end{aligned} \quad (2.87)$$

For k_{+-}^2 we found respectively

$$k_{+-}^2 = -\frac{2\alpha m^2}{\pi} \int_0^\omega \frac{\omega d\varepsilon}{\varepsilon \varepsilon'} s_3 \kappa'^2 \int_0^\infty e^{-it} \frac{\varphi_p}{\nu \sinh \nu t} \tanh^2 \frac{\nu t}{2} dt. \quad (2.88)$$

Here the coefficients s_1 and s_2 are defined in Eq.(2.42),

$$s_3 = \frac{2\varepsilon\varepsilon'}{\omega^2}, \quad \boldsymbol{\kappa}' = \frac{\varepsilon\varepsilon'}{\omega^2}\boldsymbol{\kappa}, \quad \nu = 2\sqrt{iq}, \quad q = QL_c, \quad L_c \equiv L(\varrho_c) = \ln \frac{a_{s_2}^2}{\lambda_c^2 \varrho_c^2},$$

$$\varphi_p \equiv \varphi(\boldsymbol{\kappa}', \nu, t) = \exp \left[-\frac{4i\boldsymbol{\kappa}'^2 t}{\nu^2} \left(1 - \frac{2}{\nu t} \tanh \frac{\nu t}{2} \right) \right], \quad (2.89)$$

where $\boldsymbol{\kappa}$ is defined in Eq.(2.78), Q is defined in Eq.(2.3), the parameter ϱ_c is defined by the set of equations (compare with Eq.(2.61)):

$$\varrho_c = 1 \quad \text{for} \quad 4(\boldsymbol{\kappa}'^2 + QL_1) \leq 1;$$

$$4\varrho_c^4 (\boldsymbol{\kappa}'^2 \varrho_c^2 + QL_c) = 1 \quad \text{for} \quad 4(\boldsymbol{\kappa}'^2 + QL_1) \geq 1, \quad (2.90)$$

In the absence of external field ($\boldsymbol{\kappa}' = 0$, $\varphi_p = 1$) we have

$$k_{++}^2 = \frac{\alpha m^2}{2\pi} \int_0^\omega \frac{\omega d\varepsilon}{\varepsilon\varepsilon'} \int_0^\infty e^{-it} \left[s_2 \nu \tanh \frac{\nu t}{2} - \frac{s_3}{2t} \left(\frac{\nu}{\sinh \nu t} - \frac{1}{t} \right) \right] dt$$

$$= -\frac{\alpha m^2}{2\pi} \int_0^\omega \frac{\omega d\varepsilon}{\varepsilon\varepsilon'} \left[s_1 \left(\ln p - \psi \left(p + \frac{1}{2} \right) \right) + s_2 \left(\psi(p) - \ln p + \frac{1}{2p} \right) \right],$$

$$k_{+-}^2 = 0, \quad (2.91)$$

where $p = i/2\nu$, $\psi(p)$ as above is the logarithmic derivative of the gamma function. Substituting the result obtained into formula (2.86) we have the probability of pair creation which agrees with Eq.(2.43).

In the absence of multiple scattering ($\nu \rightarrow 0$) we get

$$k_{++}^2 = \frac{\alpha m^2}{\pi} \int_0^\omega \frac{\omega d\varepsilon}{\varepsilon\varepsilon'} \int_0^\infty e^{-it} \left[s_2 \boldsymbol{\kappa}'^2 t \varphi_F - \frac{s_3}{2t} (\varphi_F - 1) \right] dt,$$

$$k_{+-}^2 = -\frac{\alpha m^2}{2\pi} \int_0^\omega \frac{\omega d\varepsilon}{\varepsilon\varepsilon'} s_3 \boldsymbol{\kappa}'^2 \int_0^\infty e^{-it} \varphi_F t dt, \quad (2.92)$$

where

$$\varphi_F = \exp \left(-i \frac{\boldsymbol{\kappa}'^2 t^3}{3} \right) \quad (2.93)$$

For this case the expressions for $k_{1,2}^2$ (2.10) after substitution results of Eq.(2.92) agree with masses squared of photon calculated in an external electromagnetic field (see [8] and references therein).

In the case when the both characteristic parameters are small ($\nu_1^2 = 4QL_1 \ll 1$, $\kappa \ll 1$), the main terms of decomposition of the functions k^2 are the sum of independent corrections to the photon mass squared

both on account of the multiple scattering and an external field

$$\begin{aligned}
k_{++}^2 &= \frac{\alpha m^2}{\pi} \left[-i \frac{7}{9} \frac{\omega}{\omega_e} \left(1 - \frac{1}{21L_1} \right) + \frac{59}{225} \left(\frac{\omega}{\omega_e} \right)^2 \right. \\
&\quad \left. - i \frac{3\sqrt{3}\pi}{16\sqrt{2}} \frac{\omega}{\omega_F} \exp \left(-\frac{8\omega_F}{3\omega} \right) - \frac{11}{90} \left(\frac{\omega}{\omega_F} \right)^2 \right], \\
k_{+-}^2 &= \frac{\alpha m^2}{\pi} \left[i \frac{\sqrt{3}\pi}{16\sqrt{2}} \frac{\omega}{\omega_F} \exp \left(-\frac{8\omega_F}{3\omega} \right) + \frac{1}{30} \left(\frac{\omega}{\omega_F} \right)^2 \right]; \\
\omega &\ll \omega_e, \quad \omega_F = m \frac{H_0}{|\mathbf{F}|}, \quad \omega \ll \omega_F,
\end{aligned} \tag{2.94}$$

where ω_e is defined in Eq.(2.48) and H_0 in Eq.(1.22). The correction $\propto 1/L_1$ follows from the first term of decomposition of the type Eq.(2.20). Let us remind that in gold the value ω_e is $\omega_e = 10.5$ TeV, this is the typical value for the heavy elements.

In Fig.7 the functions $\text{Re } k_{++}^2$ (curve 2) and $\text{Im } k_{++}^2$ (curve 1) are given for the case when the influence of a medium is taken into account only (Eq. (2.91)). The both curves are normalized to the asymptotics given by Eq. (2.94) in the limit $\omega_F \rightarrow \infty$.

It should be noted that beginning with some photon energy $\omega = \omega_b$ the radiative correction to the value $\text{Re } \mathcal{E}_{jk}$ in the absence of a field ($\boldsymbol{\kappa} = 0$) becomes larger than ω_0^2/ω^2 (see Eq.(2.75)). The estimate of ω_b is following

$$\omega_b \sim \sqrt{\frac{\alpha}{\pi} \frac{L_{rad}}{\lambda_c}} \omega_0. \tag{2.95}$$

For gold one obtains $\omega_b \sim 40$ GeV.

A propagation of high-energy photons in oriented single crystals is one of interesting applications of the result obtained in this subsection. In this case we have both the dense matter with strong effect of multiple scattering and high fields of crystal axes or planes. As we saw, the LPM effect is most pronounced in the heavy elements. The same is valid for the process under consideration. Let the high-energy photon incident on crystal. The angle of incidence is small and such that the distance from axis $\boldsymbol{\rho}$ (or the distance from plane x) can be considered as a constant on the formation length of process (the constant field approximation is applicable, see Sections 12,15 in [10]).

For the case of orientation of a crystal along an axis the ratio of density

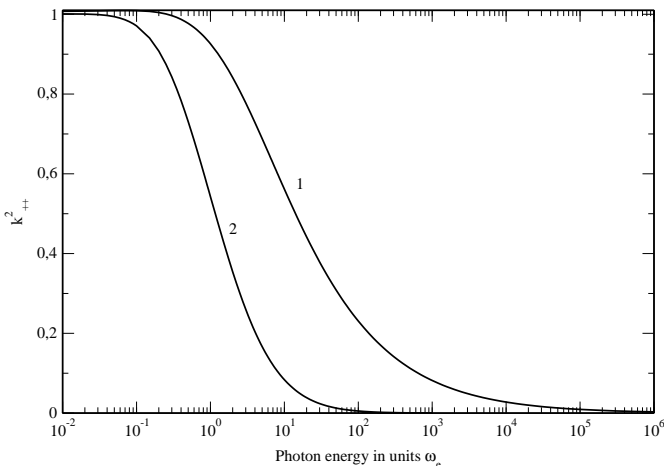


Figure 7: The functions $\text{Re } k_{++}^2$ (curve 2) and $\text{Im } k_{++}^2$ (curve 1) versus the photon energy taken in units ω_e (because of this the curves are universal) for the case when the influence of a medium is taken into account only (Eq.(2.91)). The both curves are normalized to the asymptotics given by Eq.(2.94) in the limit $\omega_F \rightarrow \infty$.

of atoms in the vicinity of axis $n(\boldsymbol{\rho})$ to the mean density n_a is

$$\xi_{ax}(\boldsymbol{\rho}) = \frac{n(\boldsymbol{\rho})}{n_a} = \frac{\exp(-\rho^2/2u_1^2)}{2\pi u_1^2 dn_a}, \quad (2.96)$$

where u_1 is the amplitude of thermal vibrations of atoms, d is the mean distance between atoms which form the axis. This ratio is maximal at $\boldsymbol{\rho} = 0$. For numerical estimates we use for definiteness the tungsten single crystal. For the axis $\langle 111 \rangle$ in W the ratio $\xi_{ax}(0)=370$ at the room temperature ($T = 293$ K) and $\xi_{ax}(0)=1020$ at $T = 77$ K. The effect of multiple scattering becomes strong at characteristic photon energy $\omega_e(n_a) \simeq 11$ TeV and this value is inversely proportional to the density. So we have that $\omega_e(\rho = 0) \simeq 30$ GeV at $T = 293$ K and $\omega_e(\rho = 0) \simeq 11$ GeV at $T = 77$ K. It should be noted that within logarithmic accuracy we neglect by relatively small variation of L_1 due to substitution the screening radius a_s^2 by the value $2u_1^2$.

It is useful to compare these estimates with known threshold energies ω_t at which the probability of pair creation in the field of axis is equal to the probability of the Bethe-Heitler mechanism, see Table 12.1 in [10]. For photon energy $\omega \geq \omega_t$ the process of pair creation in the field of axis dominates. In

W crystal for $\langle 111 \rangle$ axis $\omega_t = 22$ GeV at $T=293$ K and $\omega_t = 13$ GeV at $T=77$ K. It is seen that for these energies the ratio ω/ω_e which characterize the strength the LPM effect is of the order of unity. At $\omega \sim \omega_t$ the maximal value of the parameter $\kappa(\boldsymbol{\varrho})$ which determines the probability of pair creation by a photon in a field is also of the order of unity (at $\varrho \simeq u_1$, see the mentioned Table). So we reach the conclusion that at some energy (for axial orientation of crystal) all the discussed effects are essential simultaneously. For example, to calculate the influence of the field of axis on the polarization tensor one have to average the general formula (2.87) over all values of $\boldsymbol{\varrho}$ (this is integration over $d^2\varrho$ with the weight n_\perp , where $n_\perp = n_a d$ is the density of axis in the perpendicular to them plane).

2.6 An influence of multiple scattering on coherent scattering of photon

Investigation of the coherent photon scattering (the Delbrück scattering) has rather long history which can be found in review (see e.g.[37]). There is a special interest to study the process for heavy elements (the cross section $\propto Z^4$). However, in this case the contributions of higher orders of $Z\alpha$ into the amplitude of photon scattering are very important. This means that one needs the theory which is exact with respect to the parameter $Z\alpha$. The amplitudes of the coherent photon scattering valid for any $Z\alpha$ for high photon energy $\omega \gg m$ and small scattering angle (or small momentum transfer Δ) were calculated by several group of authors (see [38], [39], [40], [41], [42]). In the last paper the process of the coherent photon scattering was considered in frame of the quasiclassical operator method which appears to be very adequate for consideration of this problem.

As in the previous section the amplitude M of the coherent photon scattering in the quasiclassical approximation is described by diagram where the electron-positron pair is created by the initial photon with 4-momentum k_1 (ω, \mathbf{k}_1) and then annihilate into the final photon with 4-momentum k_2 (ω, \mathbf{k}_2), so that the photon momentum transfer is $\Delta = |\mathbf{k}_2 - \mathbf{k}_1|$. For high energy photon $\omega \gg m$ this process occurs over a rather long distance (see Eq.(1.12)).

It is convenient to describe the process of photon scattering in terms of helicity amplitudes. We choose the polarization vectors with helicity λ

$$\begin{aligned} \mathbf{e}_\lambda &= \frac{1}{\sqrt{2}} (\mathbf{e}_1 + i\lambda\mathbf{e}_2), & \mathbf{e}_1 &= \boldsymbol{\nu} = \frac{\boldsymbol{\Delta}}{|\boldsymbol{\Delta}|}, & \mathbf{e}_2 &= \mathbf{n} \times \boldsymbol{\nu}, & \mathbf{n} &= \frac{\mathbf{k}_1}{\omega}, \\ \lambda &= \pm 1, & \mathbf{e}_\lambda \mathbf{e}_\lambda^* &= 1, & \mathbf{e}_\lambda \mathbf{e}_{-\lambda}^* &= 0, & \mathbf{e}_\lambda \times \mathbf{n} &= i\lambda\mathbf{e}_\lambda. \end{aligned} \quad (2.97)$$

There are two independent helicity amplitudes:

$$M_{++} = M_{--}, \quad M_{+-} = M_{-+}, \quad (2.98)$$

where the first subscript is the helicity of the initial photon and the second is the helicity of the final photon. When the initial photons are unpolarized the differential cross section of scattering summed over final photons polarization contains the combination

$$2[|M_{++}|^2 + |M_{+-}|^2]. \quad (2.99)$$

The calculation of the amplitudes of photon scattering on the separate atom appears to be most simple in the case when the screening radius of atom a_s is much smaller than the formation length of process ($a_s \ll \lambda_c \omega / 2m = l_{p,max}$ Eq.(1.11)). The imaginary part of helicity amplitudes in this case can be written in the form [43]

$$\text{Im } M_{\lambda\lambda'} = \frac{4Z^2\alpha^3\omega}{m^2} \int_0^1 dx \int_0^1 dy \mu_{\lambda\lambda'} f_{\lambda\lambda'}, \quad (2.100)$$

where

$$\begin{aligned} \mu_{++} &= 1 - 2x(1-x) + 4x(1-x)y(1-y), & \mu_{+-} &= x(1-x)y^2; \\ f_{++} &= \ln(ma_s) - \frac{2s^2+1}{2s\sqrt{1+s^2}} \ln\left(s + \sqrt{1+s^2}\right) - f(Z\alpha) + \frac{41}{42}, \\ f_{+-} &= 1 - \frac{1}{s\sqrt{1+s^2}} \ln\left(s + \sqrt{1+s^2}\right), & s &= \frac{\Delta a_s}{2}, \end{aligned} \quad (2.101)$$

where the function $f(\xi)$ is defined in Eq.(2.5). The important property of Eq.(2.100) is that the dependence on the screening radius a_s originates in it from the Born approximation. In this approximation in the case of arbitrary screening the radius a_s enters only in the combination

$$\frac{1}{a_s^2} + q_{\parallel}^2, \quad q_{\parallel} = \frac{q_m}{x(1-x)y}, \quad q_m = \frac{m^2}{2\omega}. \quad (2.102)$$

Because of this we can extend Eq.(2.101) on the case of arbitrary screening making the substitution

$$\frac{1}{a_s} \rightarrow \sqrt{q_{\parallel}^2 + a_s^{-2}} \equiv q_{ef}, \quad s = \frac{\Delta}{2q_{ef}} \quad (2.103)$$

In the case $a_s \gg \omega/m^2$ (the screening radius is very large, or in other words we consider the photon scattering in the Coulomb field) we have to substitute in Eq.(2.101)

$$a_s \rightarrow \frac{1}{q_{\parallel}}, \quad s \rightarrow s_c = \frac{\Delta}{2q_{\parallel}} = \frac{\Delta\omega}{m^2} x(1-x)y. \quad (2.104)$$

In the case of the complete screening ($a_s \ll \omega/m^2$) the functions $f_{\lambda\lambda'}$ are independent of x and y and the corresponding integrals are

$$\int_0^1 dx \int_0^1 dy \mu_{++} = \frac{7}{9}, \quad \int_0^1 dx \int_0^1 dy \mu_{+-} = \frac{1}{18}. \quad (2.105)$$

For the scattering amplitudes we have

$$\begin{aligned} \text{Im } M_{++} &= \frac{28Z^2\alpha^3\omega}{9m^2} f_{++}, & \text{Im } M_{+-} &= \frac{2Z^2\alpha^3\omega}{9m^2} f_{+-}, \\ \text{Re } M_{++} &= 0, & \text{Re } M_{+-} &= 0. \end{aligned} \quad (2.106)$$

The real part of amplitudes are calculated using dispersion relations. The photon scattering amplitude in this case for arbitrary value of parameter $a_s m^2/2\omega$ for $\Delta = 0$ was found recently in [41] and for arbitrary Δ in [42].

When a photon is propagating in a medium it also dissociates with probability $\propto \alpha$ into an electron-positron pair. The virtual electron and positron interact with a medium and can scatter on atoms. In this scattering the electron and positron interaction with the Coulomb field in the course of the coherent scattering of photon is involved also. So there is a direct analogue with the LPM effect considered above. However there is the difference: in the LPM effect the particles of electron-positron pair created by a photon are on the mass shell while in the process of the coherent scattering of photon this particles are off the mass shell, but in the high energy region (this is the only region where the influence of the multiple scattering is pronounced) the shift from the mass shell is relatively small. To include this scattering into consideration the amplitude of the coherent scattering of photon should be averaged over all possible trajectories of electron and positron. This operation can be performed with the aid of the distribution function averaged over the atomic positions of scatterer in the medium in the same manner as it is done in Appendix A [43].

The photon scattering amplitudes can be written in the form

$$M_{++} = M_{++}^c + M_{++}^{(1)}, \quad M_{+-} = M_{+-}^c + M_{+-}^{(1)}, \quad (2.107)$$

where M_{++}^c is the main (logarithmic) term and $M_{++}^{(1)}$ is the first correction to the scattering amplitude. The main terms are [43]

$$\begin{aligned}
M_{++}^c &= \frac{\alpha m^2 \omega}{2\pi n_a} \int \frac{d\varepsilon}{\varepsilon \varepsilon'} \Phi_s(\nu_s), \quad M_{+-}^c = 0, \\
\Phi_s(\nu_s) &= s_1 \left(\ln p - \psi \left(p + \frac{1}{2} \right) \right) + s_2 \left(\psi(p) - \ln p + \frac{1}{2p} \right), \\
\nu_s &= 2\sqrt{iq_s}, \quad q_s = QL_s, \quad p = i/(2\nu_s), \\
Q &= \frac{2\pi Z^2 \alpha^2 \varepsilon \varepsilon' n_a}{m^4 \omega}, \quad L_s \equiv L_s(\varrho_c) = \ln \frac{a_{s2}^2}{\lambda_c^2 \varrho_c^2} - F_2 \left(\frac{\beta}{2} \right), \\
F_2(v) &= \frac{2v^2 + 1}{v\sqrt{1+v^2}} \ln \left(v + \sqrt{1+v^2} \right) - 1, \quad \beta = a\Delta, \quad (2.108)
\end{aligned}$$

where a_{s2} is defined in Eq.(2.12) and the coefficients s_1 and s_2 are defined in Eq.(2.42). The structure of the amplitude M_{++}^c is quite similar to the structure of the pair creation probability Eq.(2.43) under influence of the multiple scattering (the fact that the amplitude is expressed in terms of the probability is the common feature of the coherent photon scattering description). This result is not occasional and connected with origin of coherent scattering of photon as a process which is going through dissociation of a photon into electron-positron pair. However the expression for the basic parameter ν_s differs from corresponding expression in Eq.(2.43).

The first corrections to the amplitudes are defined by

$$\begin{aligned}
M_{++}^{(1)} &= -\frac{\alpha m^2 \omega}{4\pi n_a L_s} \int \frac{d\varepsilon}{\varepsilon \varepsilon'} F_s(\nu_s), \quad M_{+-}^{(1)} = \frac{\alpha m^2 \omega}{4\pi n_a L_s} F_1 \left(\frac{\beta}{2} \right) \int \frac{d\varepsilon}{\varepsilon \varepsilon'} F_3(\nu_s), \\
F_s(\nu_s) &= \int_0^\infty \frac{dz e^{-it}}{\sinh^2 z} [s_1 f_1(z) - 2is_2 f_2(z)], \quad F_1(v) = 1 - \frac{\ln(v + \sqrt{1+v^2})}{v\sqrt{1+v^2}}, \\
F_3(\nu_s) &= i\nu_s s_3 \int_0^\infty \frac{dz e^{-it}}{\sinh^3 z} g(z) = \frac{s_3}{2} \left[1 + \frac{1}{2p} - p \zeta(2, p) \right] \quad (2.109)
\end{aligned}$$

here the functions $f_1(z)$ and $f_2(z)$ are defined in Eq.(2.45), the coefficient s_3 is defined in Eq.(2.89), $\zeta(s, a)$ is the generalized Riemann zeta function. Use of the given representations of functions $F_3(\nu_s)$ and $G(z)$ in $f_1(z)$ simplifies the numerical calculation. The functions $F_1(z)$ and $F_2(z)$ in Eqs.(2.108), (2.109) encountered in the radiation theory.

In the region of the weak effect of scattering ($|\nu_s| \ll 1$, $\varrho_c = 1$) we obtain

$$M_{++} = M_{++}^c + M_{++}^{(1)} = i \frac{14Z^2\alpha^3\omega}{9m^2} \left[L_{s1} \left(1 + i \frac{59\omega}{175\omega_e} \frac{L_{s1}}{L_1} - \frac{3312}{2401} \left(\frac{\omega}{\omega_e} \frac{L_{s1}}{L_1} \right)^2 \right) - \frac{1}{21} \right], \quad (2.110)$$

$$M_{+-} = M_{+-}^{(1)} = i \frac{2Z^2\alpha^3\omega}{9m^2} F_1 \left(\frac{\beta}{2} \right) \left(1 + i \frac{16\omega}{25\omega_e} \frac{L_{s1}}{L_1} - \frac{384}{245} \left(\frac{\omega}{\omega_e} \frac{L_{s1}}{L_1} \right)^2 \right),$$

here

$$L_{s1} - \frac{1}{21} = 2 \left[\ln \frac{a_s}{\lambda_c} - \frac{1}{2} \left(F_2 \left(\frac{\Delta a_s}{2} \right) + 1 \right) - f(Z\alpha) + \frac{41}{42} \right], \quad (2.111)$$

ω_e is defined in Eq.(2.48) and L_1 is defined in Eq.(2.12). The characteristic energy ω_e encountered in analysis of influence of the multiple scattering on the probability of pair photoproduction [21], in gold $\omega_e=10.5$ TeV. The amplitudes Eq.(2.111) coincide with the formulas in absence of multiple scattering if we neglect the terms $\propto \omega/\omega_e$ and $(\omega/\omega_e)^2$. The terms $\propto \omega/\omega_e$ define the appearing real part of the scattering amplitudes while the terms $\propto (\omega/\omega_e)^2$ are the corrections to the imaginary part.

In the region where the effect of scattering is strong ($|\nu_s| \gg 1$) we obtain

$$\begin{aligned} M_{++} &= (i-1) \frac{3\pi Z^2\alpha^3\omega}{2\sqrt{2}\Delta_s^2} \sqrt{L_{s3}} \left[1 - \frac{1}{4L_{s3}} \left(2C + \frac{1}{3} + i\frac{\pi}{2} \right) \right], \\ M_{+-} &\simeq (i-1) \frac{\pi Z^2\alpha^3\omega}{8\sqrt{2}\Delta_s^2} \frac{1}{\sqrt{L_{s3}}} F_1 \left(\frac{\beta}{2} \right), \quad L_{s3} = L_{s2} + \frac{1}{2} \ln L_{s2}, \\ L_{s2} &= L_{s1} + \frac{1}{2} \ln \frac{\omega}{\omega_e} = 2 \ln(a_s \Delta_s) + 1 - F_2 \left(\frac{\Delta a_s}{2} \right) - 2f(Z\alpha), \\ \Delta_s^4 &= 2\pi Z^2\alpha^2\omega n_a, \quad \nu_s^2 = i \frac{\omega}{\omega_e} \frac{4\varepsilon\varepsilon'}{\omega^2} \left(L_{s3} + \frac{1}{2} \ln \frac{4\varepsilon\varepsilon'}{\omega^2} \right). \end{aligned} \quad (2.112)$$

the real and imaginary parts of the amplitudes are equal (if we neglect the term $\propto 1/L_{s3}$ in M_{++}). Moreover the amplitudes Eq.(2.112) don't depend on the electron mass m . In place of it we have the value Δ_s .

The influence of a medium on the process of the coherent photon scattering illustrated in Fig.8a and b, where $\text{Im } M_{++}$ and $\text{Re } M_{++}$ as well as $\text{Im } M_{+-}$ and $\text{Re } M_{+-}$ are given as a function of photon energy ω in gold.

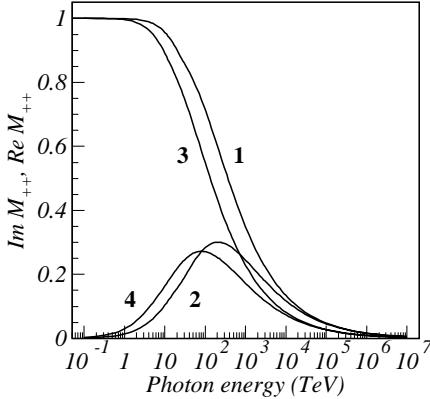


Figure 8: (a) The amplitude M_{++} of the coherent photon scattering in gold under influence of the multiple scattering at the different momentum transfer to the photon Δ in terms of the amplitude $\text{Im}M_{++}$ (2.106) calculated for the screened Coulomb potential.

Curve 1 is $\text{Im}M_{++}$ for $\Delta = 0.4435 m$.
 Curve 2 is $\text{Re}M_{++}$ for $\Delta = 0.4435 m$.
 Curve 3 is $\text{Im}M_{++}$ for $\Delta = 0.0387 m$.
 Curve 4 is $\text{Re}M_{++}$ for $\Delta = 0.0387 m$.

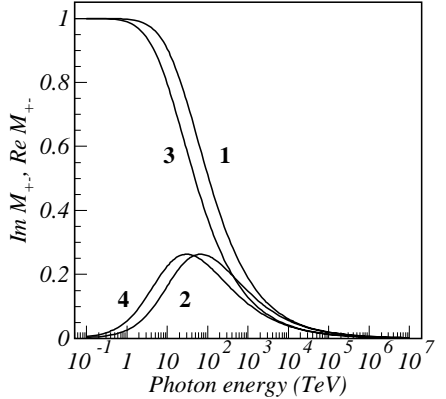


Figure 8: (b) The same as in Fig.1 but for the amplitude M_{+-} in terms of the amplitude $\text{Im}M_{+-}$ (2.106) calculated for the screened Coulomb potential.

This influence is due to the multiple scattering of electron and positron of the virtual pair on the formation length of the process (see Eqs.(1.12) and (1.13))

$$l_f = \frac{\omega}{2(q_s^2 + m^2 + \Delta^2)}. \quad (2.113)$$

In the region $\Delta^2 \ll q_s^2 + m^2$ this formation length is independent of Δ and its value coincides practically with the formation length of pair creation by a photon l_c considered in the previous subsection. There is some difference connected with the logarithmic dependence of ν_s^2 value on Δ^2 :

$$|\nu_s^2| = \frac{q_s^2}{m^2} = \frac{4\pi Z^2 \alpha^2}{m^2} n_a l_f \int_{q_{min}^2}^{q_{max}^2} \frac{dq^2}{q^2} \quad (2.114)$$

where $q_{max}^2 = m^2 + q_s^2$ and $q_{min}^2 = \Delta^2 + a_s^{-2}$, a_s is the screening radius of atom (1.13). This defines the weak (logarithmic) dependence of $\text{Im}M_{++}$ on Δ in the region $\Delta < \sqrt{q_s^2 + m^2}$. This can be seen in Fig.8a where the curves 1 and 3 represent behavior of $\text{Im} M_{++}$ for $\Delta=0.4435 m$ and $\Delta=0.0387 m$ respectively. For lower value of Δ the minimal momentum transfer q_{min} (1.13) diminishes thereby the interval of contributing the multiple scattering angles increases, so the multiple scattering affects the photon scattering amplitude at a lower energy (and smaller formation length). Because of this the curve 3 is shifted to the left respect the curve 1. Note that the curve 3 ($\Delta^{-1} \sim a_{s2}$) is very similar to the curve 2 in Fig.4 which represents the behavior of the probability of pair photoproduction in gold vs photon energy.

The new property of influence of a medium is the appearance of the real part of the coherent photon scattering amplitudes at high energy ω . In the region $\omega \ll \omega_e$ the value of $\text{Re}M$ is small accordingly Eq.(2.111). In the asymptotic region $\omega \gg \omega_e$ we have $-\text{Re} M = \text{Im} M$ according to Eq.(2.112). This property is seen clearly in Figs.8a and b. So the value of $-\text{Re} M$ is small at low and very high energies of photon. At intermediate energies the value of $-\text{Re} M$ have the maximum at $\omega \simeq 220$ TeV for $\Delta = 0.4435 m$ and at $\omega \simeq 80$ TeV for $\Delta = 0.0387 m$. In Fig.8b the same curves are shown for amplitude M_{+-} . These curves are very similar to curves in Fig.8a. The curves in both figures are normalized to imaginary part of the corresponding amplitude in the absence of the multiple scattering. The ratio these imaginary parts $r = \text{Im}M_{+-}/\text{Im}M_{++}$ is very small: it is $r = 0.04435$ for $\Delta = 0.4435 m$ and $r = 0.003018$ for $\Delta = 0.0387 m$.

2.7 The polarization of a medium and the bremsstrahlung process

When one considers bremsstrahlung of enough soft photons $\omega \leq \omega_0\gamma$ (see Eq.(1.4)), one has to take into account the effect of a polarization of the medium. This effect diminishes the formation length (see Eq.(1.5)) as well as the probability of radiation (see [4], the qualitative discussion may be found in [6]). For analysis we use the general expression for the probability of radiation, see Eq.(A.1), Appendix A. The factor in front of exponent in this expression (see Eq.(A.2)) contains two terms A and \mathbf{B} , the term A is not changed and the term \mathbf{B} contains combination

$$\mathbf{v} - \frac{\mathbf{k}}{\omega} \simeq \boldsymbol{\vartheta} + \mathbf{n} \frac{\kappa_0^2}{2\gamma^2}, \quad \kappa_0 = \frac{\omega_p}{\omega}, \quad \omega_p = \omega_0\gamma, \quad (2.115)$$

and its dependence on κ_0 (term of the order $1/\gamma^2$) may be neglected also. So, the dependence on ω_0 manifests itself in the exponent of Eq.(A.1), and respectively in the exponent of (A.20) only:

$$a \rightarrow 2 \frac{\omega \varepsilon}{\varepsilon - \omega} \left(1 - \frac{k}{\omega} v - \frac{\omega_0^2}{2\varepsilon \omega} \right) \simeq a \kappa \equiv \tilde{a}, \quad \kappa \equiv 1 + \kappa_0'^2, \quad \kappa_0'^2 = \frac{\varepsilon'}{\varepsilon} \kappa_0^2. \quad (2.116)$$

where the term with ω_0^2 arises in the case of virtual photon: $k^2 \equiv k_\mu k^\mu \neq 0$. Performing the substitution $a \rightarrow \tilde{a}$ in Eq.(2.1) we obtain for the potential (see Eqs.(2.1) (2.3), (2.4), (2.12))

$$\begin{aligned} V(\underline{\varrho}) &\rightarrow \tilde{V}(\tilde{\varrho}) = \tilde{Q} \tilde{\varrho}^2 \left(L \left(\frac{\tilde{\varrho}}{2\sqrt{\kappa}} \right) - 2C \right) = \tilde{V}_c(\tilde{\varrho}) + \tilde{v}(\tilde{\varrho}), \quad \tilde{\varrho} = |\tilde{\underline{\varrho}}| = \varrho \sqrt{\kappa}, \\ \tilde{V}_c(\tilde{\varrho}) &= \tilde{q} \tilde{\varrho}^2, \quad \tilde{q} = \tilde{Q} \tilde{L}(\tilde{\varrho}_c), \quad \tilde{Q} = \frac{Q}{\kappa^2}, \quad \tilde{L}(\tilde{\varrho}_c) = \ln \frac{\kappa}{\gamma^2 \vartheta_2^2 \tilde{\varrho}_c^2}, \\ \tilde{v}(\tilde{\varrho}) &= -\frac{\tilde{q} \tilde{\varrho}^2}{\tilde{L}} \left(2C + \ln \frac{\tilde{\varrho}^2}{4\tilde{\varrho}_c^2} \right). \end{aligned} \quad (2.117)$$

The substitution Eq.(2.116) in the expression for the probability of radiation Eq.(2.2) gives

$$R_1 \rightarrow R_1, \quad R_2 \rightarrow R_2 \kappa \equiv \tilde{R}_2. \quad (2.118)$$

The value of the parameter $\tilde{\varrho}_c$ in (2.117) is determined by equation (compare with Eqs.(2.10), (2.25))

$$4\tilde{\varrho}_c^4 \tilde{Q} \tilde{L}(\tilde{\varrho}_c) = 1, \quad \text{for} \quad 4\tilde{Q} \tilde{L}(1) \geq 1. \quad (2.119)$$

In the opposite case $\tilde{\varrho}_c = 1$ and this is possible in two intervals of the photon energy ω :

1. for $\kappa_0 \ll 1$ when the multiple scattering and effects of the polarization of a medium are weak;
2. for $\kappa_0 \gg 1$ when effects of the polarization of a medium become stronger then effects of the multiple scattering ($\nu_0 < \kappa$).

In an intermediate region we substitute $\tilde{\varrho}_c^2 \rightarrow \varrho_c^2 \kappa$ in Eq.(2.119). After it we obtain the equation for ϱ_c which coincides with Eq.(2.10), see also Eq.(2.25):

$$\frac{1}{\varrho_c^4} = \nu_0^2(\varrho_c), \quad \nu_0^2(\varrho_c) = 4QL(\varrho_c). \quad (2.120)$$

Thus, for $\tilde{\varrho}_c < 1$ we have

$$\tilde{\nu}_0 = \sqrt{4\tilde{Q}\tilde{L}(\tilde{\varrho}_c)} = \frac{1}{\tilde{\varrho}_c^2} = \frac{1}{\varrho_c^2\kappa} = \frac{\nu_0}{\kappa}, \quad \tilde{L}(\tilde{\varrho}_c) = L(\varrho_c), \quad (2.121)$$

while for $\tilde{\nu}_0 < 1$ we have

$$\tilde{\nu}_0 = \sqrt{4\tilde{Q}\tilde{L}(1)} = \frac{2}{\kappa}\sqrt{\tilde{Q}}\ln\left(\frac{a_{s2}^2\kappa}{\lambda_c^2}\right). \quad (2.122)$$

The spectral distribution of the probability of radiation Eq.(2.29) with allowance for the polarization of a medium have the form

$$\frac{dW}{d\omega} = \frac{\alpha}{2\pi\gamma^2}\text{Im}\left[\tilde{\Phi}(\tilde{\nu}) - \frac{1}{2\tilde{L}(\tilde{\varrho}_c)}\tilde{F}(\tilde{\nu})\right], \quad (2.123)$$

where

$$\tilde{\Phi}(R_1, R_2) = \Phi(R_1, \tilde{R}_2), \quad \tilde{F}(R_1, R_2) = F(R_1, \tilde{R}_2),$$

In the case $\nu_0 \ll \kappa_0^2$, the characteristic momentum transfer in the used units (ζ_c) are defined by value $\kappa_0^2(\tilde{\varrho}_c^2 = 1)$, one can use asymptotic expansion Eq.(2.28) and we have for the spectral distribution of the probability of radiation

$$\frac{dW}{d\omega} = \frac{16}{3}\frac{Z^2\alpha^3n_a}{m^2\omega\kappa_0^2}\left(L_p + \frac{1}{12} - f(Z\alpha)\right) = \frac{4}{3\pi}\frac{Z\alpha^2\omega}{m\gamma^2}\left(L_p + \frac{1}{12} - f(Z\alpha)\right), \quad (2.124)$$

where $f(Z\alpha)$ is defined in (2.5), $L_p = \ln(183Z^{-1/3}\kappa_0)$. The results obtained agree with given in [4] where calculations are fulfilled within a logarithmic accuracy and without Coulomb corrections. It is seen that the dependence of spectral distribution on photon energy ($\omega d\omega$) differs essentially from the Bethe-Maximon one ($d\omega/\omega$), and the probability is independent on the density n .

3 Impact of a medium for a target of finite thickness

3.1 General consideration

In the case under consideration probability of radiation is defined not only by the relative time $\tau = t_2 - t_1$ as in Sec. 2.1. The used radiation theory

is formulated in terms of two times (see Eqs.(A.1) - (A.3) of Appendix A). Proceeding from this formulation we can obtain more general expression for the radiation probability. With allowance for the polarization of a medium we have for the spectral distribution of the probability of radiation (compare with Eq.(2.2))

$$\begin{aligned} \frac{dw}{d\omega} &= \frac{4\alpha}{\omega} \text{Re} \int_{-\infty}^{\infty} dt_2 \int_{-\infty}^{t_2} dt_1 \exp \left(-i \int_{t_1}^{t_2} \mu(t) dt \right) \\ &\times [r_1 \varphi_0(0, t_2, t_1) - ir_2 \nabla \varphi(0, t_2, t_1)], \end{aligned} \quad (3.1)$$

where

$$\mu(t) = 1 + \kappa_0'^2 g(t), \quad \kappa_0'^2 = \frac{\varepsilon'}{\varepsilon} \kappa_0^2, \quad r_1 = \frac{\omega^2}{\varepsilon^2}, \quad r_2 = 1 + \frac{\varepsilon'^2}{\varepsilon^2}, \quad (3.2)$$

here the function $g(t)$ describes the density of atoms on the projectile trajectory, κ_0 is defined in Eq.(2.115). The functions $\varphi_\mu(\mathbf{q}, t_2, t_1)$, ($\varphi_\mu = (\varphi_0, \boldsymbol{\varphi})$) satisfy the equation (2.3), but now the potential V depends on time

$$\begin{aligned} i \frac{\partial \varphi_\mu}{\partial t} &= H(t) \varphi_\mu, \quad H(t) = \mathbf{p}^2 - iV(\mathbf{q})g(t); \\ \varphi_0(\mathbf{q}, t_1, t_1) &= \delta(\mathbf{q}), \quad \boldsymbol{\varphi}(\mathbf{q}, t_1, t_1) = \mathbf{p} \delta(\mathbf{q}). \end{aligned} \quad (3.3)$$

So, the functions $\kappa_0'^2$ and $V(\mathbf{q})$ in Eqs.(3.2) and (3.3) depend now on mean density of atoms on the projectile trajectory while the function $g(t)$ describes the modulation of the density as a function of time

$$g(t) = \frac{n_a(t)}{\bar{n}}$$

Using an operator form of a solution of Eq.(3.3) (compare with Eq.(2.6)) we can present the probability Eq.(3.1) in the form

$$\begin{aligned} \frac{dw}{d\omega} &= \frac{4\alpha}{\omega} \text{Re} \int_{-\infty}^{\infty} dt_2 \int_{-\infty}^{t_2} dt_1 \exp \left(-i \int_{t_1}^{t_2} \mu(t) dt \right) \\ &\times \langle 0 | r_1 S(t_2, t_1) + r_2 \mathbf{p} S(t_2, t_1) \mathbf{p} | 0 \rangle, \quad S(t_2, t_1) = \mathbb{T} \exp \left[-i \int_{t_1}^{t_2} H(t) dt \right], \end{aligned} \quad (3.4)$$

where the symbol \mathbb{T} means the chronological product. Note, that in Eqs.(3.1) and (3.4) it is implied that a subtraction is made at $V = 0$, $\mu(t) = 1$.

3.2 Boundary effects for a thick target

For the homogeneous target of finite thickness l the radiation process in a medium depends on interrelation between l and formation length l_f Eq.(1.5). In the case when $l \gg l_f$ we have the thick target where radiation on the boundary should be incorporated. In the case when $l \ll l_f$ we have the thin target where the mechanism of radiation is changed essentially and in the case when $l \sim l_f$ we have intermediate thickness. Integrals over time in Eq.(3.5) we present as integrals over four domains:

1. $t_1 \leq 0, 0 \leq t_2 \leq T$;
2. $0 \leq t_1 \leq T, 0 \leq t_2 \leq T$;
3. $0 \leq t_1 \leq T, t_2 \geq T$;
4. $t_1 \leq 0, t_2 \geq T$;

where

$$\mu(t) = \vartheta(-t) + \vartheta(t - T) + \kappa \vartheta(t) \vartheta(T - t), \quad T = \frac{l}{l_{f0}} = \frac{l \omega m^2}{2 \varepsilon \varepsilon'}, \quad \kappa = 1 + \kappa_0'^2. \quad (3.5)$$

In two more domains $t_{1,2} \leq 0$ and $t_{1,2} \geq T$ an electron is moving entirely free and there is no radiation. We consider in this subsection the case, when the thickness of a target l is much larger than formation length l_f Eq.(1.5) or $(\nu_0 + \kappa)T \gg 1$. In this case domain 4. doesn't contribute. The contributions of other domains are

$$\begin{aligned} I_1 &\simeq \int_{-\infty}^0 dt_1 \int_0^\infty dt_2 \exp(i(t_1 - \kappa t_2)) \exp(-iHt_2) \exp(iH_0 t_1) \\ &= -\frac{1}{H + \kappa} \frac{1}{H_0 + 1}, \\ I_2 &= \int_0^T dt_2 \int_0^{t_2} dt_1 \exp(-i(H + \kappa)(t_2 - t_1)) \\ &\simeq T \int_0^\infty d\tau \exp(-i(H + \kappa)\tau) - \int_0^\infty \tau d\tau \exp(-i(H + \kappa)\tau) \\ &= -i \frac{T}{H + \kappa} + \frac{1}{(H + \kappa)^2}, \quad I_3 \simeq -\frac{1}{H_0 + 1} \frac{1}{H + \kappa}, \end{aligned} \quad (3.6)$$

where $H_0 = \mathbf{p}^2$. The term in I_2 : $-iT/(H + \kappa)$ describes the probability of radiation considered in previous subsections. All other terms define the

probability of radiation of boundary photons ¹. So, making the mentioned subtraction we have for the spectral distribution of the probability of radiation of boundary photons

$$\begin{aligned} \frac{dw_b}{d\omega} &= \frac{4\alpha}{\omega} \text{Re} \langle 0 | r_1 M + r_2 \mathbf{p} M \mathbf{p} | 0 \rangle, \\ M &= \left(\frac{1}{H + \kappa} - \frac{1}{\mathbf{p}^2 + 1} \right)^2 \end{aligned} \quad (3.7)$$

In the case when both the LPM effect and effect of polarization of a medium are weak one can decompose combination in M in Eq.(3.7)

$$\frac{1}{H + \kappa} - \frac{1}{\mathbf{p}^2 + 1} \simeq \frac{1}{\mathbf{p}^2 + 1} (iV - \kappa_0'^2) \frac{1}{\mathbf{p}^2 + 1}. \quad (3.8)$$

Using this decomposition one can find an estimate for probability of radiation

$$\frac{dw_b}{d\omega} \simeq \frac{\alpha}{\pi} \left(-c_1 \nu_1^4 + c_2 \kappa_0'^4 \right), \quad (3.9)$$

where c_1 and c_2 are some positive coefficients. So, in the case under consideration the probability of boundary photon radiation is negligible small.

In the case when $\nu_1 \ll \kappa_0'^2 \geq 1$ one can omit the potential V in Eq.(3.8), so that the effect of polarization of a medium is essential, then

$$\begin{aligned} \frac{dw_b}{d\omega} &= \frac{4\alpha}{\omega(2\pi)^2} \int \langle 0 | r_1 M + r_2 \mathbf{p} M \mathbf{p} | 0 \rangle d^2 p \\ &= \frac{\alpha}{\pi\omega} \left\{ r_1 \left(1 + \frac{1}{\kappa} - \frac{2}{\kappa - 1} \ln \kappa \right) + r_2 \left[\left(1 + \frac{2}{\kappa - 1} \right) \ln \kappa - 2 \right] \right\}. \end{aligned} \quad (3.10)$$

This result is the quantum generalization of the transition radiation probability [58].

Let us estimate the probability of radiation Eq.(3.7) in the case when both the LPM effect and effect of polarization of a medium are strong ($\nu_0 + \kappa \gg 1$). In this case we can neglect the term $1/(H + \kappa)$ in the term $\propto r_1$ in M Eq.(3.7). In the term $\propto r_2$ one can put $V(\mathbf{q}) \simeq \nu_0^2 \mathbf{q}^2 \sim \nu_0^2 / \mathbf{p}^2$ so that

$$\int \mathbf{p}^2 \left(\frac{1}{H + \kappa} - \frac{1}{\mathbf{p}^2 + 1} \right)^2 d^2 p \simeq \pi \ln(\nu_0 + \kappa). \quad (3.11)$$

¹Radiation of boundary photons in an inhomogeneous electromagnetic field was considered in [48].

Substituting these results into Eq.(3.7) we have up to logarithmic accuracy

$$\frac{dw_b}{d\omega} = \frac{\alpha}{\omega\pi} [r_1 + r_2 \ln(\nu_0 + \kappa)]. \quad (3.12)$$

In the case $\nu_0 \ll \kappa$ this result agrees with Eq.(3.11). The case $\nu_0 \geq \kappa$ will be considered below (see Eqs.(3.36) and (3.37)).

3.3 A thin target

We consider now a situation when the formation length of radiation is much larger than the thickness l of a target [17]

$$l \ll l_f = \frac{l_{f0}}{\zeta}, \quad \zeta = 1 + \gamma^2 \vartheta^2, \quad T = \frac{l}{l_{f0}} \ll \frac{1}{\zeta}, \quad (3.13)$$

where l_f , l_{f0} are defined in Eqs.(1.5), (1.6). In the case $\kappa T \ll 1$ the radiated photon is propagating in the vacuum and one can neglect the polarization of a medium. The spectral distribution of the probability of radiation from a thin target is

$$\frac{dw_{th}}{d\omega} = \frac{\alpha}{\pi^2 \omega} \int d^2 \varrho [r_1 K_0^2(\varrho) + r_2 K_1^2(\varrho)] (1 - \exp(-V(\varrho)T)), \quad (3.14)$$

where $V(\varrho)$ is defined in Eqs.(2.3), (2.4), K_n is the modified Bessel function. If $V(\varrho = 1)T \ll 1$ one can expand the exponent (the contribution of the region $\varrho \gg 1$ is exponentially damped because in this region $K_{0,1}(\varrho) \propto \exp(-\varrho)$). In the first order over VT using the explicit expression for the potential Eq.(2.4) one obtains in this case the Bethe-Maximon formula (with the Coulomb corrections) Eq.(2.29).

In the opposite case when the multiple scattering of a particle traversing a target is strong ($V(\varrho = 1)T \gg 1$, the mean square of multiple scattering angle $\vartheta_s^2 \gg 1/\gamma^2$). We present the function $V(\varrho)T$ (see Eqs.(2.3), (2.4) and (2.14) as

$$\begin{aligned} V(\varrho)T &= \frac{\pi Z^2 \alpha^2 n_a l}{m^2} \varrho^2 \left(\ln \frac{4a_s^2}{\lambda_c^2 \varrho^2} - 2C \right) \\ &= A \varrho^2 \ln \frac{\chi_t}{\varrho^2} = A \varrho^2 \left(\ln \frac{\chi_t}{\varrho_t^2} - \ln \frac{\varrho^2}{\varrho_t^2} \right) = k \varrho^2 \left(1 - \frac{1}{L_t} \ln \frac{\varrho^2}{\varrho_t^2} \right); \\ A \varrho_t^2 \ln \frac{\chi_t}{\varrho_t^2} &= 1, \quad L_t = \ln \frac{\chi_t}{\varrho_t^2} = \ln \frac{4a_s^2}{\lambda_c^2 \varrho_t^2} - 2C, \end{aligned} \quad (3.15)$$

where ϱ_t is the lower boundary of values contributing into the integral over ϱ . Substituting this expression into (3.14) we have the integral

$$2\pi \int_0^\infty \varrho d\varrho K_1^2(\varrho) \left\{ 1 - \exp \left[-k\varrho^2 \left(1 - \frac{1}{L_t} \ln \frac{\varrho^2}{\varrho_t^2} \right) \right] \right\} \equiv \pi J. \quad (3.16)$$

In this integral we expand the exponent in the integrand over $1/L_t$ keeping the first term of the expansion. It is convenient to substitute $z = k\varrho^2$. We find

$$\begin{aligned} J_1 &= \frac{1}{k} \int_0^\infty \left[K_0 \left(\sqrt{\frac{z}{k}} \right) K_2 \left(\sqrt{\frac{z}{k}} \right) - K_1^2 \left(\sqrt{\frac{z}{k}} \right) \right] \exp(-z) z dz, \\ J_2 &= -\frac{1}{kL_t} \int_0^\infty K_1^2 \left(\sqrt{\frac{z}{k}} \right) \exp(-z) \ln z z dz, \quad J = J_1 + J_2. \end{aligned} \quad (3.17)$$

Expanding the modified Bessel functions $K_n(x)$ at $x \ll 1$ and taking the integrals in the last expression we have

$$\begin{aligned} J &= J_1 + J_2 = \left(1 + \frac{1}{2k} \right) (\ln 4k - C) + \frac{1}{2k} - 1 + \frac{C}{L_t}, \\ k &= \frac{\pi Z^2 \alpha^2}{m^2} n_a l L_t. \end{aligned} \quad (3.18)$$

In the term with K_0^2 in Eq.(3.14) the region $\varrho \sim 1$ contributes. So we have

$$J_3 = 2 \int_0^\infty K_0^2(\varrho) (1 - \exp(-VT)) \varrho d\varrho \simeq 2 \int_0^\infty K_0^2(\varrho) \varrho d\varrho = 1. \quad (3.19)$$

Substituting found J and J_3 into Eq.(3.14) we obtain for the spectral distribution of the probability of radiation in a thin target at conditions of the strong multiple scattering

$$\frac{dw_{th}}{d\omega} = \frac{\alpha}{\pi\omega} (r_1 + r_2 J). \quad (3.20)$$

The logarithmic term in this formula is well known in theory of the collinear photons radiation at scattering of a radiating particle on angle much larger than characteristic angles of radiation $\sim 1/\gamma$. It is described with logarithmic accuracy in a quasi-real electron approximation (see [50], Appendix B2).

The formula (3.14) presents the probability of radiation in the case when the formation length $l_f \gg l$. It is known, see e.g. [8], that in this case a process of scattering of a particle is independent of a radiation process and a

differential probability of radiation at scattering with the momentum transfer \mathbf{q} can be presented in the form

$$dW_\gamma = dw_s(\mathbf{q})dw_r(\mathbf{q}, \mathbf{k}), \quad (3.21)$$

where $dw_s(\mathbf{q})$ is the differential probability of scattering with the momentum transfer \mathbf{q} which depends on properties of a target. The function $dw_r(\mathbf{q}, \mathbf{k})$ is the probability of radiation of a photon with a momentum \mathbf{k} when an emitting electron acquires the momentum transfer \mathbf{q} . This probability has a universal form which is independent of properties of a target. For an electron traversing an amorphous medium this fact is reflected in Eq.(3.14). Indeed, passing on to a momentum space we have

$$\begin{aligned} dw_r(\mathbf{q}, \mathbf{k}) &= \frac{\alpha d\omega}{\pi^2 \omega} \int d^2 \varrho [r_1 K_0^2(\varrho) + r_2 K_1^2(\varrho)] (1 - \exp(-i\mathbf{q}\boldsymbol{\varrho})) \\ &= \frac{\alpha d\omega}{\pi \omega} \left[r_1 F_1\left(\frac{q}{2}\right) + r_2 F_2\left(\frac{q}{2}\right) \right], \end{aligned} \quad (3.22)$$

where the functions $F_1(z)$ and $F_2(z)$ are defined in Eqs.(2.109) and (2.108). Remind that q is measured in electron mass. The probability of radiation in this form was found in [52]. For a differential probability of scattering (here we consider the multiple scattering) there is a known formula (cf. Eqs.(A.13), (A.18), (2.3) and (2.4))

$$\begin{aligned} dw_s(\mathbf{q}) &= F_s(\mathbf{q})d^2 q, \quad F_s(\mathbf{q}) = \frac{1}{(2\pi)^2} \int d^2 \varrho \exp(-i\mathbf{q}\boldsymbol{\varrho}) \exp(-V_s(\varrho)l), \\ V_s(\varrho) &= n_a \int d^2 q (1 - \exp(-i\mathbf{q}\boldsymbol{\varrho})) \sigma(\mathbf{q}), \end{aligned} \quad (3.23)$$

where $\sigma(\mathbf{q})$ is the cross section of single scattering.

The formula (3.23) is the exact solution of the kinetic equation for the pure scattering problem (without radiation). Let us consider scattering of relativistic electrons in the case when scattering angles $\vartheta_s \ll 1$ and the condition $\vartheta_s \gg \vartheta_1 = \frac{1}{a_s \varepsilon}$ is fulfilled (the angle ϑ_1 is defined in Appendix A, Eq.(A.13)). For combination $V_s(\varrho)l$ in Eq.(3.23) one can use Eq.(3.15). Let us remind that the impact parameters ϱ measured in the Compton wavelengths λ_c , which is conjugate to space of the transverse momentum transfers

q measured in the electron mass m .

$$\begin{aligned}
 V_s(\varrho)l &\simeq V(\varrho)T = \frac{\varrho^2}{\varrho_t^2} - \frac{1}{L_t} \frac{\varrho^2}{\varrho_t^2} \ln \frac{\varrho^2}{\varrho_t^2}, \\
 L_t &= l_t + \ln(L_t), \quad \frac{1}{\varrho_t^2} = AL_t \\
 l_t &= \ln(A\chi_t) = \ln(4\pi Z^2 \alpha^2 n_a l_a^2) + 1 - 2C - 2f(Z\alpha). \quad (3.24)
 \end{aligned}$$

Substituting Eq.(3.24) into Eq.(3.23) and passing to the variable $\nu = q\varrho_t/2$ we obtain

$$\begin{aligned}
 dw_s(\nu) &= f(\nu)\nu d\nu, \\
 f(\nu) &= \int_0^\infty u J_0(\nu u) \exp\left(-\frac{u^2}{4} + \frac{u^2}{4L_t} \ln \frac{u^2}{4}\right) du. \quad (3.25)
 \end{aligned}$$

Solution of scattering problem in angular variables is given in the end of Appendix A (see Eq.(A.24)).

On the adopted assumptions ($\vartheta_s^2/\vartheta_1^2 = A\chi_t \gg 1$, $l_t \gg 1$, $L_t \gg 1$) one can expand in Eq.(3.25) over powers of $1/L_t$:

$$\begin{aligned}
 f(\nu) &= \sum_{n=0}^{\infty} \frac{1}{n!} \int_0^\infty u J_0(\nu u) \exp\left(-\frac{u^2}{4}\right) \left(\frac{u^2}{4L_t} \ln \frac{u^2}{4}\right)^n du \\
 &= f^{(0)}(\nu) + \frac{1}{L_t} f^{(1)}(\nu) + \frac{1}{L_t^2} f^{(2)}(\nu) + \dots \quad (3.26)
 \end{aligned}$$

It is instructive to compare these results with the classical paper Bethe on multiple scattering [44]. The obtained formula Eq.(3.26) is consistent with Eq.(25) of [44]. However there is difference in evaluation of the Coulomb corrections entering into the expression for the function l_t Eq.(3.24) (see e^b in Eq.(22) in [44]). In the last formula in [44] the Coulomb correction is contained in the form $-\ln(1 + 3.34Z^2\alpha^2)$ (it should be noted that a) Bethe was referring to the numerical coefficient at $(Z\alpha)^2$ calculated by Molière [45] as "only approximate"; b) the Coulomb corrections to the cross sections of bremsstrahlung and pair creation by photon which contain the famous function $f(Z\alpha)$ defined in Eq.(2.5) were found after publication of [44]) while in Eq.(3.24) enters different correction: $-2f(Z\alpha)$. To compare these results numerically let us consider case $Z\alpha \ll 1$. In this case the correction in [44] is $-3.34Z^2\alpha^2$ while for Eq.(3.24) we have the correction $-2\zeta(3)Z^2\alpha^2 = -2.404Z^2\alpha^2$. Besides, for accounting the inelastic scattering on electrons the use of Eq.(2.34) for the potential $V_s(\varrho)$ gives more accurate results than the simple substitution $Z^2 \rightarrow Z(Z+1)$ done in [44].

The main term of the expansion in Eq.(3.26) has the Gaussian form

$$f^{(0)}(\nu) = 2e^{-\nu^2} \quad (3.27)$$

The next terms contains the corrections to the Gaussian form. They were analyzed in detail in [44].

Using the formula (3.22) one can easily obtain to within logarithmic accuracy expressions (3.20),(3.12). Both a radiation of boundary photons and a radiation in a thin target may be considered as a radiation of collinear photons (see e.g. [50]) in the case when an emitting particle deviates at large angle ($\vartheta_s \gg 1/\gamma, q \gg 1$). Using Eq.(3.22) at $x \gg 1$ we find

$$\begin{aligned} dw_r(q) &\simeq \frac{\alpha d\omega}{\pi\omega} [r_1 + r_2 (\ln q^2 - 1)]; \\ \int d^2q dw_r(q) F_s(\mathbf{q}) &\simeq \frac{\alpha d\omega}{\pi\omega} [r_1 + r_2 (\ln \overline{q^2} - 1)]. \end{aligned} \quad (3.28)$$

For a thin target value of $\overline{q^2}$ is defined by mean square of multiple scattering angle on a thickness of a target l , and for boundary photons is the same but on the formation length l_f . However, if one intends to perform computation beyond a logarithmic accuracy, the method given in this subsection has advantage since there is no necessity to calculate $F_s(\mathbf{q})$. Radiation from a thin target using the path integral method was considered in [54] and [55].

3.4 A target of intermediate thickness

In the case when a target has intermediate thickness ($l \sim l_f$) the separation of contributions on photon emission inside target and boundary photon emission becomes senseless. We consider this case [18] neglecting by the correction

term $v(\underline{\rho})$. We present the spectral probability of radiation as

$$\begin{aligned}
\frac{dw}{d\omega} &= \frac{\alpha}{\pi\omega} \sum_{k=1}^5 \left[-r_1 \text{Im} J_k^{(1)} + r_2 \text{Re} J_k^{(2)} \right]; \\
J_1^{(m)} &= J_3^{(m)} = \int_0^\infty dt_1 \int_0^T dt_2 e^{-i(t_1 + \kappa t_2)} \left[(t_1 + t_2)^{-m} - N_1^m \right], \\
J_2^{(m)} &= \int_0^T dt (T-t) e^{-i\kappa t} \left[t^{-m} - N_2^m \right], \\
J_4^{(m)} &= \int_0^\infty dt_1 \int_0^\infty dt_2 e^{-i(t_1 + t_2 + \kappa T)} \left[(t_1 + t_2 + T)^{-m} - N_4^m \right], \\
J_5^{(m)}(T) &= 2 \int_0^\infty dt_1 \int_0^T dt_2 \frac{e^{-it_1}}{(t_1 + t_2)^m} (e^{-it_2} - e^{-i\kappa t_2}) \\
&\quad + \int_0^T dt \frac{(T-t)}{(t-i0)^m} (e^{-it} - e^{-i\kappa t}) \\
&\quad + \int_0^\infty dt_1 \int_0^\infty dt_2 \frac{e^{-i(t_1 + t_2)}}{(t_1 + t_2 + T)^m} (e^{-iT} - e^{-i\kappa T}). \quad (3.29)
\end{aligned}$$

where T is defined in Eq.(3.5), the functions N_k are

$$\begin{aligned}
N_1 &= \frac{\nu}{\sinh \nu t_2 + \nu t_1 \cosh \nu t_2}, & N_2 &= \frac{\nu}{\sinh \nu(t-i0)}, \\
N_4 &= \frac{\nu}{(1 + \nu^2 t_1 t_2) \sinh \nu T + \nu(t_1 + t_2) \cosh \nu T}, & \nu &= \frac{1+i}{\sqrt{2}} \nu_0, \quad (3.30)
\end{aligned}$$

here κ and ν_0 are defined in Eq.(2.116) and in Eq.(2.26).

We confine ourselves to the case $\varepsilon \ll \varepsilon_e$ when the LPM effect manifests itself for soft emitted photons ($\omega \ll \varepsilon$). So we can neglect the terms with r_1 in (3.29).

Let us consider first the case when LPM effect is weak ($\nu_1 \ll 1$). We assume here that condition $\nu_1(\omega_p) \geq 1$ (definition of ω_p see in Eq.(1.5)) is fulfilled. This means that in the region where $\nu_1 \ll 1$ one has $\omega \gg \omega_p$ and effects of the polarization of a medium are negligible. This is true for high energies ($\varepsilon \geq 10$ GeV). Then for thickness $T \ll 1/\nu_1$ the transverse shift of the projectile due to the multiple scattering in a target as a whole have no influence on coherent effects defined by the phase $\phi = \omega l(1 - \mathbf{n}\mathbf{v})$ in the factor $\exp(-i\phi)$. Indeed, for the projectile traversing a target in the case $\nu_1 T \ll 1$ an increment of the phase ϕ is small

$$\Delta\phi \sim \omega l \vartheta_s^2 \sim \omega l \frac{\nu_1^2 T}{\gamma^2} \sim \nu_1^2 T^2 \ll 1. \quad (3.31)$$

The angle of multiple scattering ϑ_s is small also comparing with an characteristic angle of radiation $1/\gamma$ ($\gamma^2\vartheta_s^2 = \nu_1^2 T \ll 1$). So, in the case $\nu_1 \ll 1$, $\nu_1 T \ll 1$ the radiation originates on separate atoms of a target and an interference on target boundaries is defined by the value $\omega l(1 - v) = T$. At $T \ll 1$ this interference is weak, while at $T \gg 1$ there is a damping of the interference terms due to integration over photon emission angles. Expanding over ν_1 in Eq.(3.29) we obtain ($\kappa = 1$):

$$J^{(2)}(T) \equiv \text{Re} \sum_{k=1}^4 J_k^{(2)}(T) \simeq \frac{\nu_1^2 T}{3} \left[1 - 3T \int_1^\infty \frac{(x-1)^2}{x^3} \sin(xT) dx \right] \quad (3.32)$$

$$= \frac{\nu_1^2 T}{3} \left[1 + 3T \left(\left(1 - \frac{T^2}{2} \right) \text{si}(T) - 2T \text{ci}(T) + \frac{3}{2} \sin T - \frac{T}{2} \cos T \right) \right],$$

where $\text{si}(T)$ ($\text{ci}(T)$) is the integral sine (cosine). For case $T \ll 1$

$$J^{(2)}(T) \simeq \frac{\nu_1^2 T}{3} \left[1 - \frac{3\pi}{2} T + 6T^2 \left(\ln \frac{1}{T} + 1 - C \right) \right], \quad (3.33)$$

and for case $T \gg 1$

$$J^{(2)}(T) \simeq \frac{\nu_1^2 T}{3} \left(1 + 6 \frac{\cos T}{T^2} \right). \quad (3.34)$$

Thus, in the case $\nu_1 \ll 1$, $\nu_1 T \ll 1$ the probability of radiation is defined by Bethe-Maximon formula both for $T \ll 1$ and for $T \gg 1$. However, for $T \sim 1$ the interference on the target boundaries is essential. If we present as above $J^{(2)}$ as product of $\nu_1^2 T/3$ (Bethe-Maximon formula) and some interference factor, then this factor attains 0.53 at $T = 0.32$ (minimum of the interference factor) and 1.33 at $T = 1.84$ (maximum of the interference factor).

When the parameter $\nu_1 T$ is large ($\nu_1 \ll 1$, $\nu_1 T \gg 1$) the radiation is formed inside a target and the interference terms are damped exponentially. In this case formulae derived for thick target in Sec.2.1 are applicable. Taking into account the contribution of boundary photons (see Sec.3.2) we have

$$J^{(2)}(\infty) = \frac{\nu_1^2 T}{3} \left(1 + \frac{1}{6L_1} - \frac{16\nu_1^4}{21} \right) - \frac{2\nu_1^4}{21}, \quad (3.35)$$

where L_1 and ν_1 are defined in Eqs.(2.12) and (2.25).

We consider now the case when the LPM effect is strong ($\nu_0 \gg 1$) and the parameter $T \ll 1$ while the value which characterize the thickness of a

target $\nu_0 T \sim 1$. We find for $\kappa T \ll 1$ ($r_2 \simeq 2$)

$$\begin{aligned} \frac{dw}{d\omega} &= \frac{2\alpha}{\pi\omega} \left(J^{(2)} + J_5^{(2)} \right), \quad J_5^{(2)} \simeq \frac{(\kappa - 1)^2}{2} \left(\ln \frac{1}{T} + \frac{1}{2} - C \right), \\ J^{(2)} &\simeq \text{Re} \left\{ \ln(\nu \sinh \nu T) - 1 - C - \kappa \frac{\pi T}{4} \right. \\ &+ \frac{2i}{\nu \tanh \nu T} \left[\ln(\nu \tanh \nu T) + 1 - C - \frac{i\pi}{2} \right] + i\kappa T \left(\ln \frac{\cosh \nu T}{\tanh \nu T} - \frac{\nu T}{\tanh \nu T} \right) \\ &\left. + \frac{i\kappa}{\nu} \int_0^{\nu T} dt \left(\frac{4t}{\sinh 2t} - \frac{t^2}{\sinh^2 t} \right) \right\}, \quad \nu = \exp\left(i\frac{\pi}{4}\right) \nu_0. \end{aligned} \quad (3.36)$$

For a relatively thick target ($\nu_0 T \gg 1$) we have from Eq.(3.36)

$$\begin{aligned} J^{(2)} &\simeq \ln \nu_0 - 1 - C - \ln 2 + \frac{\sqrt{2}}{\nu_0} \left(\kappa \frac{\pi^2}{24} + \ln \nu_0 + 1 - C + \frac{\pi}{4} \right) \\ &+ \frac{\nu_0 T}{\sqrt{2}} \left(1 - \frac{\pi\kappa}{2\sqrt{2}\nu_0} \right) \end{aligned} \quad (3.37)$$

Here the terms without T are the contribution of boundary photons (see Eq.(4.14) in [17]) while the term $\propto T$ gives the probability of radiation inside target (with correction $\sim \kappa/\nu_0$ but without corrections $\sim 1/L$). The relative value of the last corrections at $\nu_0 \gg 1$ is given by Eq.(2.33).

In the limiting case when a target is very thin and $\nu_0 T \ll 1$ but when $\nu_0^2 T \gg 1$ we have from Eq.(3.36)

$$\begin{aligned} J^{(2)} &\simeq \left(1 + \frac{2}{\nu_0^2 T} \right) [\ln(\nu_0^2 T) + 1 - C] - 2 + \delta, \\ \delta &= \frac{(\nu_0 T)^4}{180} + \frac{2(\nu_0 T)^2}{45} T (\ln \nu_0^2 T - C) - \frac{\kappa T}{6} (\nu_0 T)^2. \end{aligned} \quad (3.38)$$

The terms without δ in this expression coincide with Eq.(3.20) (up to terms $\propto C/L_t$).

In the photon energy region where $\nu_0 T \ll 1$ the contribution of the terms $J_k^{(m)}$ ($k=1,2,3$) is very small ($\sim \delta$) and decreases with photon energy reduction ($\propto \omega$), so that in the spectral distribution of radiation only the terms $J_4^{(m)}, J_5^{(m)}$ contribute. We obtain for the function $J_4^{(2)}$ in the case when $(1 + \nu_0)T \ll 1$ and when the parameter $\nu_0^2 T$, which characterizes the mean square angle of the multiple scattering in a target as a whole, has an arbitrary

value

$$\begin{aligned}
J_4^{(2)} e^{i\kappa T} &= \int_0^\infty dx x \int_0^\infty \frac{dt_1}{t_1^2} \int_0^\infty \frac{dt_2}{t_2^2} \exp\left(-\left(1 + \frac{x}{t_1 t_2}\right)(t_1 + t_2)\right) \\
&\quad \times [1 - \exp(-x\nu_0^2 T)] \\
&= 4 \int_0^\infty dx K_1^2(2\sqrt{x}) [1 - \exp(-x\nu_0^2 T)] \\
&= 2 \int_0^\infty d\rho \rho K_1^2(\rho) [1 - \exp(-k\rho^2)], \quad 4k = \nu_0^2 T, \quad (3.39)
\end{aligned}$$

where $K_1(\rho)$ is the modified Bessel function. Formula (3.39) corresponds at $\kappa = 1$ to result for a thin target obtained above (see Eq.(3.14)) without terms $\propto 1/L$. Since the dependence on the parameter κ is contained in Eq.(3.39) as a common phase multiplier $\exp(-i\kappa T)$, one can write more accurate expression for $J_4^{(2)}$ (with terms $\propto 1/L$) using the found results (see Eq.(3.15)):

$$J_4^{(2)} = 2e^{-i\kappa T} \int_0^\infty d\rho \rho K_1^2(\rho) [1 - \exp(-V(\rho)T)], \quad (3.40)$$

where $V(\rho)T$ is defined in Eq.(3.15). For the case $\nu_0^2 T \gg 1$ it has the form

$$e^{i\kappa T} J_4^{(2)} = \left(1 + \frac{1}{2k}\right) [\ln 4k + 1 - C] - 2 + \frac{C}{L_t}, \quad (3.41)$$

where k and L_t are defined in Eq.(3.18) and Eq.(3.15). In the case when parameter k is not very high one has to use an exact expression Eq.(3.14). For $k \ll 1$ one can expand the exponent in the integrand of Eq.(3.40). Then we find

$$e^{i\kappa T} J_4^{(2)} = \frac{\nu_1^2 T}{3} \left(1 + \frac{1}{6L_1}\right), \quad \nu_1^2 T = \frac{4\pi Z^2 \alpha^2 n_{al}}{m^2} L_1. \quad (3.42)$$

At $\kappa T \ll 1$ the spectral distribution of probability is

$$\frac{dw}{d\omega} = \frac{2\alpha}{3\pi\omega} \nu_1^2 T \left(1 + \frac{1}{6L_1}\right) \left(1 - \frac{\omega}{\varepsilon}\right). \quad (3.43)$$

This is the Bethe-Maximon formula for not very hard photons (terms $\propto \left(\frac{\omega}{\varepsilon}\right)^2$ are omitted).

When a photon energy decreases, the parameter κ increases as well as the combination $\kappa T \propto 1/\omega$, while the value $(\nu_0 T)^2$ decreases $\propto \omega$. Just this value defines an accuracy of Eq.(3.40). Using Eq.(3.29) at $T \ll 1, \kappa T \geq 1$ we find for the probability of transition radiation ($J_5^{(2)}$) the following expression

$$\frac{dw_{tr}}{d\omega} \simeq \frac{2\alpha}{\pi} \left\{ \left(1 + \frac{2}{\kappa - 1} \right) \left[\ln \kappa - \text{ci}(\kappa T) + \cos(\kappa T)(\ln T + C) + \frac{\pi}{2} \sin(\kappa T) \right] + \kappa T \text{si}(\kappa T) - 4 \sin^2 \frac{\kappa T}{2} \right\}. \quad (3.44)$$

In the limiting case $\kappa T \gg 1$ the probability Eq.(3.44) turns into standard probability of the transition radiation (3.11) with oscillating additions

$$\begin{aligned} \frac{dw_{tr}}{d\omega} &= \frac{2\alpha}{\pi} \left[J_{tr} + \cos(\kappa T) (\ln T + C + 1) + \frac{\pi}{2} \sin(\kappa T) \right], \\ J_{tr} &= \left(1 + \frac{2}{\kappa - 1} \right) \ln \kappa - 2. \end{aligned} \quad (3.45)$$

Note, that there is a qualitative difference in a behaviors of interference terms in Eqs.(3.34) and (3.45). In the former an amplitude of oscillation with ω increase decreases as $1/\omega^2$ while in the latter the corresponding amplitude weakly (logarithmically) increases with ω decrease.

From the above analysis follows that in the case when $\nu_0 T \ll 1$ ($\nu_0 \gg 1$) the spectral distribution of probability of radiation with the polarization of a medium taken into account has the form

$$\frac{dw}{d\omega} = \frac{dw_{tr}}{d\omega} + \cos(\kappa T) \frac{dw_{th}}{d\omega}, \quad (3.46)$$

where $dw_{th}/d\omega$ is the spectral distribution of probability of radiation in a thin target without regard for the polarization of a medium. In the case $4k = \nu_0^2 T \gg 1$ the probability $dw_{th}/d\omega$ is defined by Eqs.(3.18), (3.20) and for the case $k \ll 1$ it is defined by Eq.(3.35). More accurate representation of the probability of radiation $dw_{th}/d\omega$ may be obtained using Eq.(3.40). It follows from Eqs.(3.45) and (3.46) that if we make allowance for multiple scattering at $\kappa T \gg 1$ this results in decreasing of oscillations of the transition radiation probability by magnitude of the bremsstrahlung probability in a thin target.

The radiation of the boundary photons with regard for the multiple scattering was considered in [51] (for $\omega \ll \varepsilon$), the effect of polarization of a

medium was included into consideration of the problem in [52] and [53]. In these papers the probability of radiation of boundary photons (under condition of applicability of Eqs.(3.37) and (3.38)) was analyzed also to within the logarithmic accuracy (see Eq.(20) in [52] and Eq.(15) in [53]). This accuracy is insufficient for parameters connected with experiment [14]-[18]. For example, for $\varepsilon = 25$ GeV and in heavy elements the value ν_0 equates κ for $\nu_0 \sim 20$. One can see from Eqs.(3.37) and (3.38) that in this case $\ln \nu_0$ is nearly completely compensated by constant terms. Our results, which are consistent with obtained [52], are more accurate and presented in more convenient for application form and the Coulomb corrections are included.

3.5 Multiphoton effects in energy loss spectra

It should be noted that in the experiments [12]-[14] the summary energy of all photons radiated by a single electron is measured. This means that besides mentioned above effects there is an additional "calorimetric" effect due to the multiple photon radiation. This effect is especially important in relatively thick used targets. Since the energy loss spectrum of an electron is actually measured, which is not coincide in this case with the spectrum of photons radiated in a single interaction, one have to consider the distribution function of electrons over energy after passage of a target [19]. As it is known, this distribution function is the solution of the corresponding kinetic equation. However, the problem can be simplified essentially if one is interested in the soft part of the energy loss spectrum. Just this situation was in the experiments [12]-[14], since the measurements were performed in the region of the photon energies of one to five orders of magnitude lower than the electron energy.

We consider first the spectral distribution of the energy loss. The probability of the successive radiation of n soft photons with energies $\omega_1, \omega_2, \dots, \omega_n$ by a particle with energy ε ($\omega_k \ll \varepsilon, k = 1, 2 \dots n$) on the length l in the energy intervals $d\omega_1 d\omega_2 \dots d\omega_n$ is given by expression

$$\begin{aligned} dw(\omega_1, \omega_2, \dots, \omega_n) &= A \int_0^l dW(\omega_1) dl_1 \int_0^{l_1} dW(\omega_2) dl_2 \dots \int_0^{l_{n-1}} dW(\omega_n) dl_n \\ &= \frac{A}{n!} dw(\omega_1) dw(\omega_2) \dots dw(\omega_n), \end{aligned} \quad (3.47)$$

where A is the normalization constant, $dW(\omega)/d\omega$ is the differential probability of the photon radiation per unit length, $dw(\omega)/d\omega = ldW(\omega)/d\omega$ is the differential probability of the photon radiation per length l . If the probability $dw/d\omega$ doesn't depend on the particle energy ε then integrating Eq.(3.47)

over all photon energies we obtain

$$w_n = \frac{A}{n!} w^n, \quad w = \int \frac{dw}{d\omega} d\omega. \quad (3.48)$$

The value A is defined by the condition that probability of all the possible events with radiation of any number of photons or without photon radiation is equal to unit.

$$\sum_{n=0}^{\infty} w_n = A \sum_{n=0}^{\infty} \frac{1}{n!} w^n = A \exp w = 1, \quad A = \exp(-w). \quad (3.49)$$

Using Eqs.(3.47),(3.49) we can write the expression for the differential distribution of the energy loss in the form

$$\frac{1}{\omega} \frac{d\varepsilon}{d\omega} = \sum_{n=1}^{\infty} \frac{1}{n!} \exp(-w) \int \frac{dw}{d\omega_1} \frac{dw}{d\omega_2} \cdots \frac{dw}{d\omega_n} \delta \left(\sum_{k=1}^n \omega_k - \omega \right) d\omega_1 \dots d\omega_n. \quad (3.50)$$

Here on the right-hand side we have the sum of the probabilities of radiation of n photons with summary energy ω .

Using standard parametrization of δ -function

$$\delta \left(\sum_{k=1}^n \omega_k - \omega \right) = \frac{1}{2\pi} \int_{-\infty}^{\infty} \exp \left(i s \left(\omega - \sum_{k=1}^n \omega_k \right) \right) ds$$

we obtain

$$\begin{aligned} \frac{d\varepsilon}{d\omega} &= \frac{\omega}{2\pi} \int_{-\infty}^{\infty} \exp(is\omega - w) \sum_1^{\infty} \frac{1}{n!} \left(\int \frac{dw}{d\omega_1} \exp(-is\omega_1) d\omega_1 \right)^n ds \\ &= \frac{\omega}{2\pi} \int_{-\infty}^{\infty} \exp(is\omega) \exp \left\{ - \int_0^{\infty} \frac{dw}{d\omega_1} [1 - \exp(-is\omega_1)] d\omega_1 \right\} ds \quad (3.51) \\ &= \frac{1}{\pi} \operatorname{Re} \int_0^{\infty} \exp(ix) \exp \left\{ - \int_0^{\infty} \frac{dw}{d\omega_1} \left[1 - \exp \left(-ix \frac{\omega_1}{\omega} \right) \right] d\omega_1 \right\} dx. \end{aligned}$$

The formula (3.51) was derived by Landau [60] (see also [1]) as solution of the kinetic equation under assumption that energy loss are much smaller than particle's energy (the paper [60] was devoted to the ionization energy loss). Let us notice the following. The energy loss are defined by the hard part of the radiation spectrum. In the soft part of the energy loss spectrum Eq.(3.51) the probability of radiation of one hard photon only is taken into

account accurately. To calculate the probability of the emission of two and more hard photons one has to take into account step by step the recoil in previous acts of the photon emission. The probability of radiation of two and more hard photons is of the order $(l/L_{rad})^2$ and so on. Thus, the formula (3.51) is applicable for the thin targets and has accuracy l/L_{rad} . If we want to improve accuracy of Eq.(3.51) and for the case of thick targets $l \geq L_{rad}$ one has to consider radiation of an arbitrary number of hard photons. This problem is solved in Appendix of [19] for the case when hard part of the radiation spectrum is described by the Bethe-Maximon formula. In this case the Eq.(3.51) acquires the additional factor. As a result we extend this formula on the case of thick targets.

We will analyze first the interval of photon energies where the Bethe-Maximon formula is valid. We write it in the form (within the logarithmic accuracy)

$$\omega \frac{d\omega}{d\omega} = \frac{l}{L_{rad}} \left[\frac{4}{3} \left(1 - \frac{\omega}{\varepsilon} \right) + \frac{\omega^2}{\varepsilon^2} \right] \vartheta(\varepsilon - \omega) = \beta \left(1 - x_1 + \frac{3}{4} x_1^2 \right) \vartheta(1 - x_1), \quad (3.52)$$

where l is the thickness of the target, L_{rad} is the radiation length,

$$\beta = \frac{4l}{3L_{rad}}, \quad x_1 = \frac{\omega}{\varepsilon}.$$

The integral in the curly brackets in Eq.(3.51) is

$$J \simeq \beta \left(\ln x + \mu + i \frac{\pi}{2} \right), \quad \mu = \ln \frac{\varepsilon}{\omega} - \frac{5}{8} + C \quad (3.53)$$

Substituting this result into Eq.(3.51) we have

$$\frac{d\varepsilon}{d\omega} = \beta \frac{\exp(-\beta\mu)}{\Gamma(1 + \beta)} = \beta f_{BH}, \quad (3.54)$$

where $\Gamma(z)$ is the Euler gamma function. If we consider radiation of the one soft photon, we have from Eq.(3.51) $d\varepsilon/d\omega = \beta$. Thus, the formula (3.54) gives additional "reduction factor" f_{BH} which characterizes the distortion of the soft Bethe-Maximon spectrum due to multiple photons radiation. The derivation of Eq.(3.54) is based on expression (3.51) in which the statistical independence of photon radiation acts is assumed (the Poisson distribution). This statistical independence is broken when two or more hard photons (energies of which are of the order of the energy of the initial electron) are emitted. Since the probability of hard photon radiation is of the order of β , Eq.(3.54)

is applicable, strictly speaking, at $\beta \ll 1$ and it has the accuracy up to factor $(1 + O(\beta^2))$. However, the contribution of arbitrary number of hard photons radiated in the Beth-Maximon region is exactly calculated. This contribution is contained in the factor $g(\beta)$ (see Appendix of [19], Eqs.(A.15), (A.16)). So we obtain the reduction factor valid for $\beta \geq 1$

$$f_{BH} = g(\beta) \frac{\exp(-\beta\mu)}{\Gamma(1+\beta)} = \left(\frac{\omega}{\varepsilon}\right)^\beta (1+\beta)^{1/4} \left(1 + \frac{\beta}{2}\right)^{3/4}. \quad (3.55)$$

In Fig.9 the function $f_{BH}(\omega)$ is given for electron with the energy $\varepsilon = 25$ GeV. One can see that for $\omega = 100$ MeV the difference between the value $f_{BH}(\omega)$ and unit is 5-6 times greater than value β . Let us discuss this circumstance.

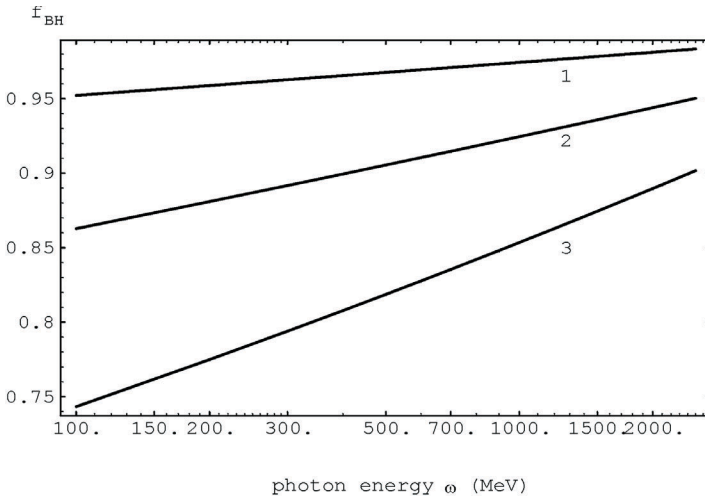


Figure 9: The reduction factor f_{BH} for the energy of the initial electron $\varepsilon = 25$ GeV. The curves 1,2 and 3 are respectively for $\beta = 0.01, 0.03$ and 0.06 .

The emission of accompanying photons with energy much less or of the order of ω (we consider in this figure the situation connected with SLAC experiment [12]-[14] where $\omega \ll \varepsilon$, $\beta \ll 1$) changes the spectral distribution on quantity order of β . However, if one photon with energy $\omega_r > \omega$ is emitted, at least, then photon with energy ω is not registered at all in the corresponding channel of the calorimeter. Since mean number of photons with energy larger than ω

is determined by the expression (see Eqs.(3.47)-(3.52))

$$\sum_{n=0}^{\infty} n w_n = w_{\omega} = \int_{\omega}^{\varepsilon} \frac{dw}{d\omega} d\omega, \quad (3.56)$$

the probability of the event when no photon with energy $\omega_r > \omega$ is radiated is defined by $\exp(-w_{\omega})$. This is just the main factor in the expression for the reduction factor f_{BH} (3.55). In the case, when radiation is described by the Bethe-Maximon formula the value w_{ω} increases as a logarithm with ω decrease ($w_{\omega} \simeq \beta \ln \varepsilon/\omega$) and for large ratio ε/ω the value w_{ω} is much larger than β . Thus, amplification of the effect is connected with a large interval of the integration ($\omega - \varepsilon$) at evaluation of the radiation probability.

The Bethe-Maximon formula becomes inapplicable for the photon energies $\omega \leq \omega_c$, (ω_c is defined in Eq. (2.27)), where LPM effect starts to manifest itself (see Eqs.(2.17), (2.18)). Calculating the integral in Eq.(3.51) we find for the distribution of the spectral energy loss

$$\frac{d\varepsilon}{d\omega} = 3\beta \sqrt{\frac{\omega}{2\omega_c}} f_{LPM}, \quad f_{LPM} = g(\beta) \left(1 + \frac{3\pi}{2\sqrt{2}} \beta \sqrt{\frac{\omega}{\omega_c}} \right) \exp(-w_c), \quad (3.57)$$

where f_{LPM} is the reduction factor in the photon energy range where the LPM effect is essential,

$$w_c = \beta \left(\ln \frac{\varepsilon}{\omega_c} + C_2 \right), \quad C_2 \simeq 1.959. \quad (3.58)$$

In this expression the terms $\sim 1/L$ (see Sec.2.1) are not taken into account. In Fig.10 the function $f_{LPM}(\omega)$ is shown for $\omega < 100$ MeV ($\varepsilon = 25$ GeV, $\omega_c = 228$ MeV). It is seen in Fig.10 that the reduction factor f_{LPM} changes appreciably in the region of high photon energies solely. This is due to the fact that here the total probability of photon radiation is finite (in contrast to the Bethe-Maximon formula) and the integral which defines this probability converges at $\omega \rightarrow 0$.

In the above analysis we neglected an influence of the polarization of a medium on the bremsstrahlung. This is correct if $\kappa \ll \nu_0$ (see Eqs.(2.115), (2.116),(2.26), Sec. 2.6) where

$$\kappa = 1 + \frac{\omega_p^2}{\omega^2} \equiv 1 + \kappa_0^2, \quad \omega_p = \gamma\omega_0, \quad \nu_0^2 = \frac{\omega_c}{\omega}. \quad (3.59)$$

We assume, for definiteness, that $\omega_p \ll \omega_c$. This is true in any case for a dense matter if electron energy $\varepsilon \geq 10$ GeV. In the opposite case when

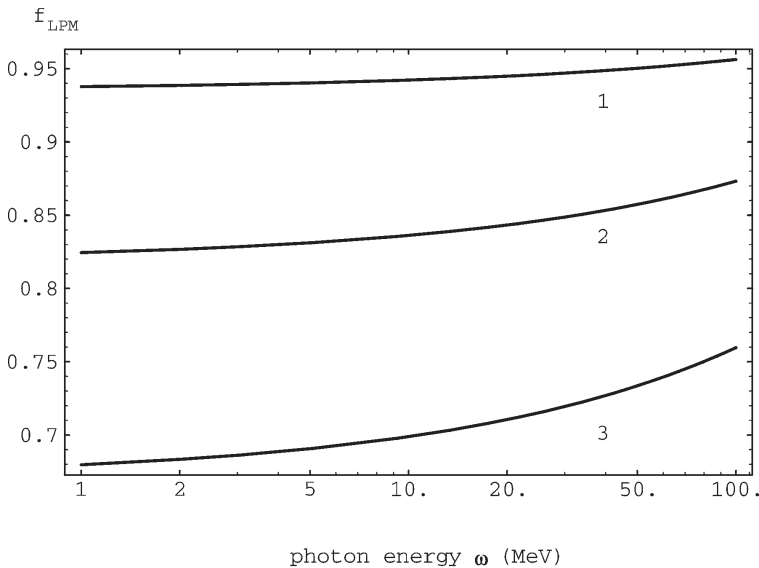


Figure 10: The reduction factor f_{LPM} for energy of the initial electron $\varepsilon=25$ GeV in tungsten ($\omega_c=228$ MeV). The curves 1, 2 and 3 are respectively for $\beta=0.01, 0.03$ and 0.06 .

$\kappa \gg \nu_0 \gg 1$ there is an additional suppression of the bremsstrahlung (see Sec. 2.6):

$$\omega \frac{dw}{d\omega} \simeq \frac{3l}{4\kappa L_{rad}} = \frac{\beta}{\kappa} \quad (3.60)$$

and this contribution into reduction factor (3.57) can be neglected.

The main contribution into effect considered for the photon energies such that $\omega \ll \omega_p$ gives the transition radiation Eqs.(3.10), (3.45). Let us note, that for the transition radiation the given above derivation of the formula (3.51) is directly inapplicable. However, for application of formula (3.51) it is enough that acts of radiation of soft photons are statistically independent. Taking integrals in Eq.(3.51) and taking into account that $\eta \ll 1$ (but it may be that $\eta\sigma \sim 1$) we obtain

$$\begin{aligned} \frac{d\varepsilon}{d\omega} = & \frac{g(\beta)}{\pi} \exp(-w_c) \exp \left[-\eta \left(\sigma^2 - \frac{3\pi^2}{4} + \psi^2(1 - 2\eta\sigma) + \psi'(1 - 2\eta\sigma) \right) \right] \\ & \times \sin [2\pi\eta(\sigma + \psi(1 - 2\eta\sigma))] \Gamma(1 - 2\eta\sigma), \end{aligned} \quad (3.61)$$

where $\psi(z) = d \ln \Gamma(z)/dz$, $g(\beta)$ is defined in Eq.(3.55),

$$\eta = \frac{2\alpha}{\pi}, \quad \sigma = \ln \frac{\omega_p}{\omega} + C - 1. \quad (3.62)$$

In the case $\eta\sigma \ll 1$ we have

$$\begin{aligned} \frac{d\varepsilon}{d\omega} &= 2\eta \left(\ln \frac{\omega_p}{\omega} - 1 \right) g(\beta) \exp(-w_c) f_{tr}, \\ f_{tr} &= \exp \left[-\eta \left(\ln \frac{\omega_p}{\omega} - 1 \right)^2 \left(1 + \frac{\eta\pi^2}{3} \right) + \frac{\eta\pi^2}{4} \right]. \end{aligned} \quad (3.63)$$

The case of a thin target, with thickness l where the photon formation length is

$$l_f = \frac{2\gamma^2}{\omega} (\kappa + \nu_0) \geq l \quad (3.64)$$

should be analyzed separately. We consider situation when effects of the polarization of a medium are weak ($\kappa_0^2 < \nu_0$) In this case the scattering takes place on a target as a whole during the radiation process and the spectral probability $dw/d\omega$ in Eqs.(3.48)-(3.52) depends on the momentum transfer $q = \gamma\vartheta$ (see Eq.(3.22))

$$\frac{dw_r}{d\omega} = \frac{2\alpha}{\pi} \frac{d\omega}{\omega} F_2 \left(\frac{q}{2} \right) \equiv \beta_1(q) \frac{d\omega}{\omega}, \quad (3.65)$$

where $F_2(x)$ is defined in Eq.(2.108). On the final step one have to average $d\varepsilon_r/d\omega$ over \mathbf{q} with the distribution function $F_s(\mathbf{q})$ Eq.(3.23).

Since the expression for the spectral distribution (3.65) has the same form as in the Bethe-Maximon case, one can use Eq. (3.54) for calculation of the reduction factor. As a result we have for the contribution of the thin target region

$$f_{th} = \frac{1}{\langle \beta_1(q) \rangle} \left\langle \beta_1(q) \exp \left[-\beta_1(q) \ln \frac{\omega_{th}}{\omega} \right] \right\rangle \simeq 1 - \frac{2\alpha}{\pi} \frac{\langle F_2^2 \left(\frac{q}{2} \right) \rangle}{\langle F_2 \left(\frac{q}{2} \right) \rangle} \ln \frac{\omega_{th}}{\omega}, \quad (3.66)$$

where ω_{th} is the boundary energy starting from which the target becomes thin. The lower limit of the applicability of Eq.(3.66) is determined from the condition $l_f = l$. The expression (3.66) depends essentially on the mean square of the momentum transfer q_s^2 associated with the target thickness. In the case $q_s^2 \ll 1$ when an influence of the multiple scattering is weak ($\vartheta_s^2 \ll 1/\gamma^2$)

$$F_s(q) = \frac{4Z^2\alpha^2}{(q^2 + \alpha_s^2)^2} \frac{n_a l}{m^2}, \quad \alpha_s = \frac{\lambda_c}{a_{s2}}, \quad (3.67)$$

where a_{s2} is the effective screening radius Eq.(2.12). When the multiple scattering is strong ($q_s^2 \gg 1$, $\vartheta_s^2 \gg 1/\gamma^2$), the reduction factor can be calculated using the Gaussian distribution for $F_s(q)$

$$F_s(q) = \frac{1}{\pi q_s^2} \exp\left(-\frac{q^2}{q_s^2}\right),$$

$$q_s^2 = \frac{4\pi Z^2 \alpha^2}{m^2} n_a l \int_0^{q_s^2+1} \frac{q^2 dq^2}{(q^2 + \alpha_s^2)^2} \simeq \frac{4\pi Z^2 \alpha^2}{m^2} n_a l \ln \frac{q_s^2 + 1}{\alpha_s^2}. \quad (3.68)$$

In the first case ($q_s^2 \ll 1$) one has $\langle F_2^2 \rangle \ll \langle F_2 \rangle$ and one can neglect the correction to unit in Eq.(3.66). In the opposite case ($q_s^2 \gg 1$) the main contribution into entering mean values of F_2 gives values $q \gg 1$ where

$$F_2(q) \simeq \ln q^2 - 1 + \frac{2}{q^2}. \quad (3.69)$$

In this case the effect under consideration may be noticeable.

From the above analysis one can find an approximate expression for the reduction factor in the general form. One can present the integral over ω_1 in Eq.(3.51) as

$$\int_0^\infty \frac{d\omega}{d\omega_1} \left[\exp\left(-ix \frac{\omega_1}{\omega}\right) - 1 \right] d\omega_1$$

$$\simeq - \int_\omega^\infty \frac{d\omega}{d\omega_1} d\omega_1 + \int_0^\omega \frac{d\omega}{d\omega_1} \left[\exp\left(-ix \frac{\omega_1}{\omega}\right) - 1 \right] d\omega_1. \quad (3.70)$$

The second integral on the right-hand side of Eq.(3.70) (as well as terms omitted in the first integral) has an order $\omega d\omega/d\omega$. For the case $\beta \ll 1$ this value is small

$$\omega \frac{d\omega}{d\omega} \leq \frac{4l}{3L_{rad}} \equiv \beta \quad (\omega \geq \omega_p);$$

$$\omega \frac{d\omega}{d\omega} \simeq \frac{4\alpha}{\pi} \left(\ln \frac{\omega_p}{\omega} - 1 \right) = 2\eta(\sigma - C), \quad (\omega \ll \omega_p). \quad (3.71)$$

Let us note that a contribution of the transition radiation can be enlarged n times if one makes a target as a collection of n plates conserving the total thickness l provided that definite conditions are fulfilled for the plate thicknesses and gaps between plates. In that case $\eta \rightarrow n\eta$ and above formulae are valid if $n\eta \leq 1$.

Expanding the exponential in Eq.(3.51) with the second integral of Eq.(3.70) and integrating over x we have

$$\begin{aligned} & \frac{1}{2\pi} \int_{-\infty}^{\infty} \exp(ix) dx \int_0^{\omega} \frac{dw}{d\omega_1} \left[\exp\left(-ix \frac{\omega_1}{\omega}\right) - 1 \right] d\omega_1 \\ &= \int_0^{\omega} \frac{dw}{d\omega_1} \delta\left(1 - \frac{\omega_1}{\omega}\right) d\omega_1 = \omega \frac{dw}{d\omega}. \end{aligned} \quad (3.72)$$

Thus, the spectral distribution of the energy loss and reduction factor f have the following general form

$$\frac{d\varepsilon}{d\omega} = \omega \frac{dw}{d\omega} f, \quad f = \exp\left[-\int_{\omega}^{\infty} \frac{dw}{d\omega_1} d\omega_1\right] \left(1 + O\left(\omega \frac{dw}{d\omega}\right)\right) \quad (3.73)$$

3.6 Radiation from structured target

The radiation from several plates for the relatively hard part of the spectrum in which the bremsstrahlung in the condition of the strong LPM effect dominates was investigated recently in [61]. A rather curious interference pattern in the spectrum of the radiation was found which depends on a number (and a thickness) of plates and the distance between plates (the polarization of a medium was neglected). In the present section the probability of radiation in a radiator consisting of N plates is considered [20]. The transition radiation dominates in the soft part of the considered spectrum, while the bremsstrahlung under influence of the strong LPM effect dominates in the hard part. The intermediate region of the photon energies where contributions of the both mentioned mechanisms are of the same order is of evident interest. We analyze this region in detail. In this region effects of the polarization of the medium are essential.

Here we consider the case when the target consists of N identical plates of thickness l_1 with the equal gaps l_2 between them. The case $l_1 \ll l_f$ will be analyzed where l_f is the characteristic formation length of radiation in absence of a matter ($\omega_0 = 0$), see Eqs.(1.4)-(1.6)

$$l_f = \frac{l_{f0}}{1 + \gamma^2 \vartheta_c^2} = \frac{l_{f0}}{1 + p_c^2}, \quad T_{1,2} = \frac{l_{1,2}}{l_{f0}}, \quad \frac{l_1}{l_f} = (1 + p_c^2) T_1 \ll 1, \quad T_1 + T_2 = T, \quad (3.74)$$

where ϑ_c is the characteristic angle of radiation.

One can split the spectral distribution of the probability of radiation into two parts

$$\frac{dw}{d\omega} = \frac{dw_{br}}{d\omega} + \frac{dw_{tr}}{d\omega}, \quad (3.75)$$

where $dw_{br}/d\omega$ is the spectral distribution of the probability of bremsstrahlung with allowance for the multiple scattering and polarization of a medium and $dw_{tr}/d\omega$ is the probability of the transition radiation for the N -plate target. For $dw_{br}^{(N)}/d\omega$ one has:

$$\frac{dw_{br}^{(N)}}{d\omega} = \frac{\alpha}{\pi\omega} \operatorname{Re} \sum_{n_1, n_2=0}^{N-1} \int d\tau_2 \int d\tau_1 \exp[-i(\tau_1 + \tau_2 + \kappa T_1 + (n-1)\bar{\kappa}T)] \times [r_1 (G_n - G_n(0)) + r_2 (G_n^2 - G_n^2(0))], \quad (3.76)$$

where the coefficient r_1 and r_2 are defined in Eq.(3.2),

$$G_n^{-1} = \beta_n [(d_n - d_{n-1})^2 - 1] + i(d_n - d_{n-1})(\tau_1 + \tau_2) - \beta_n^{-1}\tau_1\tau_2; \\ N \geq n = n_2 - n_1 + 1 \geq 1; \quad n_1 = 0, \quad 0 \leq \tau_1 < \infty; \quad n_2 = N - 1, \quad 0 \leq \tau_2 < \infty; \\ n_1 \geq 1, \quad 0 \leq \tau_1 \leq T; \quad n_2 \leq N - 2, \quad 0 \leq \tau_2 \leq T, \\ \bar{\kappa} = 1 + \frac{\overline{\kappa_0^2}}{\kappa_0^2}, \quad \overline{\kappa_0^2} = \kappa_0^2 \frac{l_1}{l_1 + l_2} \quad (3.77)$$

The function d_n can be presented in the form

$$d_n = \frac{\sinh n\eta}{\sinh \eta}, \quad \sinh \eta = 2\sqrt{iqT_1T(1 + iqT_1T)}. \quad (3.78)$$

For the case $\eta \ll 1$ one has

$$\eta \simeq 2\sqrt{iqT_1T} \equiv 2T\sqrt{i\bar{q}}, \quad \bar{q} = q\frac{T_1}{T} = q\frac{l_1}{l_1 + l_2}. \quad (3.79)$$

In above formulas

$$T = T_1 + T_2, \quad b = \frac{1}{4qT_1}, \quad \beta_n = \frac{b}{d_n}, \quad G_n(0) = G_n(q=0) \quad (3.80)$$

Note for the subtraction procedure one has that when $q \rightarrow 0$, the function b , $\beta_n \rightarrow \infty$.

For one plate ($N = 1$) we have $n_1 = n_2 = 0$, $n = 1$ and

$$G_1^{-1} = i(\tau_1 + \tau_2) - \frac{1}{b}\tau_1\tau_2, \quad G_1^{-1}(0) = i(\tau_1 + \tau_2). \quad (3.81)$$

In the integral (3.76) we rotate the integration contours over τ_1 , τ_2 on the angle $-\pi/2$ and substitute variables $\tau_{1,2} \rightarrow -ix_{1,2}$. Then we carry out change

of variables $x = x_1 + x_2$, $x_2 = zx$. We have

$$\begin{aligned}
\frac{dw_{br}^{(1)}}{d\omega} &= \frac{\alpha}{\pi\omega} \cos \kappa T_1 \int_0^\infty \exp(-x) dx \int_0^1 \left[r_1 \left(1 - \frac{1}{g(x, z)} \right) \right. \\
&\quad \left. + r_2 \left(1 - \frac{1}{g^2(x, z)} \right) \right] dz \\
&= \frac{\alpha b}{\pi\omega} \cos(\kappa T_1) \int_0^\infty \exp(-bx) \left[r_1 F_1 \left(\sqrt{\frac{x}{4}} \right) + r_2 F_2 \left(\sqrt{\frac{x}{4}} \right) \right], \\
g(x, z) &= 1 + \frac{x}{b} z(1 - z), \tag{3.82}
\end{aligned}$$

where the functions $F_1(x)$ and $F_2(x)$ are defined in (2.109) and (2.108).

The special case is when a target consists of two plates ($N = 2$). Since the formation length is enough long for the soft photons ($\omega \ll \varepsilon$) only, we consider the term with r_2 in Eq.(3.76) as far as $r_1 = \omega^2/\varepsilon^2 \ll 1$. For the case ($N = 2$) the sum in Eq.(3.76) consists of three terms: 1) $n_1 = n_2 = 0$; 2) $n_1 = n_2 = 1$; 3) $n_1 = 0, n_2 = 1$. For the two first $n = 1$ and we have from Eq.(3.81)

$$\begin{aligned}
\frac{dw_{br1}^{(2)}}{d\omega} &= \frac{dw_{br2}^{(2)}}{d\omega} = \frac{\alpha r_2}{\pi\omega} \operatorname{Re} \left[\exp(-i\kappa T_1) \int_0^\infty d\tau_2 \int_0^T \exp(-i(\tau_1 + \tau_2)) \right. \\
&\quad \left. \times \left[\frac{1}{(\tau_1 + \tau_2)^2} - \frac{1}{(\tau_1 + \tau_2 + i\tau_1\tau_2/b)^2} \right] d\tau_1 \right]. \tag{3.83}
\end{aligned}$$

For the third term $n = 2$, $d_2 = 2 \cosh \eta = 2(1 + 2iqT_1T)$ (see Eq.(3.78)) and we have

$$\begin{aligned}
G_2^{-1} &= iT + i \left(1 + \frac{iT}{b} \right) (\tau_1 + \tau_2) - \frac{2}{b} \left(1 + \frac{iT}{2b} \right) \tau_1 \tau_2 \\
&= i(T + \tau_1 + \tau_2) - \frac{2}{b} \tau_1 \tau_2 + \frac{iT}{b} \left[i(\tau_1 + \tau_2) - \frac{\tau_1 \tau_2}{b} \right], \tag{3.84}
\end{aligned}$$

so that

$$\begin{aligned}
\frac{dw_{br3}^{(2)}}{d\omega} &= \frac{\alpha r_2}{\pi\omega} \operatorname{Re} \left[\exp(-i(\kappa T + \kappa T_1)) \int_0^\infty dx_1 \int_0^\infty \exp(-(x_1 + x_2)) \times \right. \\
&\quad \left. \left[\frac{1}{(iT + x_1 + x_2)^2} - \frac{1}{\left[iT + x_1 + x_2 + \frac{2}{b} x_1 x_2 + \frac{iT}{b} (x_1 + x_2 + \frac{x_1 x_2}{b}) \right]^2} \right] dx_2 \right]. \tag{3.85}
\end{aligned}$$

Here we rotate the integration contours over τ_1, τ_2 on the angle $-\pi/2$ and substitute variables $\tau_{1,2} \rightarrow -ix_{1,2}$.

In the case of the weak multiple scattering ($b \gg 1$) neglecting the effect of the polarization of a medium ($\kappa = 1$) and expanding the integrand in Eqs.(3.83) and (3.86) over $1/b$ we have for the probability of radiation

$$\begin{aligned} \frac{dw_{br}^{(2)}}{d\omega} &= 2 \frac{dw_{br1}^{(2)}}{d\omega} + \frac{dw_{br3}^{(2)}}{d\omega} \simeq \frac{2\alpha r_2}{3\pi\omega b} \left[1 - \frac{3}{10b} + \frac{1}{b} G(T) \right], \\ G(T) &= T^2 \int_0^\infty \frac{x^3 \exp(-x)}{(x^2 + T^2)^2} \left[\left(1 - \frac{3x^2}{10T^2} \right) \cos \left(T - 4 \arctan \frac{x}{T} \right) \right. \\ &\quad \left. + \frac{2x}{T} \sin \left(T - 4 \arctan \frac{x}{T} \right) \right]. \end{aligned} \quad (3.86)$$

Note that the main term of the decomposition in Eq.(3.86) is the Bethe-Maximon probability of radiation from two plates which is independent of the distance between plates. This means that in the case considered we have independent radiation from each plate without interference in the main order over $1/b$. The interference effects appear only in the next orders over $1/b$.

In the case of the strong multiple scattering we have $b \ll 1$, $p_c^2 \gg 1$. When the formation length is much longer than the target thickness as a whole ($T \ll b$) we find for the probability of radiation

$$\frac{dw_{br}^{(2)}}{d\omega} \simeq \frac{\alpha r_2}{\pi\omega} \left[(1+b) \left(\ln \frac{2}{b} + 1 - C \right) - 2 \right] \cos(2\kappa T_1). \quad (3.87)$$

In the opposite case $b \ll T \ll 1$ neglecting the effect of the polarization of a medium ($\kappa T_1 \ll 1$) we have

$$\frac{dw_{br}^{(2)}}{d\omega} \simeq \frac{\alpha r_2}{\pi\omega} \left[(1+2b) \left(\ln \frac{T}{b^2} + 1 - C \right) - 2 \right]. \quad (3.88)$$

The case of the strong multiple scattering ($b \ll 1$) for the photon energies where the value $T \geq 1$ is of the special interest. In this case we can neglect the polarization of a medium $\kappa = \bar{\kappa} = 1$, and disregard the terms $\propto \kappa T_1$ in the exponent of the expressions (3.83) and (3.85) since $T_1 \ll 1$. We obtain

as a result

$$\begin{aligned} \frac{dw_{br}^{(2)}}{d\omega} &= 2\frac{dw_{br1}^{(2)}}{d\omega} + \frac{dw_{br3}^{(2)}}{d\omega} \simeq 2\frac{dw_{br}^{(2)}}{d\omega} - \frac{dw_{br3}^{(2)}}{d\omega}, \quad \frac{dw_{br3}^{(2)}}{d\omega} = \frac{\alpha r_2}{\pi\omega} F(T), \\ \text{Re } F(T) &= \int_0^\infty d\tau_2 \int_T^\infty d\tau_1 \frac{1}{(\tau_1 + \tau_2)^2} \exp(-i(\tau_1 + \tau_2)) \\ &= \int_T^\infty \frac{d\tau}{\tau^2} \exp(-i\tau)(\tau - T) = -(\text{ci}(T) + T\text{si}(T) + \cos T), \end{aligned} \quad (3.89)$$

where $\text{si}(z)$ is the integral sine and $\text{ci}(z)$ is the integral cosine. At $T \gg 1$ we have

$$F(T) = -\frac{\cos T}{T^2}. \quad (3.90)$$

Let us turn to the case of large N ($N \geq 3$). If the formation length of the bremsstrahlung is shorter than the distance between plates ($T > 1$) the interference of the radiation from neighboring plates takes place. Using the probability of radiation from two plates (3.86) we obtain in the case of weak multiple scattering ($b \gg 1$)

$$\frac{dw_{br}^{(N)}}{d\omega} \simeq \frac{N\alpha r_2}{3\pi\omega b} \left[1 - \frac{3}{10b} + 2\frac{N-1}{Nb}G(T) \right], \quad (3.91)$$

where for $T \gg 1$ the function $G(T)$ is defined in Eq.(3.86). In the case of strong multiple scattering ($b \ll 1$) and large T we have (compare with Eqs.(3.89) and (3.90))

$$\frac{dw_{br}^{(N)}}{d\omega} \simeq N \left(\frac{dw_{br}^{(1)}}{d\omega} + \frac{\alpha r_2}{\pi\omega b} \frac{N-1}{Nb} \frac{\cos T}{T^2} \right). \quad (3.92)$$

The behavior of the spectral distribution $\omega \frac{dw}{d\omega}$ can be discussed using as an example the case of two plates with the thickness l_1 and the distance between plates $l_2 \geq l_1$ which was analyzed in detail above. For plates with the thickness $l_1 \geq 0.2\%L_{rad}$ and in the energy interval $\omega > \omega_p$, in which the effects of the polarization of a medium can be discarded, the condition (3.74) is fulfilled only for enough high energy ε so that $\omega_p \ll \omega_c$ (see Eqs.(1.5), (2.27)). We study the situation when the LPM suppression of the intensity of radiation takes place for relatively soft energies of photons: $\omega \leq \omega_c \ll \varepsilon$.

For the hard photons $\omega_c \ll \omega < \varepsilon$ the formation length l_{f0} Eq.(1.6) is much shorter than the plate thickness l_1 ($T_1 \gg 1$), the radiation intensity

is the incoherent sum of radiation from two plates and it is independent of the distance between plates. In this interval the Bethe-Maximon formula is valid.

For $\omega \leq \omega_c$ the LPM effect turns on, but when $\omega = \omega_c$ the thickness of plate is still larger than the formation length l_{f0}

$$\frac{l_1}{l_{f0}(\omega_c)} = T_1(\omega_c) \equiv T_c \simeq \frac{2\pi}{\alpha} \frac{l_1}{L_{rad}} > 1, \quad (3.93)$$

so that the formation of radiation takes place mainly inside each of plates. With ω decreasing we get over to the region where the formation length $l_{f0}(\omega_c) > l_1$, but effects of the polarization of a medium are still weak ($\omega > \omega_p$). Within this interval (for $\omega < \omega_{th}$) the main condition (3.74) is fulfilled. To estimate the value ω_{th} we have to take into account the characteristic radiation angles (p_c^2 in Eq.(3.74)), connected with mean square angle of the multiple scattering. Using the definition of the parameter $b = 1/(4qT_1)$ in Eq.(3.80)) we have

$$p_c^2 \leq \frac{1}{b} = \frac{2\pi}{\alpha} \frac{l_1}{L_{rad}} \left(1 - \frac{\ln \varrho_b}{\ln(a_{s2}/\lambda_c)} \right) \simeq T_c \left(1 + \frac{\ln T_c}{2 \ln(a_{s2}/\lambda_c)} \right);$$

$$\omega_{th} = \frac{\omega_c}{T_c(1+p_c^2)} \geq \omega_b = \frac{\omega_c}{T_c(1+T_c)}, \quad (3.94)$$

where the parameter ϱ_b is defined by a set of equations (we rearranged terms in (3.15)):

$$\varrho_b = 1, \quad L_b = L_1 \quad \text{for} \quad 4QL_1T_1 = \frac{2\pi}{\alpha} \frac{l_1}{L_{rad}} \leq 1, \quad q = QL_1;$$

$$4QL(\varrho_b)T_1\varrho_b^2 = \frac{2\pi}{\alpha} \frac{l_1}{L_{rad}} \varrho_b^2 \left(1 - \frac{\ln \varrho_b^2}{L_1} \right) = 1, \quad \text{for} \quad 4QL_1T_1 > 1, \quad (3.95)$$

here $L_1 = \ln(a_{s2}/\lambda_c)^2$. One can show (see discussion after Eq.(3.6) in [18]) that $\omega_{th} \simeq 4\omega_b$. Naturally, $\omega_{th} < \omega_c/T_c$, and when $\omega = \omega_c/T_c$ one has $T_1 = 1$, $l_1 = l_0$. It is seen from Eq.(3.94) that when the value l_1 decreases, the region of applicability of results of this subsection grows.

So, when $\omega < \omega_{th}$ the formation length is longer than the thickness of the plate l_1 and the coherent effects depending on the distance between plates l_2 turn on. For the description of these effects for $T = (1 + l_2/l_1) T_1 \geq 1$ one can use Eq.(3.89). For $T \geq \pi \gg 1$ one can use the asymptotic expansion (3.90) and it is seen that at $T = \pi$ the spectral curve has minimum. Let us note an accuracy of formulas is better when ω decreases, and the description is more accurate for $T \gg T_1$ ($l_2 \gg l_1$).

With further decreasing of the photon energy ω the value T diminishes and the spectral curve grows until $T \sim 1$. When $T < 1$ the spectral curve decreases $\propto \ln T$ according with Eq.(3.88). So, the spectral curve has maximum for $T \sim 1$. The mentioned decreasing continues until the photon energy ω for which $(1 + 2/b)T \sim 1$. For smaller ω the thickness of the target is shorter than the formation length.

The results of numerical calculations are given in Fig.11. The formulas (3.83), (3.85) were used. The spectral curves of energy loss were obtained for the case of two gold plates with the thickness $l_1 = 11.5 \mu m$ with different gaps l_2 between plates. The initial energy of electrons is 25 GeV. The characteristic parameters for this case are:

$$\begin{aligned} \omega_c \simeq 240 \text{ MeV}, \quad T_c \simeq 2.9, \quad b^{-1} \simeq 3.3, \quad \omega_{th} \simeq 80 \text{ MeV}, \\ \omega_p \simeq 3.9 \text{ MeV}, \quad \omega_1 \simeq 30 \text{ keV}, \quad \frac{T}{T_1} \equiv k = \frac{l_1 + l_2}{l_1} = 3, 5, 7, 9, 11. \end{aligned} \quad (3.96)$$

At $\omega > 80$ MeV the radiation process occurs independently from each plate according with theory of the LPM effect given above. The interference pattern appears at $\omega < 80$ MeV where the formation length is longer than the thickness of one plate and the radiation process depends on the distance between plates T . According to Eqs.(3.90), (3.91) the curves 1-5 have minimums at $\omega \simeq \pi\omega_{th}/k$ ($T = \pi$) which are outside of Fig.11 and will be discussed below. In accord with the above analysis the spectral curves in Fig. 11 have the maximums at photon energies $\omega \simeq \omega_{th}/k$ ($T = 1$). These values (in MeV) are $\omega \simeq 27, 16, 11, 9, 7$ for curves 1, 2, 3, 4, 5 respectively. At further decrease of $\omega(T)$ the spectral curves diminish according to Eq.(3.88) and attain the minimum at $\omega_{min} = \omega_{th}/(k(1 + 2/b))$ ($T(1 + 2/b) = 1$). The corresponding values (in MeV) are $\omega \simeq 3.5, 2, 1.4, 1.2$ for curves 1, 2, 3, 4. The least value of $\omega_{min} \simeq 1$ MeV has the curve 5. However, one has to take into account that at $\omega \leq 1.5$ MeV ($\kappa_0^2 = p_c^2 \simeq 2/b$) the contribution of the transition radiation becomes significant. Starting from $\omega \leq 0.6$ MeV the contribution of the transition radiation dominates.

The approach presented in this subsection is applicable in the interval of photon energies where effects of the polarization of a medium are essential. It includes also the soft part of the LPM effect. For the case given in Fig.11 our results are given up to $\omega_{max} \sim 20$ MeV. On the other hand, in [61] the hard part of the LPM effect spectrum was analyzed where one can neglect the effects of the polarization of a medium ($\omega > 5$ MeV for the mentioned case). Although here (as in [20]) in and in [61] the different methods are used, the results obtained in overlapping regions are in a quite reasonable agreement among themselves.

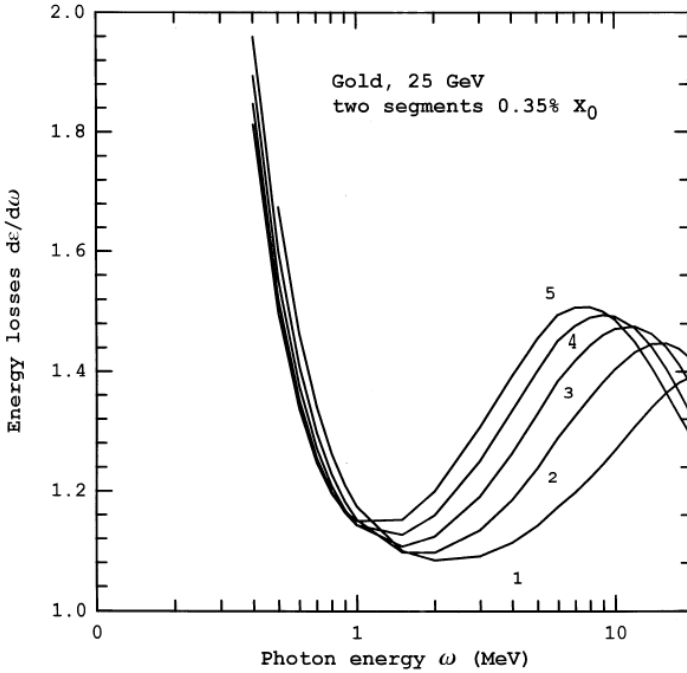


Figure 11: The energy losses spectrum $\frac{d\varepsilon}{d\omega}$ in units $\frac{2\alpha}{\pi}$, in the target consisting of two gold plates with thickness $l_1 = 11.5 \mu m$ for the initial electrons energy $\varepsilon=25$ GeV.

Curve 1 is for distance between plates $l_2 = 2l_1$;

Curve 2 is for distance between plates $l_2 = 4l_1$;

Curve 3 is for distance between plates $l_2 = 6l_1$;

Curve 4 is for distance between plates $l_2 = 8l_1$;

Curve 5 is for distance between plates $l_2 = 10l_1$.

It is interesting to discuss behavior of the spectral curves obtained in [61] from the point of view of our results. We consider the low value l_1 (T_c is not very large) and a situation when corrections to the value b in Eq.(3.94) which neglected in [61] are less than 20%. This leads to the difference in results less than 10%. We concentrate on the case of gold target with the total thickness $Nl_1 = 0.7\% L_{rad}$. The case $N = 1$ where $T_c = 5.8$, $b^{-1} = 7.3$, $\omega_c \simeq 240$ Mev, $\omega_{th} = 4\omega_c/(T_c(1 + T_c)) \simeq 24$ MeV was considered in detail in [61] (see Sec. 2). The curves in figures in [61] are normalized on the Bethe-Heitler probability of radiation (no the Coulomb corrections),

i.e. they measured in units $\alpha r_2 T_c / (3\pi)$. In the region where our results are applicable $\omega < \omega_{th} \simeq 24$ MeV in Fig.2 of [61] ($G = 0$) one can see plateau the ordinate of which is 10% less than calculated according with Eq.(3.82). The case of two plates ($T_c \simeq b^{-1} \simeq 3$, $\omega_c \simeq 240$ MeV, $\omega_{th} \simeq \omega_c / T_c = 80$ MeV) is given in Fig.3 of [61]. The lengths of the gaps are the same as in our Fig.11, except $k = 9$. The positions and ordinates of the minimums and the maximums in the characteristic points ($\omega \simeq \pi\omega_{th}/k$ for minimums and $\omega \simeq \omega_{th}/k$ ($T = 1$) for maximums, see above) as well as behavior of the spectral curves is described quite satisfactory by our formulas (see e.g. asymptotic Eqs.(3.87)-(3.90)).

3.7 Comparison of the results obtained in different papers

As it was said above, Migdal have calculated the probability of the bremsstrahlung and pair creation in the logarithmic approximation [2]. This result, now considered as classic one, was confirmed in the most of subsequent calculation.

We developed the method of calculation [17, 18, 19, 20] which goes beyond the logarithmic approximation. The formula (2.17) gives the spectral distribution of the probability of radiation which coincides formally with the probability calculated by Migdal (Eq.(49) in [2]). However, here Coulomb corrections are included into parameter ν in contrast to [2], [3]. As it was noted, the parameter ϱ_c entering into the parameter ν (see Eqs.(2.17), (2.12) and (2.10)) is defined up to the factor ~ 1 , what is inherent in the logarithmic approximation. However, we calculated also the next term of the decomposition over $v(\boldsymbol{\varrho})$ (an accuracy up to the "next to leading logarithm") and this permits to obtain the result which is independent of the parameter ϱ_c . It was shown that the definition of the parameter ϱ_c minimizes corrections to Eqs.(2.17) and (2.43) practically for all values of the parameter ϱ_c . It should be emphasized also that here the Coulomb corrections are included into the parameter ν in contrast to [3]. Moreover, the procedure of fine tuning presented above (see [17]) permits one (after adding the term $dW_1/d\omega$ (2.22)) to obtain more accurate expression for the probability of radiation, which has power accuracy in the limit of weak multiple scattering, see (2.29), while the probability calculated by Migdal [2] has logarithmic accuracy only in the mentioned limit. The interrelation between the main term $dW_c/d\omega$ and the first correction $dW_1/d\omega$ depends essentially on fine tuning procedure which was chosen, as it was just said, in a such way that minimize the value of the first correction. For example, one can see that the maximal value of $dW_1/d\omega$

is of the order 7 % of the main term for all four spectral curves shown in the Fig.3. This means that in our case there are more rigid requirements on fine tuning procedure than used by Migdal.

In the approach used by Blankenbecler and Drell (BD) [22] the scattering process was considered in the second approximation of the eikonal formalism and an analysis of scattering in medium was based on the model of a random medium. The radiation was calculated for all possible paths and averaged. One advantage of this approach is that it treats naturally finite thickness targets. There are a few short-comings in the BD approach. The Gaussian distribution of scattered electrons was obtained by Migdal [2] as a solution of the Fokker-Planck equation, while in BD approach this is an input. Actually there are deviations from the Gaussian distribution, see end of Sec.3.3. The calculation of the probability $dW/d\omega$ is quite unwieldy in BD approach and general formula for $dW/d\omega$ (Eq.(5.32) in [22]) is written down in an implicit form only, and the functions $\eta(z_2, z_1, l)$ and $\lambda(z_2, z_1, l)$ in the mentioned formula have to be calculated in the each case separately. This means that comparison of BD probability with that calculated by Migdal can be done in limiting cases only. In the case of weak multiple scattering the probability in [22] coincides with the Bethe-Heitler probability taken with logarithmic accuracy (just as in Migdal paper [2]). However, in the limit of the strong LPM effect, where the probability of radiation is given by Eqs.(2.17) and (2.31) above and which coincides with obtained by Migdal Eq.(52) in [2] (if one omits the Coulomb corrections included into the parameter ν_0), the probability calculated by BD (the term with R_2) differs from (2.31) by factor $\sqrt{3\pi/8}=1.0854$. The origin of this discrepancy was not analyzed in [22].

In the paper of R.Baier, Dokshitzer, Mueller, Peigne, and Schiff (BDMPS) [25] the multiple scattering of high-energy electrons off a large number of scatterers (presented as a screened Coulomb potential) is analyzed within eikonal formalism. Radiation of soft photons only is included using the classical current approach, although this approach gives no significant simplification for the problem under consideration. All the results are obtained within logarithmic accuracy. No general formula of the type of Eq.(2.18) is written down. In the "Bethe-Heitler limit" the result of [25] does not completely match the standard Bethe-Heitler formula. Since the method used consists in direct summation over scatterers it naturally included the consideration of a target of finite thickness. For thin target ($T \leq l_{f0}$) the result of [25] is similar to logarithmic term in Eq.(3.18) where $r_2 = 2$ for soft photons. The explicit formula for radiation spectrum is given in [25] in the limit of strong LPM effect where it is similar to Eq.(2.32) if $\omega \ll \varepsilon$ and the Coulomb corrections are omitted.

Note that in Migdal papers [2], [3] and in our papers the kinetic equation is the basic element of the used methods while in the both papers [25] and [22] the consideration does not include the kinetic equation. Due to this feature the calculations in the both papers [25] and [22] are more cumbersome and no general formulas for radiation spectra are obtained.

A path integral method is applied successfully for analysis of multiple scattering (see e.g. [63]). Zakharov [23], [24] is used this method to study of the LPM effect. Using a transverse Green function based on a path integral he succeeded in reduction of the problem to the two dimensional Schrödinger equation, i.e. he rederived equation a la Eq.(2.3), which was obtained earlier in [9]. The probability of radiation was calculated (see Eq.(19) in [23]) within logarithmic accuracy (as in Migdal papers [2] and [3]) although it is written down in a more cumbersome form. The procedure of fine tuning so important for Migdal calculation [2] is oversimplified in [23]. For earlier attempt to do study of the LPM effect in a such way see [63]. The formalism used in [23] has the same region of validity as in Migdal's papers [2], [3] and in our papers [9], [17] and [18] in spite of claims about "rigorous treatment of the LPM effect". The developed formalism allows naturally to consider the LPM effect in finite thickness targets [24]. As an example the calculation of spectral intensity of radiation is given for electron energy $\varepsilon = 25$ GeV and gold target with thickness $l = 0.7\%L_{rad}$. This calculation was carried out numerically with the complete potential (see Eq.(2.3)) outside of scope of logarithmic approximation. The Coulomb corrections were discarded as well as a multiple photon radiation. After arbitrary diminishing of calculated value by 7% it was found very good agreement with a portion of data (in the region of the LPM drop up to beginning of plateau). Actually this diminishing should be attributed to Coulomb corrections found in [17] (for details see [18] and below in Sec. 3.10). More late results of Zakharov see in [64].

3.8 Qualitative behavior of the spectral intensity of radiation

We consider the spectral intensity of radiation for the energy of the initial electrons when the LPM suppression of the intensity of radiation takes place for relatively soft energies of photons: $\omega \leq \omega_c \ll \varepsilon$:

$$\nu_0(\omega_c) = 1, \quad \omega_c = \frac{16\pi Z^2 \alpha^2}{m^2} \gamma^2 n_a \ln \frac{a_s 2}{\lambda_c}, \quad (3.97)$$

see Eqs.(2.3), (2.12), (2.24)-(2.27). This situation corresponds to the experimental conditions [12, 13, 14, 15].

The ratio of the thickness of the target l and the formation length of radiation $l_f(\omega)$ (1.5) is an important characteristics of the process. In Eq.(1.5) both the multiple scattering and the polarization of a medium are taken into account. This ratio may be written as

$$\beta(\omega) \equiv \frac{l}{l_f(\omega)} = T(\nu_0 + \kappa) \simeq T_c \left[\frac{\omega}{\omega_c} + \sqrt{\frac{\omega}{\omega_c}} + \frac{\omega_p^2}{\omega\omega_c} \right],$$

$$T = \frac{l\omega}{2\gamma^2}, \quad \omega_p = \omega_0\gamma, \quad T_c \equiv T(\omega_c) \simeq \frac{2\pi}{\alpha} \frac{l}{L_{rad}}, \quad (3.98)$$

where we put that $\nu_0 \simeq \sqrt{\frac{\omega_c}{\omega}}$. Below we assume that $\omega_c \gg \omega_p$ which is true under the experimental conditions.

If $\beta(\omega_c) \gg 1$ ($T_c \gg 1$) then at $\omega \geq \omega_c$ a target is thick and one has the LPM suppression for $\omega \leq \omega_c$. There are two opportunities depending on the minimal value of the parameter β :

$$\beta_m \simeq \frac{3}{2}T_c\sqrt{\frac{\omega_1}{\omega_c}}, \quad \omega_1 = \omega_p \left(\frac{4\omega_p}{\omega_c} \right)^{1/3}, \quad \beta_m \simeq 2T_c \left(\frac{\omega_p}{\omega_c} \right)^{2/3}. \quad (3.99)$$

If $\beta_m \ll 1$ then for photon energies $\omega > \omega_1$ it will be ω_b such that

$$\beta(\omega_b) = 1, \quad \omega_b \simeq \frac{\omega_c}{T_c^2} \quad (3.100)$$

and for $\omega < \omega_b$ the thickness of a target becomes smaller than the formation length of radiation so that for $\omega \ll \omega_b$ the spectral distribution of the radiation intensity is described by Eqs. (3.36), (3.40). Under these conditions for $4k = \nu_0^2 T = T_c \gg 1$ the spectral curve has a plateau

$$\frac{dI}{d\omega} = \frac{2\alpha J}{\pi} = \text{const} \quad (3.101)$$

in accordance with Eq.(3.20). Under conditions $\kappa T \ll 1, \omega < \omega_b$ the spectral intensity of radiation is independent of photon energy ω . It should be noted that due to smallness of the coefficients in expression for δ Eq.(3.38), such behaviors of the spectral curve begins at $\omega < \omega_{th} = 4\omega_b \simeq 4\omega_c/T_c^2$. It will continue until photon energies where one has to take into account the polarization of a medium and connected with it a contribution of the transition radiation.

At $\beta_m \gg 1$ a target remains thick for all photon energies and radiation is described by formulae of Sections 2.2 and 2.6. In this case at $\omega \ll \omega_c$ ($\nu_0 \gg 1$)

and $\omega \gg (\omega_p/\omega_c)^{1/3} \omega_p$ ($\nu_0 \gg \kappa$) the spectral intensity of radiation formed inside a target is given by Eqs.(2.17) and (2.22) and the contribution of the boundary photons is given by Eq.(3.12).

It is important to include also the contribution of boundary photons. Since the contribution into the spectral intensity of radiation from a passage of the electron inside the target ($\propto T$) is diminishing and a contribution of the boundary photons is increasing with ω decrease, the spectral curve has a minimum at $\omega = \omega_m$. The value of ω_m may be estimated from equations (see (2.31), (3.36)-(3.37))

$$\begin{aligned} \frac{d}{d\omega} \left(\frac{\nu_0 T}{\sqrt{2}} + \ln \nu_0 + \frac{\pi^2 \sqrt{2} \kappa}{24 \nu_0} \right) &= 0, & \frac{\nu_0 T}{\sqrt{2}} &\simeq 1 + \frac{\pi^2 (\kappa - 1)}{4\sqrt{2} \nu_0}, \\ T_c &\simeq \left(\frac{2\omega_c}{\omega_p} \right)^{1/2} \sqrt{x} + \frac{\pi^2}{4} x^2, & x &= \frac{\omega_p}{\omega}. \end{aligned} \quad (3.102)$$

When the value of T_c is high enough, the solution of Eq.(3.102) does not satisfy the condition $\nu_0 \gg \kappa$ and in this case the equation (3.102) ceases to be valid. For determination of ω_m in this case we use the behavior of the spectral intensity of radiation at $\kappa \gg \nu_0$. In this case the contribution into radiation from inside passage of the target is described by Eq.(2.124) while the radiation of the boundary photons reduces to the transition radiation and its contribution is given by Eq.(3.10). Leaving the dominant terms ($\nu_0^2 T$ is ω independent) we have

$$\frac{d}{d\omega} \left(\frac{\nu_0^2 T}{3\kappa} + \ln \kappa \right) = 0, \quad \frac{\nu_0^2 T}{3\kappa} = 1, \quad \kappa_m = \frac{T_c}{3}, \quad \omega_m \simeq \sqrt{\frac{3}{T_c}} \omega_p. \quad (3.103)$$

Since the value $\pi^2/12 \simeq 0.8$ is of the order of unity, the solution of (3.102) at $\kappa_m \gg \nu_0$ differs only slightly from ω_m . Because of this, if the condition $2T_c(\omega_p/\omega_c)^{2/3} \gg 1$ is fulfilled, the position of the minimum is defined by Eq.(3.102). The formulas (3.102) and (3.103) show the position of a minimum of the spectral intensity curve which is the sum of contributions of radiation inside a target and boundary radiation. Due to the LPM effect the intensity of radiation inside a target diminishes with ω decreasing. However at low ω the contribution of the boundary radiation is sharply increasing and this results in appearance of a minimum of spectral curve. Eq.(3.102) gives its position at small T_c while Eq.(3.103) gives minimum position at large T_c .

If $\beta(\omega_c) = 2T_c \ll 1$ then at $\omega = \omega_c$ a target is thin and the Bethe-Maximon spectrum of radiation which is valid at $\omega \gg \omega_c$ ($\frac{dI(\omega)}{d\omega} = \text{const}$)

will be also valid at $\omega \leq \omega_c$ in accordance with Eq.(3.40) since $4k = \nu_0^2 T = T_c \ll 1$. This behavior of the spectral curve will continue with ω decrease until photon energies where a contribution of the transition radiation become essential. In this case the spectral distribution of radiation has the form (3.46) for all ω

$$\frac{d\omega}{d\omega} = \frac{d\omega_{tr}}{d\omega} + \cos(\kappa T) \frac{d\omega_{BM}}{d\omega}, \quad (3.104)$$

Since for soft photons ($\omega \ll \varepsilon$)

$$\frac{dI}{d\omega} = \frac{2\alpha}{\pi} \left[J_5^{(2)} + \frac{T_c}{3} \left(1 + \frac{1}{6L_1} \right) \cos(\kappa T) \right] \quad (3.105)$$

and $T_c/3 \ll 1$ a contribution of the transition radiation become visible already at $\kappa T \ll 1$. For $\omega > \omega_c$ ($T_c \ll 1$) the probability of radiation is defined by Eqs.(3.33)-(3.34). In this case a considerable distinction from Bethe-Maximon formula will be in the region $\omega \sim \omega_c/T_c$.

As well known, for soft photons ($\omega \ll \varepsilon$) the Bethe-Maximon formula for the spectral intensity of radiation doesn't depend on a photon energy as well. So, the ratio of these spectral intensities (see Eqs. (3.40) and (3.43)) is an important characteristics of the phenomenon under consideration:

$$R = \frac{dI_{th}}{d\omega} / \frac{dI_{BM}}{d\omega} = \frac{6}{T_c} \left(1 + \frac{1}{6L_1} \right)^{-1} \int_0^\infty d\varrho \varrho K_1^2(\varrho) [1 - \exp(-V(\varrho)T)]. \quad (3.106)$$

For $T_c \ll 1$ one has $R = 1$ and for $T_c \gg 1$ one has using expression (3.18)

$$R \simeq \frac{3}{T_c} \left(1 + \frac{1}{2k} \right) [\ln 4k + 1 - C] - 2 + \frac{C}{L_t}. \quad (3.107)$$

For estimates one can put with a good accuracy $4k \simeq T_c$ and $L_t \simeq L_1$.

There is, in principle, an opportunity to measure the electron energy (in region of high energies) using the LPM effect. For this one can measure the spectral curve on a target with thickness a few percent of L_{rad} and compare the result with the theory prediction.

Existence of the plateau of the spectral curve in a region of photon energies where a target is thin was first found in [52] within Migdal approach (quantum theory). Recently this item was discussed in [59] (in classical theory), [22] and [24].

3.9 Experimental investigation of the LPM effect

Bremsstrahlung or pair creation suppression can be studied with high energy electron or photon beams. Because pair creation suppression requires photons

with $\omega > \omega_e$ (see Eq.(2.48)), beyond the reach of current accelerators, pair creation has been studied only with cosmic rays, with consequently very limited statistics. The best suppression studies have used electron beams at accelerators. Besides the LPM effect, these beams have been used to study dielectric suppression.

3.9.1 Early experiments

The first tests of LPM suppression came shortly after Migdal's appeared. These were cosmic rays experiments with high energy photons ($\omega > 1$ TeV) and studied the depth of pair conversion in a dense target [65]-[68], see also more recent [69]. All of the air shower experiments suffered from some common problems, by far the largest being the poor statistics (high energy photons are not common). Uncertainties in the photon spectrum complicated the analysis. So, these experiments are at best qualitative verification of the LPM effect.

The first accelerator based study of LPM effect was done in Serpukhov [70]. Bremsstrahlung photons from 40 GeV electrons hitting dense target were detected in an sodium iodide calorimeter. Photons with energy $20 \text{ MeV} < \omega < 70 \text{ MeV}$ emitted from carbon, aluminium, lead and tungsten targets were analyzed. It were several limitations: because the electron beamline was in air, and included a few scintillation counters used as triggers, there was a significant light element bremsstrahlung background, it was also background due to muon contamination in used beam. The results agreed with Migdal's predictions.

3.9.2 SLAC E-146

In 1992, the E-146 collaboration at Stanford Linear Accelerator Center (SLAC) proposed the experiment to perform a precision measurement of LPM suppression, and study dielectric suppression. The experimental setup was conceptually similar to the Serpukhov experiment, but heavily optimized to minimize background. The experimenters collected a very large data set. The experiment was approved in December, 1992, and took data in March-April, 1993.

Fig.12 shows a diagram of the experiment. An 8 or 25 GeV electron beam entered SLAC End Station A and passed through a thin target. The target used are listed in Table 1. The beam was then bent downward by a 3.25 T-m dipole magnet, through six wire chamber planes which measured electron momenta and into an array of lead glass blocks which accurately counted

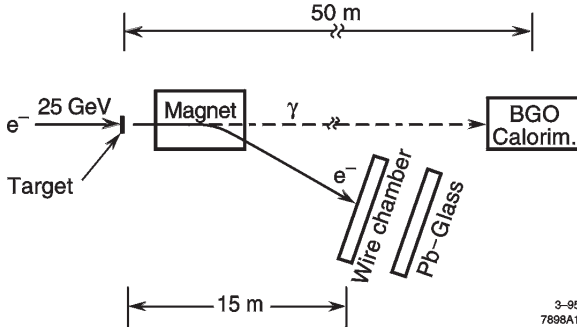


Figure 12: Diagram of the SLAC E-146 apparatus, from [15].

electrons. Produced photons continued downstream 50 meters into a BGO calorimeter array. To minimize backgrounds, the electron path visible to the calorimeter and the photon flight path were kept in vacuum.

The calorimeter comprised 45 BGO crystals in a 7 by 7 array with missing corners; each crystal was 2 cm square by 20 cm (18 L_{rad}) deep. This segmentation provided excellent spatial resolution for separating synchrotron radiation from bremsstrahlung photons. Scintillation light from each crystal was measured separately by a photomultiplier tube (PMT). The light yield was about 1 detected photoelectron per 30 keV, providing good statistics down to 200 keV. The calorimeter resolution was about 8% (FWHM) at 100 MeV, with a nonlinearity of about 3%. The calorimeter temperature was monitored throughout the experiment, and the data corrected using the measured drifts.

The collaboration used several methods to calibrate the calorimeter, to obtain both an absolute energy calibration and a crystal to crystal inter-calibration. The primary tools for measuring the relative gain were nearly vertical cosmic-ray muons, selected by a plastic scintillator paddle trigger; the gain in each crystal channel was adjusted to produce equal signals.

The absolute energy scale of the calorimeter was primarily determined using a 500 MeV electron beam. This calibration was checked with data by comparing the electron energy loss, measured by the wire chamber, with the calorimeter energy measurement. Because of the steeply falling photon spectrum and the non-Gaussian errors in the momentum measurement, this was useful only as a cross-check.

Because of the large bremsstrahlung cross section, the experiment required a beam intensity of about 1 electron per pulse. Because it would have been very uneconomical to use the SLAC linac to produce a single electron

Table 1. The characteristics of the LPM effect.

Listed are the charge of nucleus Z , the density ρ , the radiation length L_{rad} , ε_e (see Eq.(2.26)), ω_e (see Eq.(2.48)), ω_c Eq.(2.27)), ω_p Eq.(2.115)), l is the target thickness in percent of the radiation length L_{rad} (all photon energies ω_c and ω_p are for the electron energy $\varepsilon = 25$ GeV).

Material	Z	$\rho(g/cm^3)$	$L_{rad}(cm)$	$\varepsilon_e(TeV)$	$\omega_e(TeV)$	$\omega_c(MeV)$	$\omega_p(MeV)$	l
C	6	2.2	18.8	144	580	4.3	1.5	2.1, 6
Al	13	2.7	8.9	68	270	9.2	1.6	3.5, 6
Fe	26	7.87	1.76	14	56	46	2.7	2.8, 6.1
Pb	82	11.35	0.56	4.3	17.2	150	3.0	2.7
W	74	19.3	0.35	2.7	10.8	230	3.9	2.7, 6.4
U	92	18.95	0.32	2.5	10	250	3.8	2.2, 4.2
Au	79	19.32	0.33	2.6	10	240	3.9	0.1, 0.7
Water	-	1	36.1	277	1100	2.6	-	-
Std.rock	11	2.65	10.0	77	300	8.1	-	-

per pulse, the collaboration developed a method to run parasitically during SLAC linear collider (SLC) operations, by using the off-axis electrons and positrons that are removed from the beam by scrapers in the beam switchyard.

Normally, about 10% of the SLC beam is scraped away by collimators in the last 200 meters of the linac. The collimators are only $2.2 L_{rad}$ thick, so a usable flux of high energy photons emerged from their back and sides. Some of these photons travel down the beampipe, past the magnets that bend the electrons and positrons into the SLC arcs, and into the beam switchyard, where a $0.7 L_{rad}$ target converted them into e^+e^- pairs. Some of the produced electrons were captured by the transport line optics, collimated, selected for energy, and transported into the end station.

The beam worked well, with the size, divergence and yield matching simulations. At 8 and 25 GeV, the beam intensity was adjustable up to about 100 electrons/pulse. At 1 electron/pulse, the beam emittance was limited by the optics, with a typical momentum bite of $\Delta p/p < 0.5\%$. The beam optics were adjusted to minimize the photon spot size at the calorimeter; spot sizes there were typically a few mm in diameter. The beam spot was stable enough and small enough that beam motion was not a major source of error.

Data was collected and written to tape on every beam pulse (120 Hz). With the beam intensity averaging 1 electron/pulse, over 500,000 single electron events could be collected per eight hour shift. The experiment ran for a month, and good statistics were obtained with a variety of targets.

3.9.3 Data Analysis and Results

The E-146 analysis selected events containing a single electron, as counted by the lead glass blocks. The photon energy was found by summing the energies of hit BGO crystals using a cluster-finding algorithm. The cluster finding reduced the noise level by eliminating random noise hits.

The experiment studied the photon energy range from 200 keV to 500 MeV, a 2500:1 dynamic range. This exceeded the linear dynamic range of the PMTs and electronics, so data was taken with two different PMT gains, varied by changing the PMT high voltage. The high- ω running corresponded to 1 count per 100 keV and the low- ω running was 1 count per 13 keV, with the relative gains calibrated with the cosmic ray data. The high- ω data was used for $5 \text{ MeV} < \omega < 500 \text{ MeV}$ while the low- ω data covered $200 \text{ keV} < \omega < 20 \text{ MeV}$, with a weighted average used in the overlap region.

These two sets of data differed in several significant ways. There were large differences in calorimeter behavior and background levels, as well as the physics topics. For $\omega > 10 \text{ MeV}$, photons largely interacted by pair conversion, producing an electromagnetic shower. Showers typically deposited energy in 3-20 crystals in the calorimeter. For $\omega < 2 \text{ MeV}$, the photons interacted by single or multiple Compton scattering. Usually, Compton scattering deposited energy in a single calorimeter crystal. Sometimes, the photon Compton scattered once and then escaped from the calorimeter, taking some energy with it. This added a low energy tail to the energy deposition curve. While the high- ω data had very low backgrounds, the low- ω data had significant backgrounds due to synchrotron radiation, at least for the 25 GeV beams. Finally, the two data sets emphasize different physics, with the high- ω data most relevant for the LPM effect, with the low- ω data more useful for studying dielectric suppression. For these reasons, the two sets of data were analyzed quite independently, and combined in the final histograms.

3.9.4 Backgrounds and Monte Carlo

One advance introduced by E-146 was the use of a detailed, high statistics Monte Carlo. The main purpose of the Monte Carlo was to understand multi-photon pileup. This occurred when a single electron passing through the target interacted twice, radiating two photons. The Monte Carlo also simulated photon absorption in the target [14] and modelled the detector. Transition radiation was treated as an integral part of the physics, rather than a background.

The Monte Carlo tracked electrons through the material in small steps, allowing for the possibility of bremsstrahlung in the material and transition

radiation at each edge. LPM suppression was implemented using simple formulae with dielectric suppression incorporated using results of Migdal [2],[3]. For consistency, the Bethe-Heitler cross sections were included by turning LPM suppression off from Migdal's formulae, rather than using a more modern formula.

The expected and measured backgrounds were both small. The major background was synchrotron radiation from the spectrometer magnet. Synchrotron radiation was significant for $\omega < 1$ MeV in the 25 GeV data.

Non-target related backgrounds were measured with target empty runs. The backgrounds were typically 0.001 photons with $\omega > 200$ keV per electron, much less than the number of bremsstrahlung photons with $\omega > 200$ keV per electron. Target related backgrounds were expected to be small; photonuclear interaction rates are small, and the events are unlikely to appear in the E-146 analysis.

3.9.5 Results

Because of the high statistics and low background, the E-146 data allowed for detailed tests of the theory; photon spectra could be easily compared with different predictions.

Figures 13-16 show a sampling of E-146 results. Photon energies were histogrammed logarithmically, using 25 bins per decade of energy, so that each bin had a fractional width $\Delta\omega \sim 10\%\omega$. The logarithmic scale is needed to cover the 2500:1 energy range. The logarithmic binning $dN/d\ln\omega = \omega dN/d\omega$ was chosen so that a $1/\omega$ Bethe-Heitler (BH) spectrum will have an equal number of events in each bin, simplifying the presentation and statistical analysis.

Fig.13 shows the photon spectrum (points with error bars) from 8 and 25 GeV electrons passing through 2% and 6% L_{rad} carbon targets. Also shown are 3 Monte Carlo (MC) histograms. The top histogram (dashed line) is a simulation of BH bremsstrahlung plus conventional transition radiation; the transition radiation is substantial below $\omega_p \simeq 1.4$ (0.4) MeV at 25 (8) GeV (see (2.115)). Above ω_p , the spectrum is sloped because there is a finite probability of a single electron interacting twice while passing through the target. Because the calorimeter cannot separate single photons from multiple hits, but instead measures total energy deposition, this depletes the low energy end of the spectrum (shown here), while increasing the number of calorimeter overflows. In the absence of multiple interactions, the Bethe-Heitler spectrum would be flat at $(1/L_{rad})dN/d\ln\omega = 4/3 \ln(\omega_{max}/\omega_{min}) = 0.129$ for bins with logarithmic widths $\omega_{max}/\omega_{min} = 10^{1/25} = 1.096$. The

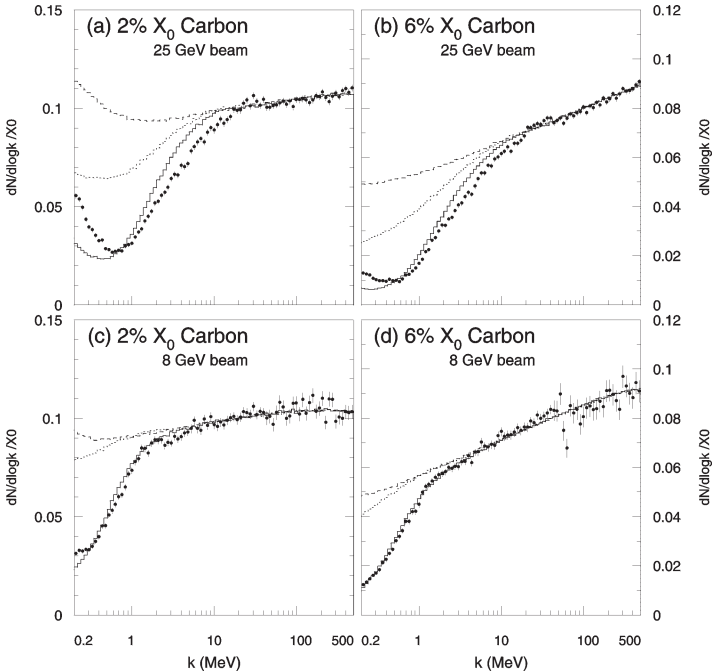


Figure 13: Comparison of data from SLAC-E-146 with MC predictions for 200 keV to 500 MeV photons from 8 and 25 GeV electrons passing through 2% and 6% L_{rad} carbon targets. The cross sections are given as $dN/d(\ln \omega)/L_{rad}$ where N is the number of events per photon energy bin per incident electron, for (a) 2% L_{rad} carbon and (b) 6% L_{rad} carbon targets in 25 GeV electron beams, while (c) shows the 2% L_{rad} carbon and (d) the 6% L_{rad} carbon target in an 8 GeV beam. Three Monte Carlo curves are shown. The solid line includes LPM and dielectric suppression of bremsstrahlung, plus conventional transition radiation. Also shown are the Bethe-Heitler plus transition radiation MC (dashed line) and LPM suppression only plus transition radiation (dotted line). Adapted from [15].

bin heights directly scale with the bin fractional width $\Delta\omega/\omega$.

To understand the qualitative features of data in Fig.13 it is helpful to use analysis made in previous subsection. For photon energy $\omega = \omega_c$, which is thickness independent, (see Eq.(3.97) and Table 1) the LPM effect is well developed. The effect becomes visible for photon energy $\omega_{vis} \sim (2 \div 3)\omega_c$. At electron energy $\varepsilon = 25$ GeV for carbon one has $\omega_c = 4.3$ MeV and

$\omega_{vis} \sim (9 \div 13)$ MeV, while for $\varepsilon = 8$ GeV one has $\omega_{vis} \sim (0.9 \div 1.3)$ MeV. The minimum of the spectral curve is situated (see Eq.(3.102)) at $\omega = \omega_m \sim \sqrt{3/T_c}\omega_p$. For target thickness $l = 2\%L_{rad}$ one has $T_c = 17.2$ and for $\varepsilon = 25$ GeV one has $\omega_p = 1.5$ MeV and $\omega_m \sim 0.4\omega_p \sim 0.6$ MeV while for $l = 6\%L_{rad}$ the value of ω_m is $\sqrt{3}$ times smaller: $\omega_m \sim 0.4$ MeV. For $\varepsilon = 8$ GeV one has for $l = 2\%L_{rad}$: $\omega_m \sim 0.2$ MeV (on the edge of figure) while for $l = 6\%L_{rad}$ the value $\omega_m \sim 0.12$ MeV is outside of figure. These estimates are in a reasonable agreement with data in Fig.13.

The dotted histogram is a simulation that includes LPM suppression, but not dielectric suppression, plus conventional transition radiation. The solid line includes LPM and dielectric suppression, along with conventional transition radiation. This was the 'standard' E-146 choice for simulation.

Both suppression mechanisms are required to approach the data. However, there are still significant discrepancies between the LPM plus dielectric MC and the data. Below 800 keV (350 keV) for 25 (8) GeV beams, the upturn in the data may be residual background, especially synchrotron radiation. The difference at higher photon energies is more complex, and will be discussed in the following subsection.

Fig.14 shows the spectrum from 8 and 25 GeV electrons passing through 3% and 6% L_{rad} aluminum targets. The same three simulations are shown. Because aluminum has twice the Z of carbon, LPM suppression is considerably enhanced, with ω_c (see Table 1) 9 MeV and 900 keV at 25 and 8 GeV respectively. Because the density is similar to carbon, dielectric suppression is similar. The agreement between the data and the standard curve is better than with carbon.

To understand the qualitative features of data in Fig.14 it is helpful to use analysis made in previous subsection just as it was done for carbon. The LPM effect becomes visible for photon energy $\omega_{vis} \sim (2 \div 3)\omega_c$. At electron energy $\varepsilon = 25$ GeV for aluminum one has $\omega_c = 9.2$ MeV and $\omega_{vis} \sim (20 \div 30)$ MeV, while for $\varepsilon = 8$ GeV one has $\omega_{vis} \sim (2 \div 3)$ MeV. The minimum of the spectral curve is situated (see Eq.(3.102)) at $\omega = \omega_m \sim \sqrt{3/T_c}\omega_p$. For target thickness $l = 3\%L_{rad}$ one has $T_c = 25.8$ and for $\varepsilon = 25$ GeV one has $\omega_p = 1.6$ MeV and $\omega_m \sim 0.6$ MeV while for $l = 6\%L_{rad}$ the value of ω_m is $\sqrt{2}$ times smaller: $\omega_m \sim 0.4$ MeV. For $\varepsilon = 8$ GeV one has for $l = 3\%L_{rad}$: $\omega_m \sim 0.2$ MeV which is on the edge of the figure. These estimates are in a reasonable agreement with data in Fig.14.

Fig.15 shows the spectrum from 8 and 25 GeV electrons passing through 3% and 6% L_{rad} iron targets, with just the 'standard' MC. The general slope of the data matches the simulation, but the behavior at higher ω for 25 GeV beams is quite different.

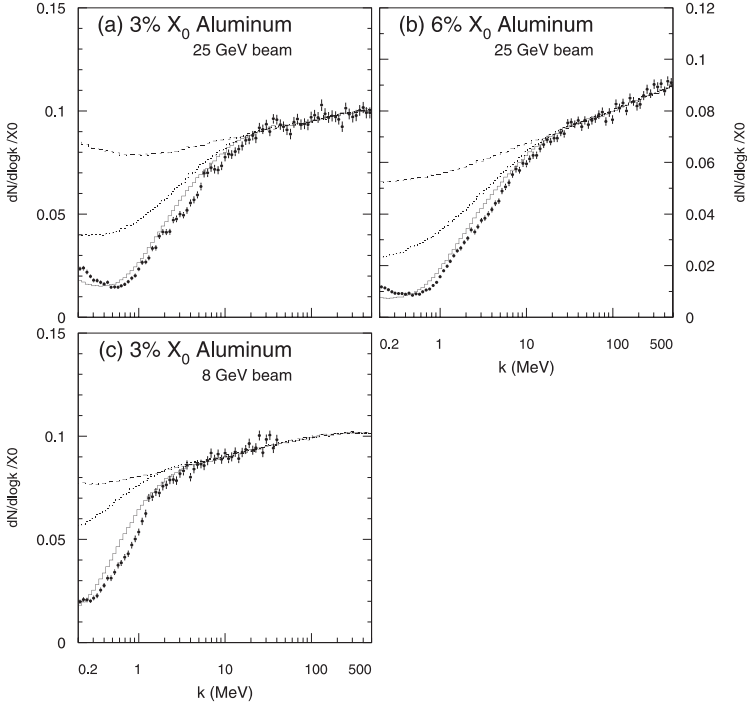


Figure 14: Comparison of data from SLAC-E-146 with Monte Carlo predictions for 200 keV to 500 MeV photons from 8 and 25 GeV electrons passing through 3% and 6% L_{rad} aluminum targets. The format and Monte Carlo curves are the same as in Fig.12. Adapted from [15].

To understand the qualitative features of data in Fig.15 we perform an analysis just as it was done for carbon and aluminum. At electron energy $\varepsilon = 25$ GeV for iron one has $\omega_c = 46$ MeV and $\omega_{vis} \sim (90 \div 140)$ MeV, while for $\varepsilon = 8$ GeV one has $\omega_{vis} \sim (9 \div 14)$ MeV. The minimum of the spectral curve is situated (see Eq.(3.102)) at $\omega = \omega_m \sim \sqrt{3/T_c} \omega_p$. For target thickness $l = 3\%L_{rad}$ one has $T_c = 25.8$ and for $\varepsilon = 25$ GeV one has $\omega_p = 2.7$ MeV and $\omega_m \sim 0.9$ MeV while for $l = 6\%L_{rad}$ the value of ω_m is $\sqrt{2}$ times smaller: $\omega_m \sim 0.7$ MeV. For $\varepsilon = 8$ GeV one has for $l = 3\%L_{rad}$: $\omega_m \sim 0.3$ MeV. These estimates are in a reasonable agreement with data in Fig. 15.

Fig.16 shows the bremsstrahlung spectra in uranium targets. Uranium is dense enough that LPM suppression is dominant, and the E-146 collaboration compared simulations with dielectric and LPM suppression, plus conventional

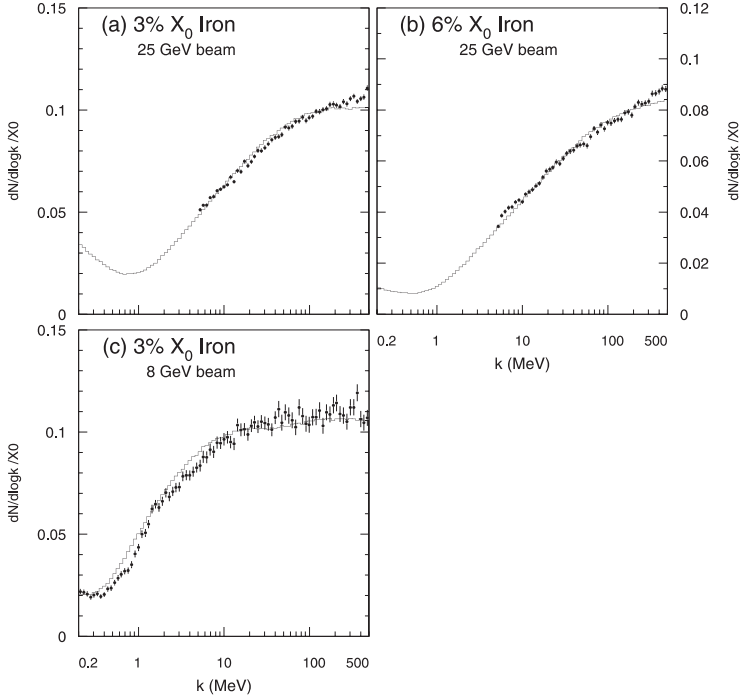


Figure 15: SLAC-E-146 measurements and Monte Carlo predictions for 8 and 25 GeV electrons passing through a 3% and 6% L_{rad} iron targets. The Monte Carlo curve is based on LPM and dielectric suppression, plus conventional transition radiation. Adapted from [15].

transition radiation (TR), or the calculations of the boundary radiation in [52] and [53] where the effect of multiple scattering is taken into account. It should be noted that the conclusions of these papers differ from each other. Our results [17] (given in Sec.3.1), which are consistent generally with obtained in [52], but more elaborated. In simulation the asymptotic formulae from [53] were used. Because of this the curve jumps at $\omega = \omega_{cr}$, around 800 keV (400 keV) at 25 (8) GeV. The curve which obtained using [52] also jumps at about 500 keV (below 200 keV) for the 25 (8) GeV data. Actually, to obtain the boundary photon contribution in the whole interval of photon energies one has to use general formulas (see Eq.(4.12) in [17] and for particular choice of parameters Eqs.(3.10), (3.36)-(3.37)) and corresponding curves have no jumps.

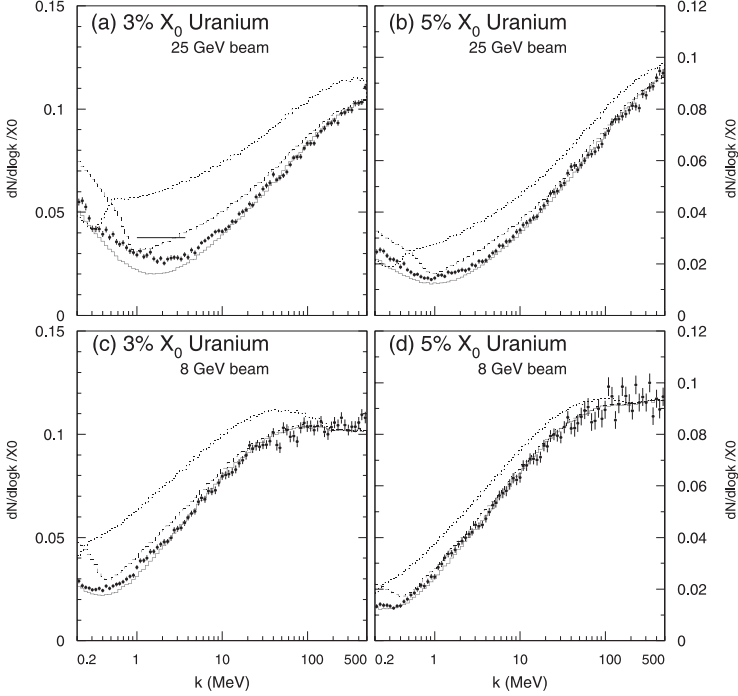


Figure 16: SLAC E-146 measurements and Monte Carlo for 3% L_{rad} and 5% L_{rad} uranium targets in 8 and 25 GeV electron beams. The solid line shows the LPM and dielectric suppression, conventional transition radiation Monte Carlo prediction. The other lines include simulations based on calculations of transition radiation due to [53] (dashed line) and [52] (dotted line). The flat solid line in panel (a) is a calculation based on [59]. Adapted from [15].

To understand the qualitative features of data in Fig.16 we perform an analysis just as it was done for carbon, aluminum and iron. At electron energy $\varepsilon = 25$ GeV for uranium one has $\omega_c = 250$ MeV and $\omega_{vis} \sim (500 \div 750)$ MeV, while for $\varepsilon = 8$ GeV one has $\omega_{vis} \sim (50 \div 80)$ MeV. The minimum of the spectral curve is situated (see Eq.(3.102)) at $\omega = \omega_m \sim \sqrt{3/T_c}\omega_p$. For target thickness $l = 3\%L_{rad}$ one has $T_c = 25.8$ and for $\varepsilon = 25$ GeV one has $\omega_p = 3.8$ MeV and $\omega_m \sim 1.3$ MeV while for $l = 5\%L_{rad}$ the value of ω_m is $\sqrt{5/3}$ times smaller: $\omega_m \sim 1$ MeV. For $\varepsilon = 8$ GeV one has for $l = 3\%L_{rad}$: $\omega_m \sim 0.4$ MeV and for $l = 5\%L_{rad}$ one has $\omega_m \sim 0.3$ MeV. These estimates are in a reasonable agreement with data in Fig.16.

In all of these plots, the Monte Carlo curves were normalized to the data by multiplication by a constant adjustment, chosen so the MC best matches the data above 20 MeV (2 MeV) at 25 (8) GeV. The thresholds were chosen to avoid thin target corrections for $l < l_{f0}$, backgrounds and transition radiation; for the 0.7% L_{rad} target discussed below, higher limits were chosen, 30 (10) MeV at 25 (8) GeV. Overall, the standard Monte Carlo curves had to be scaled up by an average of 5% (2σ) to match the data. This discrepancy would likely disappear with an input cross section where the onset of suppression was more gradual around $\omega \sim \omega_{LP}$ (ω_{LP} is defined in Eq.(1.10)).

The errors shown on the plots are statistical only. The E-146 collaboration has carefully studied the systematic errors on these measurements. The point-to-point systematic errors vary slowly with ω and correspond to a 4.6% uncertainty for $\omega > 5$ MeV. Below 5 MeV, the systematic errors rise to 9%, because of increased uncertainties in photon energy cluster finding as Compton scattering takes over from showering as the dominant energy loss. The $\pm 3.5\%$ systematic error on the normalization was determined separately.

3.10 Discussion of theory and experiment

Here we consider the experimental data (see [12]-[14],[15] and previous subsection) from the point of view of the above analysis. It was shown that the mechanism of radiation depends strongly on the thickness of the target. First, we estimate the thickness of used target in terms of the formation length. From Eq.(3.98) we have that

$$T_c = \frac{2\pi l}{\alpha L_{rad}} \geq 20 \quad \text{at} \quad \frac{l}{L_{rad}} \geq 2 \%. \quad (3.108)$$

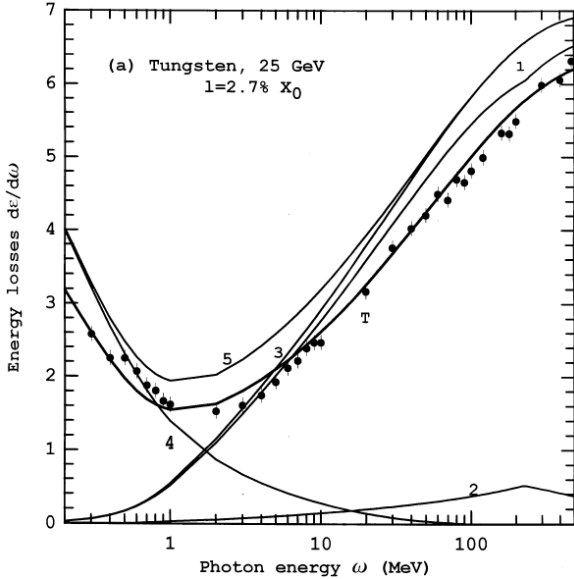
The minimal value of the ratio of the thickness of a target to the formation length is given by Eq.(3.99) ($\beta_m \simeq 2T_c(\omega_p/\omega_c)^{2/3}$). For defined value of T_c this ratio is least of all for the heavy elements. Indeed, the value of $\omega_p = \omega_0\gamma$ depends weakly on nucleus charge Z ($\omega_0 = 30 \div 80$) eV, while $\omega_c \frac{4\pi\gamma^2}{\alpha L_{rad}} \propto Z^2$. Furthermore, the ratio ω_p/ω_c decreases with the energy increase. Thus, among all the targets with thickness $l \geq 2 \%L_{rad}$ the minimal value of β_m is attained for the heavy elements (Au, W, U) at the initial energy $\varepsilon = 25$ GeV. In this case one has $\omega_c \simeq 250$ MeV, $\omega_p \simeq 4$ MeV, $\beta_m \geq 2.5$. Since the parameter T_c is energy independent and the ratio $\omega_p/\omega_c \propto 1/\varepsilon$, the minimal value $\beta_m \geq 5$ is attained at the initial energy $\varepsilon = 8$ GeV for all the targets with thickness $l \geq 2 \%L_{rad}$. So, all such targets can be considered as thick targets at both energies.

As an example we calculated the spectrum of the energy losses in the tungsten target with the thickness $l = 0.088$ mm ($=2.7\%L_{rad}$) for both initial energies shown in Fig.17(a) and (b). The characteristic parameters for this case are given in Table 2. We calculated the main (Migdal type)

Table 2. Characteristic parameters of the radiation process in tungsten with the thickness $l = 2.7\%L_{rad}$.

ε (GeV)	ω_c (MeV)	ω_p (MeV)	T_c	ω_1 (MeV)	β_m	ω_m (MeV)
25	230	3.9	21.3	1.6	2.7	2
8	23	1.3	21.3	0.76	5.7	0.5

term Eq.(2.17), the first correction term Eq.(2.22) taking into account an influence of the polarization of a medium according to Eq.(2.123), as well as the Coulomb corrections entering into parameter ν_0 Eq.(2.24) and value $L(\varrho_c)$ Eq.(2.12). The contribution of an inelastic scattering of a projectile on atomic electrons was not included into the numerical calculation (it is $\sim 1\%$), although it can be done using Eq.(2.34). We calculated also the contribution of boundary photons (see Eq.(4.12) in [17]). Here in the soft part of the spectrum $\omega < \omega_d$ ($\omega_d \simeq 2$ MeV for $\varepsilon = 25$ GeV) the transition radiation term Eq.(3.11) dominates, while in the harder part of the boundary photon



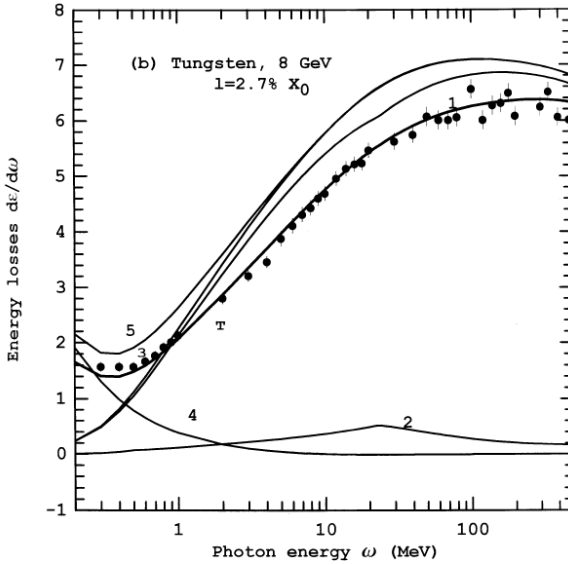


Figure 17: The energy losses $\frac{d\varepsilon}{d\omega}$ in tungsten with thickness $l = 0.088$ mm in units $\frac{2\alpha}{\pi}$, ((a) is for the initial electrons energy $\varepsilon = 25$ GeV and (b) is for $\varepsilon = 8$ GeV). The Coulomb corrections and the polarization of a medium are included: *curve 1* is the contribution of the main term describing LPM effect; *curve 2* is the correction term; *curve 3* is the sum of the previous contributions; *curve 4* is the contribution of the boundary photons; *curve 5* is the sum of the previous contributions; *curve T* is the final theory prediction with regard for the reduction factor (the multiphoton effects). Experimental data from Fig.9 of [14].

spectrum $\omega > \omega_d$ the terms depending on both the multiple scattering and the polarization of a medium give the contribution; for $\varepsilon = 8$ GeV one has $\omega_d \simeq 700$ keV. All the mentioned contribution presented separately in Fig.17. Under conditions of the experiment the multiphoton reduction of the spectral curve is very essential. The curve "T" in the Fig.17 involves the reduction factor which was constructed as the interpolation of Eqs.(3.55), (3.57) and (3.63) with the accuracy up to 1%. The curves "T" in Fig.17 (a) and (b) are the final theory prediction in units $2\alpha/\pi$.

Experimental data are taken from [14] and recalculated according with

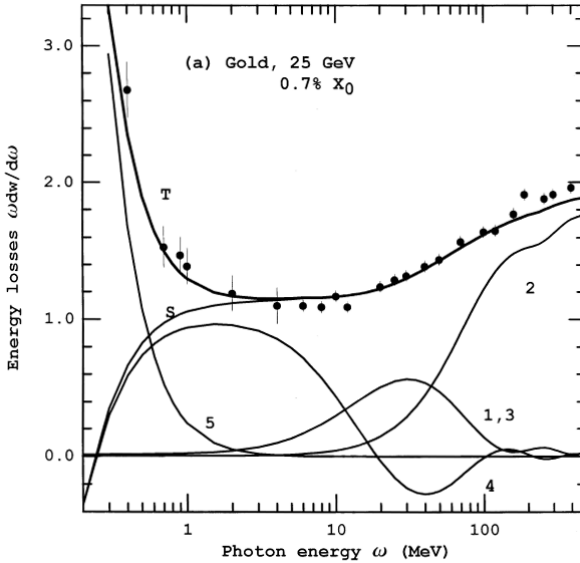
given in mentioned paper procedure:

$$\left(\frac{d\varepsilon}{d\omega}\right)_{exp} = \frac{1}{L_{rad}} \frac{N_{exp}}{k} \quad (3.109)$$

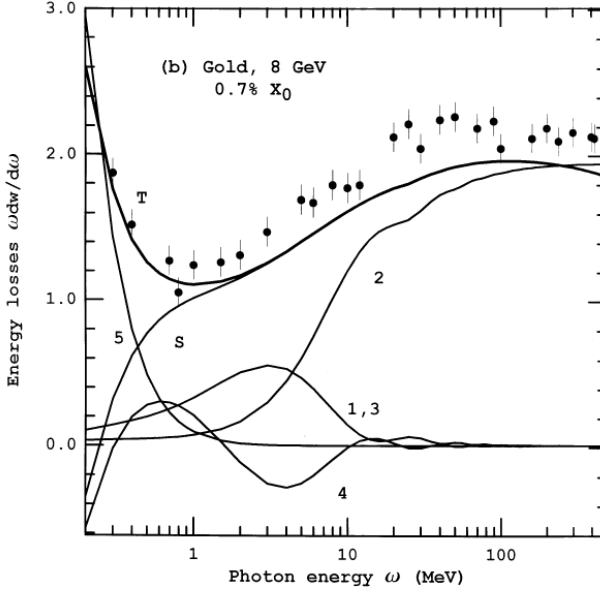
In the recent review [15] (see also the previous subsection) it is definitely indicated that $k = 0.096$ according with it definition: photon energies were histogrammed logarithmically, using 25 bins per decade of energy. In more earlier paper [14] the value $k = 0.09$ was given and we used it in our paper [17] and [18]. The data recalculated with $k = 0.096$ are also given in Fig.17. It is seen that there is a perfect agreement of the curves T with data for both energies.

The gold targets with thickness $l = 0.7\% L_{rad}$ and $l = 0.1\% L_{rad}$ are an exception and cannot't be considered as thick targets. We calculated energy losses spectra in these targets for both the initial electron energies $\varepsilon = 25$ GeV and $\varepsilon = 8$ GeV. The characteristic parameters of radiation for these cases are given in Table 3.

In Fig.18(a) results of calculations are given for target with a thickness $l = 0.7\% L_{rad}$ at $\varepsilon = 25$ GeV. The curves 1,2,3,4 present correspondingly the functions $J_1^{(2)}, J_2^{(2)}, J_3^{(2)}, J_4^{(2)}$ (3.29). At $\omega = 500$ MeV the value $\nu_1 T = \sqrt{\frac{\omega}{\omega_c}} T_c = 8.4 \gg 1$, the interference terms are exponentially small



a



b

Figure 18: The energy losses $\omega \frac{dW}{d\omega}$ in gold with thickness $l = 0.023 \text{ mm}$ in units $\frac{2\alpha}{\pi}$, ((a) is for the initial electrons energy $\varepsilon = 25 \text{ GeV}$ and (b) is for $\varepsilon = 8 \text{ GeV}$). The Coulomb corrections and the polarization of a medium are included: *curve 1* is the contribution of the term $\text{Re } J_1^{(2)} = \text{Re } J_3^{(2)}$; *curve 2* is the contribution of the term $\text{Re } J_2^{(2)}$; *curve 4* is the contribution of the term $\text{Re } J_4^{(2)}$, all (3.29); *curve S* is the sum of the previous contributions $\text{Re } J^{(2)}$; *curve 5* is the contribution of the boundary photons, see Eq.(2.20), [18]; *curve T* is the total prediction for the radiation energy losses. Experimental data from Fig.12 of [14].

Table 3. Characteristic parameters of the radiation process in gold with the thickness $l = 0.7\% L_{rad}$ and $l = 0.1\% L_{rad}$ (all photon energies ω are in MeV).

ε (GeV)	ω_c	ω_p	$T_c(0.7)$	$T_c(0.1)$	$\omega_1(0.7)$	$\beta_m(0.7)$	$\beta_m(0.1)$	ω_{th}
25	240	3.9	5.82	0.96	1.6	0.75	0.12	28
8	25	1.3	5.82	0.96	0.76	1.6	0.25	3.0

and one can use formulae for a thick target. In this case the parameter $\nu_1 = 0.69$ and contribution of boundary photons ($J_b = J_1^{(2)} + J_3^{(2)} + J_4^{(2)}$) is small ($J_b \simeq -\frac{2\nu_1^4}{21}$, see [9], Eq.(4.16)) and distinction Bethe-Maximon formula ($J_{BM} = T_c/3 = 1.94$) from $\text{Re } J^{(2)} = \text{Re } (J_1^{(2)} + J_2^{(2)} + J_3^{(2)} + J_4^{(2)})$ is of the order 10% according with asymptotic damping factor $\left(1 - \frac{16\nu_1^4}{21}\right)$. At $\omega < \omega_{th} \simeq 30$ MeV for the case $T_c \gg 1$ and $\beta_m < 1$ the spectral curve turns into plateau according with discussion in previous subsection. In this photon energy region the parameter $\nu_0 > 3$ and Eq.(3.36) for a target with intermediate thickness describes the spectral probability of radiation with a good accuracy. With the further photon energy decrease one can use limiting formula (3.38) where $\nu_0^2 T = 4k \simeq 7.4$. For this case the ratio of ordinate of the plateau to ordinate of the Bethe-Maximon intensity (see Eq.(3.107)) is $R \simeq 0.57$. Note, that in formulae for $J_1^{(2)} \div J_4^{(2)}$ the potential $V_c(\boldsymbol{\rho})$ Eq.(2.12) is used which doesn't include corrections $\sim 1/L$ ($v(\boldsymbol{\rho})$). These corrections were given above for both thin and thick targets (see Eq.(2.33)). In our case ($\nu_0 \gg 1$, $\nu_0 T \gg 1$) the expressions with corrections $\sim 1/L$ are given in Eqs.(2.33) and (3.41) for a thick target and a thin target respectively. Taking into account behaviors of correction in the region $\nu_0 \leq 1$ (see curve 2 in Fig.17(a)) we construct an interpolation factor (taking into account the term $\sim 1/L$) with accuracy of order 1%. The summary curve (T) in Fig.18(a) contains this factor.

The transition radiation contributes in the region $\omega \leq \omega_p$ (function $\text{Re } J_5^{(2)}$, curve 5 in Fig.18(a)). When $\kappa T \ll 1$ this curve is described by asymptotic of $\text{Re } J_5^{(2)}$ Eq.(3.36). The contribution of the transition radiation increases with ω decrease and for $\kappa T \sim 1$ it describes by Eq.(3.44). The contribution of the multiple scattering diminishes due to interference factor $\cos(\kappa T)$ in Eq.(3.46) (at $\omega = 0.2$ MeV, $\kappa T = 1.9$). The curve T in Fig.18(a) gives the summary contribution of the multiple scattering (the curve S , where factor $(1 - \omega/\varepsilon)$ is included) and the transition radiation (the curve 5).

In Fig.18(b) results of calculations are given for target with a thickness $l = 0.7\% L_{rad}$ at $\varepsilon = 8$ GeV. The notations are the same as in Fig.18(a). In this case the characteristic photon energy ω_c is one order of magnitude lower than for $\varepsilon = 25$ GeV, so that at $\omega = 500$ MeV the parameter ν_1 is small ($\nu_1^2 \simeq 1/20$). Because of this the right part of the curve S coincides with a good accuracy with the Bethe-Maximon formula (the Coulomb corrections are included). Note, that for this electron energy the effect of recoil (factor

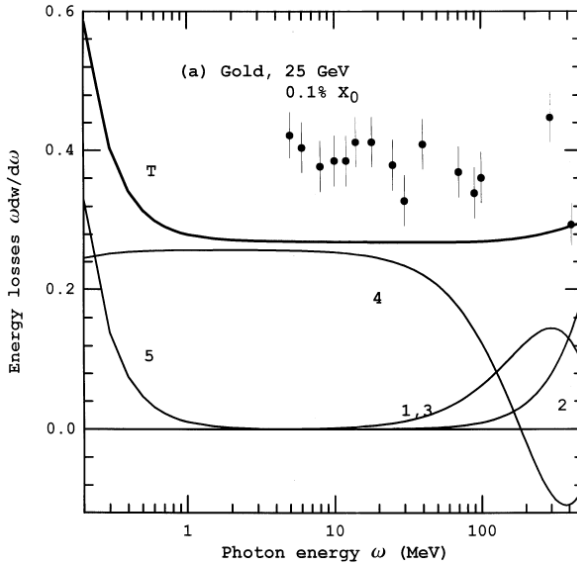
$(1 - \omega/\varepsilon)$) is more essential. Strictly speaking, a target with a thickness $0.7\%L_{rad}$ at $\varepsilon = 8$ GeV is not thin target for any photon energy ($\beta_m = 1.6$). However, for bremsstrahlung this target can be considered as a thin one for $\omega < \omega_{th} = 3$ MeV. Since the polarization of a medium becomes essential in the same region ($\omega_p = 1.25$ MeV), the interference factor $\cos(\kappa T)$ in Eq.(3.46) causes an inflection of the spectral curve S at $\omega \sim 1$ MeV. The transition radiation grows from the same photon energy ω and because of this the total spectral curve T has a minimum at $\omega \simeq 1$ MeV. As far as there is some interval of energies between ω_p and ω_{th} ($\omega_{th} - \omega_p \sim 3$ MeV), this minimum is enough wide. Moreover, the value of its ordinate coincide with a good accuracy with ordinate of the plateau of the spectral curve S in Fig.18(a) because bremsstrahlung on a thin target is independent of electron energy (3.41).It should be mentioned also that for this thickness the reduction factor due to multiple photon emission (see Eq.(3.57)) $f_{LPM} \simeq 0.94$ (so this is the effect of the same scale) but this reduction is compensated nearly exactly because of more precise definition of data (change of a bin width $\Delta k/k = 0.09$ in [12] (used in [24]) to a bin width $\Delta k/k = 0.096$ in [14], [15], see discussion in Sec.3 of [19]).

In Fig.19(a) results of calculations are given for target with a thickness $0.1\% L_{rad}$ at $\varepsilon = 25$ GeV. The notations are the same as in Fig.18(a). For this thickness $T_c = 0.96$ and one has a thin target starting from $\omega \leq \omega_c$. So, we have here very wide plateau. The left edge of the plateau is defined by the contribution of transition radiation ($\omega \sim \omega_p$). Since in this case $4k = \nu_1^2 T = T_c \simeq 1$ (see Eqs.(3.40)-(3.43)), one has to calculate the ordinate of the plateau using the exact formula for a thin target (3.40). For this case the ratio of ordinate of the plateau to ordinate of the Bethe-Maximon intensity (see Eq.(3.107)) is $R \simeq 0.85$. The same ordinate has the plateau for electron energy $\varepsilon = 8$ GeV (Fig.18(b)). However, a width of the plateau for this electron energy is more narrow (1 MeV \div 20 MeV) due to diminishing of the interval between ω_p and ω_c . For $\omega > \omega_c$ the formation length of radiation becomes shorter than target thickness ($T = T_c \omega/\omega_c > 1$) and the parameter ν_1 decreases. The value $\nu_1 T = T_c \sqrt{\omega/\omega_c}$ increases with ω growth. A target becomes thick and the spectral curves is described by the Bethe-Maximon formula in Fig.19(b) starting from photon energy $\omega \sim 100$ MeV. In Fig.19(b) the contributions of separate terms into $\text{Re } J^{(2)}$ are shown as well. Their behavior at $\omega > \omega_c$ is described quite satisfactory by Eqs. (3.33)-(3.35) (see also discussion at their derivation).

We compared our calculations with experimental data [14]. The curves T in Figs.18,19 give theory prediction (no fitting parameters!) in units $2\alpha/\pi$. It should be mentioned that in our papers [17] and [18] we put $k=0.09$ according

with the instruction given in paper [14]. But the multiphoton effects were not included. However, as was stated above one has to use $k=0.096$. So, from the one side for the gold target with the thickness $l = 0.7\% L_{rad}$ and energy $\varepsilon = 25$ GeV the reduction factor $f \simeq 0.94$ for photons with energy $\omega < 10$ MeV (plateau region). From the other side, use of the coefficient $k = 0.096$ in (3.109) instead of $k = 0.09$ lowers data upon $\sim 6\%$ and this is imitate inclusion of the reduction factor. As a result, the excellent agreement of the theory and data noted in [18] is not broken. It is seen that in Fig.18(a) there is a perfect agreement of the theory and data. In Fig.18(b) there a overall difference: data is order of 10% are higher than theory curve. For photon energy $\omega = 500$ MeV the theory coincide with Bethe-Maximon formula (with the Coulomb corrections) applicable for this energy. Note that just for this case it was similar problem with normalization of data matching with the Migdal Monte Carlo simulation (+12.2%, see Table II in [14]).

For thickness $l = 0.1\% L_{rad}$ there is a qualitative difference between our theory prediction and Monte Carlo simulation in [14]. There was a number of experimental uncertainties associated with this target. Nevertheless, we show data for $\varepsilon = 25$ GeV which are lying higher than theory curve.



a

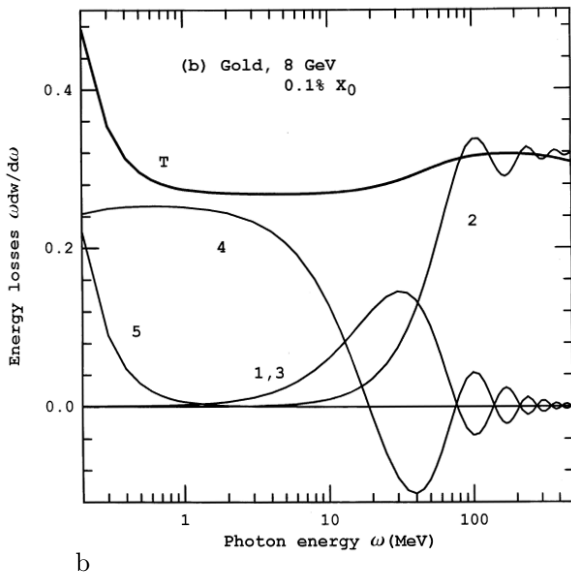


Figure 19: The energy losses $\omega \frac{dW}{d\omega}$ in gold with thickness $l = 0.0038$ mm in units $\frac{2\alpha}{\pi}$, ((a) is for the initial electrons energy $\varepsilon = 25$ GeV and (b) is for $\varepsilon = 8$ GeV). The Coulomb corrections and the polarization of a medium are included: *curve 1* is the contribution of the term $\text{Re } J_1^{(2)} = \text{Re } J_3^{(2)}$; *curve 2* is the contribution of the term $\text{Re } J_2^{(2)}$; *curve 4* is the contribution of the term $\text{Re } J_4^{(2)}$, all (3.29); *curve 5* is the contribution of the boundary photons see Eq.(2.20), [18]; *curve T* is the total prediction for the radiation energy losses. Experimental data from Fig.13 of [14].

4 Effects in colliding electron-positron beams

4.1 Mechanisms of radiation

In this section we consider the radiation at head-on collision of high energy electron and positron beams. The properties of photon emission process from a particle are immediately connected with details of its motion. It is convenient to consider the motion and radiation from particles of one beam in the rest frame of other beam (the target beam). In this case the target beam is an ensemble of the Coulomb centers. The radiation takes place at scattering

of a particle from these centers. If the target consists of neutral particles forming an amorphous medium, a velocity of particle changes (in a random way) only at small impact distances because of screening. In the radiation theory just the random collisions are the mechanism which leads to the incoherent radiation. For colliding beams significant contributions into radiation give the large impact parameters (very small momentum transfers) due to the long-range character of the Coulomb forces. As a result, in the interaction volume, which is determined also by the formation length l_f Eqs.(1.5), (1.6) (in the longitudinal direction), it may be large number of target particles. Let us note that in the case when the contribution into the radiation is given by impact parameters comparable with the transverse size of target, the number of particles in the interaction volume is determined by the ratio of the radiation formation length to the mean longitudinal distance between particles.

However, not all cases of momentum transfer should be interpreted as a result of random collisions. One have to exclude the collisions, which are macroscopic certain events. For elaboration of such exclusion we present the exact microscopic momentum transfer to the target particle in the form: $\mathbf{q} = \langle \mathbf{q} \rangle + \mathbf{q}_s$. Here $\langle \mathbf{q} \rangle$ is the mean value of momentum transfer calculated according to standard macroscopic electrodynamics rules with averaging over domains containing many particles. The longitudinal size of these domains should be large with respect to longitudinal distances between target particles and simultaneously small with respect to the radiation formation length. The motion of particle in the averaged potential of target beam, which corresponds to the momentum transfer $\langle \mathbf{q} \rangle$, determines the coherent radiation (*the beamstrahlung*). While the term \mathbf{q}_s describes the random collisions which define the process of incoherent radiation (*the bremsstrahlung*). Such random collisions we will call “scattering” since $\langle \mathbf{q}_s \rangle = 0$.

One of principal characteristics of particle motion defining the properties of coherent radiation is the ratio of variation of its transverse momentum to the mass during the whole time of passage across the opposite beam T

$$\frac{\Delta \mathbf{p}_\perp}{m} \sim \frac{eE_\perp \sigma_z}{m} \sim \frac{2\alpha N_c \lambda_c}{\sigma_x + \sigma_y} \equiv \delta, \quad (4.1)$$

where N_c is the number of particles in the opposite beam, σ_x and σ_y is its transverse dimensions ($\sigma_y \leq \sigma_x$), σ_z is the longitudinal size of opposite beam. The dispersion of particle momentum during time T is small comparing with m . It attains the maximum for the coaxial beams:

$$\frac{\langle \mathbf{q}_s^2 \rangle}{m^2} = \gamma^2 \langle \vartheta_s^2 \rangle \sim \frac{8\alpha^2 N_c \lambda_c^2}{\sigma_x \sigma_y} L \ll 1, \quad (4.2)$$

here ϑ_s^2 is the square of mean angle of multiple scattering, L is the characteristic logarithm of scattering problem ($L \sim 10$). This inequality permits one to use the perturbation theory for consideration of bremsstrahlung, and to analyze the beamstrahlung independently from the bremsstrahlung¹.

Another important characteristics of motion is the relative variation of particle impact parameter during time T

$$\frac{\Delta \varrho_i}{\varrho_i} \sim \frac{eE_{\perp} \sigma_z^2}{\varepsilon \sigma_i} \sim \frac{2\alpha N_c \lambda_c \sigma_z}{\gamma(\sigma_x + \sigma_y) \sigma_i} \equiv D_i, \quad (4.3)$$

here i is x or y . When the disruption parameter $D_i \ll 1$, the collision doesn't change the beam configuration and the particle crosses the opposite beam on the fixed impact parameter. If in addition the parameter $\delta \ll 1$ (this situation is realized in colliders with relatively low energies) then the beamstrahlung process can be calculated using the dipole approximation. The main contribution into the beamstrahlung give soft photons with an energy

$$\frac{\omega}{\varepsilon} \leq \frac{\gamma \lambda_c}{\sigma_z} \ll 1. \quad (4.4)$$

In the opposite case $\delta \gg 1$ the main part of beamstrahlung is formed when the angle of deflection of particle velocity is of the order of characteristic radiation angle $1/\gamma$ and the radiation formation length l_m is defined by

$$\frac{eE_{\perp} l_m}{m} \sim \frac{2\alpha N_c \lambda_c l_m}{(\sigma_x + \sigma_y) \sigma_z} = 1, \quad l_m = \frac{\sigma_z}{\delta}; \quad (4.5)$$

and the characteristic photon energy is

$$\omega \sim \omega_m = \frac{\gamma^2}{l_m} = \varepsilon \chi_m, \quad \chi_m \equiv 2\alpha N_c \gamma \frac{\lambda_c^2}{(\sigma_x + \sigma_y) \sigma_z} (\chi_m \ll 1). \quad (4.6)$$

Here χ is the invariant parameter Eq.(1.21) which defines properties of magnetic bremsstrahlung in the constant field approximation (CFA). For applicability of CFA it is necessary that relative variation of \mathbf{E}_{\perp} was small on the radiation formation length l_m . As far l_m is shorter than σ_z in $\delta \gg 1$ times the characteristic parameter becomes

$$D_{mi} = D_i \frac{l_m}{\sigma_z} = \frac{D_i}{\delta} = \frac{\sigma_z}{\gamma \sigma_i}, \quad (i = x, y) \quad (4.7)$$

¹ Actually more soft condition should be fulfilled:

$$\langle \mathbf{q}_s^2(l_f) \rangle / m^2 = \langle \mathbf{q}_s^2 \rangle / m^2 l_f / \sigma_z \ll 1$$

to that extent. The condition $D_{mi} \ll 1$ is fulfilled in all known cases. The mean number of photons emitted by a particle during the whole time of passage across the opposite beam T is $N_\gamma \sim \alpha\delta$, it include the electromagnetic interaction constant. Using the estimate (4.6) we get an estimate of relative energy loss

$$\frac{\Delta\varepsilon}{\varepsilon} \sim \alpha\delta\chi_m \quad (\chi_m \ll 1). \quad (4.8)$$

In the case $\chi_m \ll 1$ (this condition is satisfied in all existing facilities and proposed collider projects) the soft photons with energy $\omega \sim \omega_m = \varepsilon\chi_m \ll \varepsilon$ are mainly emitted. For $\omega \gg \omega_m$ the emission probability is exponentially suppressed. So, such photons are emitted in the bremsstrahlung process only. The boundary photon energy ω_b , starting from which the bremsstrahlung process dominates, depends on particular parameters of facility. If $\chi_m \sim 1/10$ the energy is $\omega_b \sim \varepsilon$. The formation length for $\omega \gg \omega_m$ is much shorter than l_m . On this length the particle deflection angle is small comparing with $1/\gamma$ and one can neglect the variation of transverse beam dimensions (see Eq.(4.7)). This means that all calculations of bremsstrahlung characteristics can be carried out in adiabatic approximation using local beam characteristics $\sigma_{x,y}(t), \mathbf{v}(t)$ etc, with subsequent averaging of radiation characteristics over time. Note that actually we performed a covariant analysis and the characteristic parameters are defined in a laboratory frame.

As an example we consider the situation when the configuration of beams doesn't change during the beam collision (the disruption parameter $D \ll 1$), and the total particle deflection angle during intersection of whole beam is small comparing with the characteristic radiation angle $1/\gamma$ (the dipole case). The target beam in its rest frame is the ensemble of classical potentials centers with coordinates $\mathbf{r}_a (\mathbf{x}_a, z_a)$ and the transverse coordinate of emitting particle is \mathbf{r}_\perp . In the perturbation theory the total matrix element of the radiation process can be written as

$$\mathbf{M}(\mathbf{r}_\perp) = \sum_{a=1}^{N_c} \mathbf{m}(\mathbf{r}_\perp - \mathbf{x}_a) \exp(iq_\parallel z_a) \quad (4.9)$$

We represent the combination $M_i M_j^*$ in the form

$$\begin{aligned} M_i M_j^* &= \sum_{a=b} m_i(\mathbf{r}_\perp - \mathbf{x}_a) m_j(\mathbf{r}_\perp - \mathbf{x}_b) \\ &+ \sum_{a \neq b} m_i(\mathbf{r}_\perp - \mathbf{x}_a) m_j(\mathbf{r}_\perp - \mathbf{x}_b) \exp(-iq_\parallel (z_a - z_b)). \end{aligned} \quad (4.10)$$

In the expression Eq.(4.10) we have to carry out averaging over position of scattering centers. We will proceed under assumption that there are many scattering centers within the radiation formation length $l_f = 1/q_{\parallel}$

$$N_f = n_z l_f \gg 1, \quad (4.11)$$

where for the Gaussian distribution

$$n_z = \frac{N_c}{\sqrt{2\pi}\sigma_z} \exp\left(-\frac{z^2}{2\sigma_z^2}\right), \quad (4.12)$$

here N_c and σ_z are introduced in Eq.(4.1). Note that in the situation under consideration $q_{\max} = |\mathbf{r}_{\perp} - \mathbf{x}_a|_{\max} \geq \sigma_t$, where σ_t is the characteristic transverse size of target beam. Let us select terms with approximately fixed phase $q_{\parallel}(z_a - z_b) = \phi_{ab}$ in the sum with $a \neq b$ in Eq.(4.10). If the condition (4.11) is fulfilled, there are many terms for which the phase variation is small ($\Delta\phi_{ab} \ll 1$). For this reason one can average over the transverse coordinates ($\mathbf{x}_a, \mathbf{x}_b$) of target particles in Eq.(4.10) without touching upon the longitudinal coordinates (z_a, z_b)

$$\begin{aligned} M_i M_j^* &= N_c \langle m_i m_j \rangle_{\perp} + \langle m_i \rangle_{\perp} \langle m_j \rangle_{\perp} \sum_{a \neq b} \exp(-iq_{\parallel}(z_a - z_b)) \quad (4.13) \\ &= N_c \left(\langle m_i m_j \rangle_{\perp} - \langle m_i \rangle_{\perp} \langle m_j \rangle_{\perp} \right) + \langle m_i \rangle_{\perp} \langle m_j \rangle_{\perp} \left| \sum_a \exp(iq_{\parallel}z_a) \right|^2, \end{aligned}$$

where

$$\begin{aligned} \langle m_i \rangle_{\perp} &= \int m_i(\mathbf{r}_{\perp} - \mathbf{x}) w_c(\mathbf{x}) d^2x, \\ \langle m_i m_j \rangle_{\perp} &= \int m_i(\mathbf{r}_{\perp} - \mathbf{x}) m_j(\mathbf{r}_{\perp} - \mathbf{x}) w_c(\mathbf{x}) d^2x, \quad (4.14) \end{aligned}$$

here $w_c(\mathbf{x})$ is the probability density of target particle distribution over the transverse coordinates normalized to unity. In Eq.(4.13) in the sum with $a \neq b$ we add and subtract the terms with $a = b$. We assume that the dispersion of number of scattering centers over the formation length l_f $(\Delta N)_f^2 \ll N_f$ (see Eq.(4.11)). Then on the adopted assumption the first term (proportional to N_c) on the right-hand side of Eq.(4.13) is the incoherent contribution to radiation (*the bremsstrahlung*). The second term gives the coherent part of radiation. For Gaussian distribution Eq.(4.12) performing averaging over the

longitudinal coordinate z_a one has

$$\left| \sum_a \exp(iq_{\parallel} z_a) \right|^2 \rightarrow \left| \int_{-\infty}^{\infty} n_z \exp(iq_{\parallel} z) dz \right|^2 = N_c^2 \exp(-q_{\parallel}^2 \sigma_z^2). \quad (4.15)$$

4.2 The beam-size effect in bremsstrahlung

It was pointed in Sec.1.3 that the external factors act differently on the radiating particle and on the recoil particle. This leads to a specific effect in the bremsstrahlung process at electron-electron(positron) collision. The point is that in the rest frame of recoil particle the formation length is longer by ε/m times than in the laboratory frame. Just this length determines the maximal impact parameters at scattering (e.g. the screening radius). There are a few factors which could act on the recoil electron. One of them is the presence of an external magnetic field in the region of particle collision [27] (see Sec.1.3). Another effect can appear due to smallness of the linear interval l where the collision occurs in comparison with l_v Eq.(1.6). This was pointed in [46].

The special experimental study of bremsstrahlung was performed at the electron-positron colliding beam facility VEPP-4 of Institute of Nuclear Physics, Novosibirsk [72]. The deviation of the bremsstrahlung spectrum from the standard QED spectrum was observed at the electron energy $\varepsilon = 1.84$ GeV. The effect was attributed to the smallness of the transverse size of the colliding beams. In theory the problem was investigated in [73], where the bremsstrahlung spectrum at the collision of electron-electron(positron) beams with the small transverse size was calculated to within the power accuracy (the neglected terms are of the order $1/\gamma = m/\varepsilon$). After the problem was analyzed in [74], and later on in [75] where some of results for the bremsstrahlung found in [73] were reproduced. It should be noted that in [73] (as well as in all other papers mentioned above) an incomplete expression for the bremsstrahlung spectrum was calculated. One has to perform the subtraction associated with the extraction of pure fluctuation process as it was shown above. An analogous problem encountered in the analysis of incoherent processes in the oriented crystals [83],[82] where the necessity of the subtraction procedure was indicated. Without the subtraction the results for the incoherent processes in oriented crystals would be qualitatively erroneous.

The correction to photon emission probability due to the small transverse dimensions of colliding beam for unpolarized electrons and photon was calculated in [76] basing on subtraction procedure as in Eq.(4.13). It is obtained

after integration over the azimuth angle of the emitted photon

$$dw_1 = \frac{\alpha^3}{\pi m^2} \frac{\varepsilon'}{\varepsilon} \frac{d\omega}{\omega} U(\zeta) F(\omega, \zeta) d\zeta, \quad \zeta = 1 + \gamma^2 \vartheta^2, \quad (4.16)$$

where ϑ is the photon emission angle, $\varepsilon' = \varepsilon - \omega$,

$$\begin{aligned} U(\zeta) &= v - \frac{4(\zeta - 1)}{\zeta^2}, \quad v = \frac{\varepsilon}{\varepsilon'} + \frac{\varepsilon'}{\varepsilon}, \quad F(\omega, \zeta) = F^{(1)}(\omega, \zeta) - F^{(2)}(\omega, \zeta), \\ F^{(1)}(\omega, \zeta) &= \frac{\eta^2}{\zeta^2} \int [K_0(\eta\rho)K_2(\eta\rho) - K_1^2(\eta\rho)] \rho \frac{d\Phi(\boldsymbol{\rho})}{d\rho} d^2\rho, \\ F^{(2)}(\omega, \zeta) &= \frac{2\eta^2}{\zeta^2} \int \left(\int K_1(\eta\rho) \frac{\boldsymbol{\rho}}{\rho} w_c(\mathbf{x} - \boldsymbol{\rho}) d^2\rho \right)^2 w_r(\mathbf{x}) d^2x, \end{aligned} \quad (4.17)$$

here

$$\eta = q_{min}\zeta, \quad q_{min} = m^3\omega/4\varepsilon^2\varepsilon', \quad \Phi(\boldsymbol{\rho}) = \int w_r(\mathbf{x} + \boldsymbol{\rho}) w_c(\mathbf{x}) d^2x, \quad (4.18)$$

where $w_c(\mathbf{x})$ is defined in (4.14), $w_r(\mathbf{x})$ is the same but for the radiating beam, value q_{min} is defined in c.m.frame of colliding particles. The term $F^{(2)}(\omega, \zeta)$ is the subtraction term. The total probability is $dw_\gamma = dw_0 + dw_1$, where dw_0 is standard QED probability. The analysis in [76] was based on Eqs.(4.16)-(4.17).

We considered in [76] the actual case of the Gaussian beams. The Fourier transform was used

$$\begin{aligned} w(\mathbf{x}) &= \frac{1}{(2\pi)^2} \int d^2q \exp(-i\mathbf{q}\mathbf{x}) w(\mathbf{q}); \\ w_r(\mathbf{q}) &= \exp\left[-\frac{1}{2}(q_x^2\Delta_x^2 + q_y^2\Delta_y^2)\right], \quad w_c(\mathbf{q}) = \exp\left[-\frac{1}{2}(q_x^2\sigma_x^2 + q_y^2\sigma_y^2)\right] \end{aligned} \quad (4.19)$$

where as above the index r relates to the radiating beam and the index c relates to the target beam, Δ_y and Δ_x (σ_y and σ_x) are the vertical and horizontal transverse dimensions of radiating (target) beam. Substituting Eq.(4.19) into Eq.(4.18) we find

$$\Phi(\boldsymbol{\rho}) = \frac{\Sigma_x \Sigma_y}{\pi} \exp[-\rho_x^2 \Sigma_x^2 - \rho_y^2 \Sigma_y^2]; \quad \Sigma_x^2 = \frac{1}{2(\sigma_x^2 + \Delta_x^2)}, \quad \Sigma_y^2 = \frac{1}{2(\sigma_y^2 + \Delta_y^2)}. \quad (4.20)$$

Using the relation $d\sigma_1 = \Phi^{-1}(0)dw_1$ the following expression for the correction to spectrum was found in [76] starting from Eq.(4.16)

$$d\sigma_1^{(1)} = \frac{2\alpha^3}{m^2} \frac{\varepsilon'}{\varepsilon} \frac{d\omega}{\omega} f^{(1)}(\omega), \quad f(s) = \frac{\sqrt{\pi}}{2s} (v - 8s^2) \operatorname{erfc}(s) + 4e^{-s^2} + 2\operatorname{Ei}(-s^2),$$

$$f^{(1)}(\omega) = -\frac{1}{\pi \Sigma_x \Sigma_y} \int_0^{2\pi} \frac{d\varphi}{\Sigma_x^{-2} \cos^2 \varphi + \Sigma_y^{-2} \sin^2 \varphi} \int_0^\infty F_2(z) f(s) s ds, \quad (4.21)$$

$$z^2 = \frac{s^2 q_{min}^{-2}}{\Sigma_x^{-2} \cos^2 \varphi + \Sigma_y^{-2} \sin^2 \varphi}, \quad F_2(x) = \frac{2x^2 + 1}{x\sqrt{1+x^2}} \ln(x + \sqrt{1+x^2}) - 1,$$

where $\operatorname{Ei}(x)$ is the exponential integral function and $\operatorname{erfc}(x)$ is the error function. This formula is quite convenient for the numerical calculations.

The subtraction term ($F^{(2)}(\omega, \zeta)$ in Eq.(4.17)) gives for coaxial beams

$$d\sigma_1^{(2)} = -\frac{2\alpha^3}{m^2} \frac{\varepsilon'}{\varepsilon} \frac{d\omega}{\omega} J^{(2)}(\omega), \quad (4.22)$$

where

$$J^{(2)}(\omega) = \frac{\sqrt{ab}}{\Sigma_x \Sigma_y} \int_0^\infty ds_1 \int_0^\infty ds_2 g \left(\frac{q_{min} \sqrt{s}}{2} \right) G(s_1, s_2),$$

$$G(s_1, s_2) = \frac{1}{2} \left(\frac{a_1 a_2 b_1 b_2}{AB} \right)^{1/2} \left[\frac{a_1 a_2}{A} + \frac{b_1 b_2}{B} \right] \quad (4.23)$$

Here the function $g(q)$ is:

$$g(q) = \left(v - \frac{2}{3} \right) e^{-q^2} - 2q^2 \left[\frac{\sqrt{\pi}}{2q} \left(v - \frac{8}{3} q^2 \right) \operatorname{erfc}(q) + \frac{4}{3} e^{-q^2} + \operatorname{Ei}(-q^2) \right]. \quad (4.24)$$

In Eq.(4.23) we introduced the following notations

$$a = \frac{1}{2\Delta_x^2}, \quad b = \frac{1}{2\Delta_y^2}, \quad a_{1,2} = \frac{1}{s_{1,2} + 2\sigma_x^2}, \quad b_{1,2} = \frac{1}{s_{1,2} + 2\sigma_y^2},$$

$$A = a_1 + a_2 + a, \quad B = b_1 + b_2 + b, \quad s = s_1 + s_2. \quad (4.25)$$

In the case of narrow beams one has $q_{min}/(\Sigma_x + \Sigma_y) \ll 1$. In this case of coaxial beams $d\sigma_\gamma = d\sigma_0 + d\sigma_1$ is

$$d\sigma_\gamma = \frac{2\alpha^3}{m^2} \frac{\varepsilon'}{\varepsilon} \frac{d\omega}{\omega} \left\{ \left(v - \frac{2}{3} \right) \left[2 \ln \frac{m}{\Sigma_x + \Sigma_y} + C + 2 - J_- \right] + \frac{2}{9} \right\}, \quad (4.26)$$

where

$$J_- = \frac{\sqrt{ab}}{\Sigma_x \Sigma_y} \int_0^\infty ds_1 \int_0^\infty ds_2 G(s_1, s_2) \quad (4.27)$$

The dimensions of beams in the experiment [72] were $\sigma_y = \Delta_y = 24 \mu m$, $\sigma_x = \Delta_x = 450 \mu m$, so this is the case of flat beams. The estimate for this case gives $J_- \simeq (4/3\sqrt{3})\pi\sigma_y/\sigma_x \ll 1$. This term is much smaller than other terms in Eq.(4.26). This means that for this case the correction to the spectrum calculated in [73] is very small.

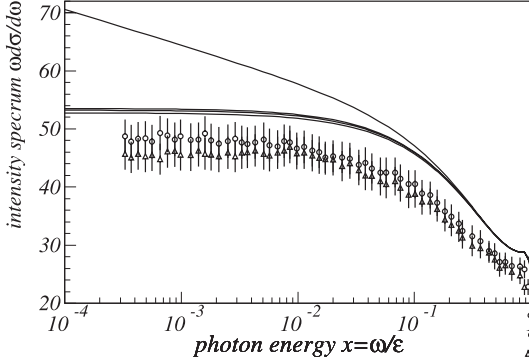


Figure 20: The bremsstrahlung intensity spectrum $\omega d\sigma/d\omega$ in units $2\alpha r_0^2$ versus the photon energy in units of initial electron energy ($x = \omega/\varepsilon$) for VEPP-4 experiment. The upper curve is the standard QED spectrum, the three close curves below are calculated for the different vertical dimensions of colliding beams (equal for two colliding beams $\sigma = \sigma_z = \Delta_z$): $\sigma = 20 \mu m$ (bottom), $\sigma = 24 \mu m$ (middle), $\sigma = 27 \mu m$ (top). The data measured in [72] are presented as circles (the experiment in 1980) and as triangles (the experiment in 1981) with 6% systematic error as obtained in [72].

The result of calculation and VEPP-4 (INP, Novosibirsk) data are presented in Fig.20 where the bremsstrahlung intensity spectrum $\omega d\sigma/d\omega$ is given in units $2\alpha r_0^2$ versus the photon energy in units of initial electron energy ($x = \omega/\varepsilon$)[76]. The upper curve is the standard QED spectrum, the three close curves below are calculated using Eqs.(4.21) and (4.22) for the different vertical dimensions of colliding beams (equal for both colliding beams $\sigma = \sigma_z = \Delta_z$): $\sigma = 20 \mu m$ (bottom), $\sigma = 24 \mu m$ (middle), $\sigma = 27 \mu m$ (top) (this is just the 1-sigma dispersion for the beams used in the experiment). All the theoretical curves are calculated to within the relativistic accuracy

(the discarded terms are of the order m/ε). It is seen that the effect of the small transverse dimensions is very essential in soft part of spectrum (at $\omega/\varepsilon = 10^{-4}$ the spectral curve diminishes in 25%), while for $\omega/\varepsilon > 10^{-1}$ the effect becomes negligible. The data measured in [72] are presented as circles (experiment in 1980) and as triangles (experiment in 1981) with 6 % systematic error as obtained in [72] (while the statistical errors are negligible). This presentation is somewhat different from [72]. It is seen that the data points are situated systematically below the theory curves but the difference is not exceed the 2-sigma level [72]. It should be noted that this is true also in the hard part of spectrum where the beam-size effect is very small.

One more measurement of beam-size effect was performed at the HERA electron-proton collider (DESY, Germany) [77]. The electron beam energy was $\varepsilon=27.5$ GeV, the proton beam energy was $\varepsilon_p=820$ GeV. The parameters of beam in this experiment were (in our notation): $\sigma_y = \Delta_y = (50 \div 58)\mu m$, $\sigma_x = \Delta_x = (250 \div 290)\mu m$. Since the ratio of the vertical and the horizontal dimensions is not very small, the contribution of subtraction term (Eq.(4.22)) is essential (more than 10%). The bremsstrahlung intensity spectrum $\omega d\sigma/d\omega$ in units $2\alpha r_0^2$ versus the photon energy in the units of initial electron energy ($x = \omega/\varepsilon$) for the HERA experiment is given in Fig.21. For details of comparison of experimental data [72], [77] with theory see [76], where we discussed also possible use of beam-size effect for linear collider tuning. It should be noted that for linear collider the condition of strong beam-size effect $\sigma_y q_{min} \ll 1$ ($\sigma_y \ll \sigma_x$) is fulfilled for the whole spectrum. This can be seen in Fig.22, where the lower curve is calculated using Eq.(4.21) and the subtraction term is very small since $\sigma_y/\sigma_x < 0.01$. As far as the narrow beams are considered in Fig.22, the lower curve is consistent also with Eq.(4.26). This curve depends on the energy and the transverse sizes of beams. It will be instructive to remind that the analysis in [76] (see Eq.(2.8)) and here is valid if $\chi_m/u \ll 1$ (see Eq.(4.6), $u = \omega/\varepsilon'$). The parameter χ_m depends also on number of particles N_c and the longitudinal beam size. So, for low N_c Fig.22 is valid for any x , but for TESLA project ($\chi_m=0.13$) it holds in hard part of spectrum only. In fact, the probability of incoherent radiation becomes larger than the probability of coherent radiation only at $x > 0.7$ where the lower curve in Fig.22 is certainly applicable.

4.3 The coherent radiation

The particle interaction at beam-beam collision in linear colliders occurs in an electromagnetic field provided by the beams. As a result, 1) the phenomena induced by this field turns out to be very essential, 2) the cross section of

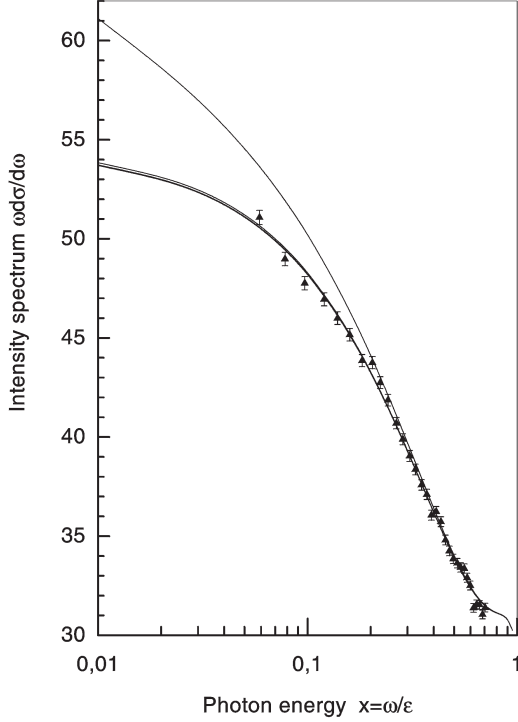


Figure 21: The bremsstrahlung intensity spectrum $\omega d\sigma/d\omega$ in units $2\alpha r_0^2$ versus the photon energy in units of initial electron energy ($x = \omega/\varepsilon$) for the HERA experiment. The upper curve is the standard QED spectrum, the two close curves below are calculated with the beam-size effect taken into account: the bottom curve is for $\sigma_z = \Delta_z = 50 \mu\text{m}$, $\sigma_y = \Delta_y = 250 \mu\text{m}$; while the top curve is for $\sigma_z = \Delta_z = 54 \mu\text{m}$, $\sigma_y = \Delta_y = 250 \mu\text{m}$. The data taken from Fig.5c in [77].

the main QED processes are modified comparing to the case of free particles. These items were considered by V.M.Strakhovenko and authors [78].

The magnetic bremsstrahlung mechanism dominates and its characteristics are determined by the value of the quantum parameter $\chi(t)$ Eq.(1.21) dependent on the strength of the incoming beam field at the moment t (the constant field limit(CFA)).

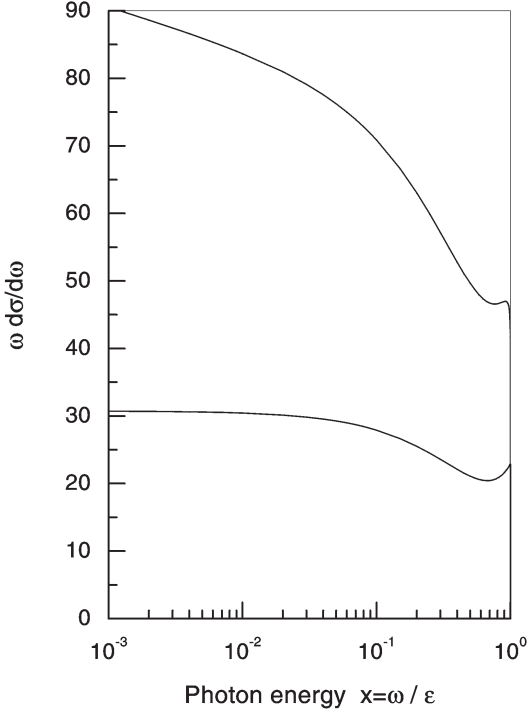


Figure 22: The bremsstrahlung intensity spectrum $\omega d\sigma/d\omega$ in units $2\alpha r_0^2$ versus the photon energy in units of initial electron energy ($x = \omega/\varepsilon$) for linear collider with beam energy $\varepsilon = 250$ GeV. The upper curve is the standard QED spectrum. The curve below is calculated with the beam-size effect taken into account for $\sigma_x = 553$ nm, $\sigma_y = 5$ nm.

In the CFA the spectral probability of radiation from an electron per unit time has the form [8], Eq.(10.25) (see also Eq.(4.24) in [10] or Eq.(90.23) in [11])

$$\frac{dw_\gamma}{dt} \equiv dW_\gamma(t) = \frac{\alpha}{2\sqrt{3}\pi\gamma^2} \int_{-\infty}^{\infty} \Phi_\gamma(t) dt d\omega,$$

$$\Phi_\gamma(t) = \left(\frac{\varepsilon}{\varepsilon'} + \frac{\varepsilon'}{\varepsilon} \right) K_{2/3}(z) - \int_z^\infty K_{1/3}(y) dy, \quad (4.28)$$

where $K_\nu(z)$ is the Macdonald functions, $z = 2u/3\chi(t)$, $u = \omega/\varepsilon'$. The corresponding probability for polarized electrons and photons is given in [84].

For the Gaussian beams

$$\chi(t) = \chi_0(x, y) \exp(-2t^2/\sigma_z^2), \quad (4.29)$$

here the function $\chi_0(x, y)$ depends on transverse coordinates.

It turns out that for the Gaussian beams the integration of the spectral probability over time can be carried out in a general form:

$$\begin{aligned} \frac{dw_\gamma}{du} &= \frac{\alpha m \sigma_z}{\pi \gamma \sqrt{6}} \frac{1}{(1+u)^2} \left[\left(1 + u + \frac{1}{1+u} \right) \right. \\ &\times \left. \int_1^\infty K_{2/3}(ay) \frac{dy}{y \sqrt{\ln y}} - 2a \int_1^\infty K_{1/3}(ay) \sqrt{\ln y} dy \right], \quad (4.30) \end{aligned}$$

where $a = 2u/3\chi_0$. In the case when $a \gg 1$ the main contribution into the integral (4.30) gives the region $y = 1 + \xi$, $\xi \ll 1$. Taking the integrals over ξ we obtain

$$\frac{dw_\gamma^{CF}}{du} \simeq \frac{\sqrt{3}\alpha m \sigma_z}{4\gamma} \frac{1+u+u^2}{u(1+u)^3} \chi_0 \exp\left(-\frac{2u}{3\chi_0}\right) \quad (4.31)$$

For round beams the integration over transverse coordinates is performed with the density

$$n_\perp(\varrho) = \frac{1}{2\pi\sigma_\perp^2} \exp\left(-\frac{\varrho^2}{2\sigma_\perp^2}\right) \quad (4.32)$$

The parameter $\chi_0(\varrho)$ we present in the form

$$\begin{aligned} \chi_0(\varrho) &= \chi_{rd} \frac{f(x)}{f_0}, \quad x = \frac{\varrho}{\sigma_\perp}, \quad f(x) = \frac{1}{x} (1 - \exp(-x^2/2)), \\ \chi_{rd} &= 0.720\alpha N_c \gamma \frac{\lambda_c^2}{\sigma_z \sigma_\perp}, \quad f'(x_0) = 0, \quad f_0 = f(x_0) = 0.451256, \end{aligned} \quad (4.33)$$

where N_c is the number of electron in the bunch.

The Laplace integration of Eq.(4.31) gives for radiation intensity $dI/du = \varepsilon u/(1+u)dW/du$

$$\frac{dI_{as}}{du} \simeq \alpha m^2 \sigma_z \frac{3}{4} \sqrt{\frac{\pi}{|f_0''|}} \frac{1+u+u^2}{\sqrt{u}(1+u)^4} f_0^{3/2} \chi_{rd}^{3/2} \exp\left(-\frac{2u}{3\chi_{rd}}\right), \quad (4.34)$$

where $f_0'' = f''(x_0) = -0.271678$.

Integration of Eq.(4.30) over transverse coordinates gives the final result for the radiation intensity. For the round beams it is shown in Fig.23 for $\chi_{rd} = 0.13$, the curve attains the maximum at $u \simeq 0.02$. The right slope of the curve agrees with the asymptotic intensity (4.34) and the left slope of the curve agrees with the standard classical intensity.

$$\frac{dI_{cl}}{du} = \frac{e^2 m^2}{\pi} 3^{1/6} \Gamma(2/3) \chi_{rd}^{2/3} u^{1/3} \quad (4.35)$$

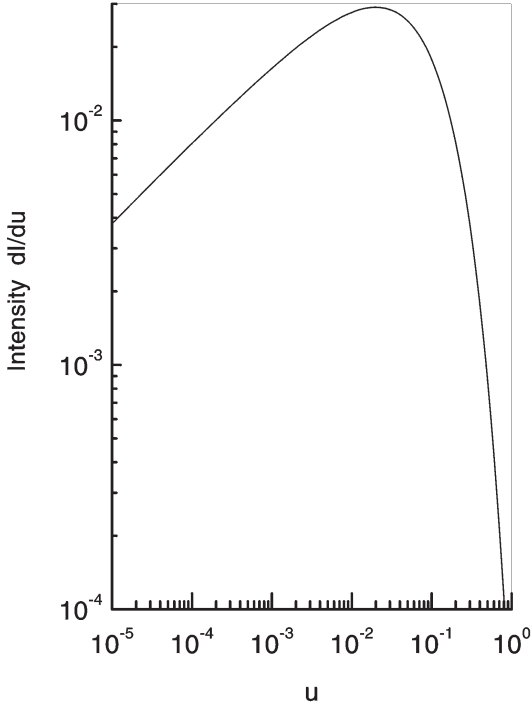


Figure 23: Spectral intensity of radiation of round beams in units $\alpha m^2 \sigma_z$ for $\chi_{rd} = 0.13$ calculated according to Eqs.(4.30),(4.33).

It will be instructive to compare the spectrum in Fig.23, found by means of integration over the transverse coordinates with intensity spectrum which follows from Eq.(4.30) (multiplied by ω) with averaged over the density

Eq.(4.32) value χ_0 Eq.(4.33): $\overline{\chi_0} = \chi_{rd} \cdot 0.8135$. The last spectrum reproduces the spectrum given in Fig.23, in the interval $10^{-3} \leq u/\overline{\chi_0} < 1$ with an accuracy better than 2% (near maximum better than 1%) while for $u/\overline{\chi_0} \leq 10^{-3}$ one can use the classic intensity (4.35) and for $u/\overline{\chi_0} \gg 1$ the asymptotics (4.34) is applicable.

For the flat beams ($\sigma_x \gg \sigma_y$) the parameter $\chi_0(\varrho)$ takes the form

$$\chi_0 = \frac{2\gamma\mathbf{E}_\perp}{H_0} = \chi_m e^{-v^2} [\mathbf{e}_y \text{erf}(w) - i\mathbf{e}_x \text{erf}(iv)], \quad \chi_m = \frac{2N_c \alpha \gamma \lambda_c^2}{\sigma_z \sigma_x}, \quad (4.36)$$

here $v = x/\sqrt{2}\sigma_x$, $w = y/\sqrt{2}\sigma_y$, $\text{erf}(z) = 2/\sqrt{\pi} \int_0^z \exp(-t^2)dt$, \mathbf{e}_x and \mathbf{e}_y are the unit vectors along the corresponding axes. The formula (4.36) is consistent with given in [79]. In [78] the term with \mathbf{e}_x was missed. Because of this the numerical coefficients in results for the flat beams are erroneous.

To calculate the asymptotics of radiation intensity for the case $u \gg \chi_m$ one has to substitute

$$\chi_0 = |\chi_0| = \chi_m e^{-v^2} [\text{erf}^2(w) - \text{erf}^2(iv)]^{1/2} \quad (4.37)$$

into Eq.(4.31) and take integrals over transverse coordinates x, y with the weight

$$n_\perp(x, y) = \frac{1}{2\pi\sigma_x\sigma_y} \exp\left(-\frac{x^2}{2\sigma_x^2} - \frac{y^2}{2\sigma_y^2}\right). \quad (4.38)$$

Integral over x can be taken using the Laplace method, while for integration over y it is convenient to introduce the variable

$$\eta = \frac{2}{\sqrt{\pi}} \int_w^\infty \exp(-t^2)dt, \quad w = \frac{y}{\sqrt{2}\sigma_y}. \quad (4.39)$$

As a result we obtain for the radiation intensity in the case of flat beams

$$\frac{dI_{fl}}{du} = \frac{9}{8\sqrt{2}(1-2/\pi)} \alpha m^2 \sigma_z \chi_m^{5/2} \frac{1+u+u^2}{u^{3/2}(1+u)^4} \exp\left(-\frac{2u}{3\chi_m}\right). \quad (4.40)$$

It is interesting to compare the high-energy end of intensity spectrum at collision of flat beams Eq.(4.40) with intensity spectrum of incoherent radiation with regard for smallness of the transverse beam sizes considered above. For calculation we use the project TESLA parameters [80]: $\varepsilon = 250$ GeV, $\sigma_x = 553$ nm, $\sigma_y = 5$ nm, $\sigma_z = 0.3$ mm, $N = 2 \cdot 10^{10}$, $\chi_m = 0.13$. The result is shown in Fig.24, where the curves calculated according to Eq.(4.40), and Eq.(4.26). It is seen that for $x = \omega/\varepsilon > 0.7$ the incoherent radiation

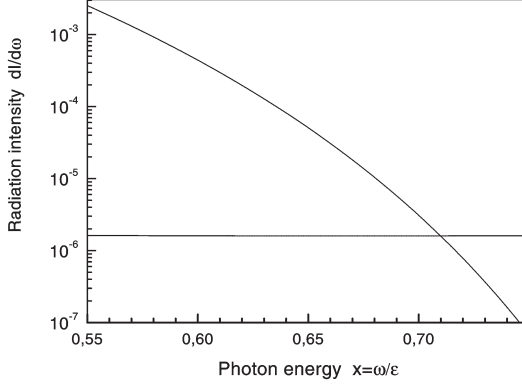


Figure 24: The spectral radiation intensity $dI/d\omega$ of coherent radiation (fast falling with $x = \omega/\varepsilon$ increase curve) and of incoherent radiation (the curve which is almost constant) in units $N\alpha^2\lambda_c/\sigma_x$ for beams with dimensions $\sigma_x = 553$ nm, $\sigma_y = 5$ nm, for $\chi_m = 0.13$.

dominates. For $x > 0.7$ the incoherent radiation may be used for a tuning of beams [76].

Along with the spectral characteristics of radiation the total number of photons emitted by an electron is of evident interest as well as the relative energy losses. We discuss an actual case of flat beams and the parameter $\chi_m \ll 1$. In this case one can use the classic expression for intensity (bearing in mind that starting from $\chi_m \sim 1/10$ the quantum effects become substantial). In classical limit the relative energy losses are

$$\left(\frac{\Delta\varepsilon}{\varepsilon}\right)_{cl} = \frac{2\alpha m^2}{3\varepsilon} \int \chi^2(t, x, y) n_{\perp}(x, y) dt dx dy. \quad (4.41)$$

Using Eqs.(4.29), (4.37), and (4.38) we get

$$\left(\frac{\Delta\varepsilon}{\varepsilon}\right)_{cl} = \frac{2}{9} \sqrt{\frac{\pi}{3}} r \chi_m^2, \quad r = \frac{\alpha \sigma_z}{\gamma \lambda_c}. \quad (4.42)$$

For mean number of emitted by an electron photons we find

$$n_{\gamma}^{cl} = \frac{5\alpha m^2}{2\sqrt{3}\varepsilon} \int \chi(t, x, y) n_{\perp}(x, y) dt dx dy = 0.59275 \frac{5}{2} \sqrt{\frac{\pi}{6}} r \chi_m = 1.072 r \chi_m. \quad (4.43)$$

If $\chi_m > 1/10$ one have to use the quantum formulas. For the energy losses one can use the approximate expression (the accuracy is better than 2% for any χ) [81]

$$d\varepsilon/dt = 2/3\alpha m^2 \chi^2 [1 + 4.8(1 + \chi) \ln(1 + 1.7\chi) + 2.44\chi^2]^{-2/3}. \quad (4.44)$$

Here χ is the local value, so this expression for $d\varepsilon/dt$ should be integrated over time and averaged over the transverse coordinates. For mean number of photons emitted by an electron there is the approximate expression (the accuracy is better than 1% for any χ_0)

$$n_\gamma(\mathbf{q}) = \frac{1.81\chi_0 r}{[1 + 1.5(1 + \chi_0) \ln(1 + 3\chi_0) + 0.3\chi_0^2]^{1/6}}, \quad (4.45)$$

where the expression should be averaged over the transverse coordinates. For the project TESLA one gets for $(\Delta\varepsilon/\varepsilon)_{cl} = 4.3\%$ according to Eq.(4.42), while the correct result from Eq.(4.44) is $\Delta\varepsilon/\varepsilon = 3.2\%$. For mean number of photons emitted by an electron we have correspondingly $n_\gamma^{cl} \simeq 1.6$ while the correct result is $n_\gamma \simeq 1.5$.

4.4 Mechanisms of e^+e^- - pair creation

The probability of pair creation by a photon in the external field can be find from formulas (4.28) using the substitution rule (see e.g.[11], [10]): $\varepsilon \rightarrow -\varepsilon$, $\omega \rightarrow -\omega$, $\omega^2 d\omega \rightarrow -\varepsilon^2 d\varepsilon$. Performing these substitutions we obtain (see also Eq.(3.50) in [10])

$$\frac{dw_e}{dt} \equiv dW_e(t) = \frac{\alpha m^2}{2\sqrt{3}\pi\omega^2} \Phi_e, \quad \Phi_e(t) = \left(\frac{\varepsilon}{\varepsilon'} + \frac{\varepsilon'}{\varepsilon} \right) K_{2/3}(y) + \int_y^\infty K_{1/3}(x) dx, \quad y = \frac{2\omega^2}{3\varepsilon\varepsilon'\kappa}, \quad \kappa = \frac{\omega F}{mH_0} \quad (4.46)$$

here ε is the energy of the created electron, $\varepsilon' = \omega - \varepsilon$ is the energy of created positron.

There are different mechanisms of electron-positron pair creation

1. Real photon radiation in the field and pair creation by this photon in the same field of the opposite beam. This mechanism dominates in the case $\chi \geq 1$.
2. Direct electroproduction of electron-positron pair in the field through virtual photon. This mechanism is also essential in the case $\chi \geq 1$.

3. Mixed mechanism(1): photon is radiated in the bremsstrahlung process, i.e. incoherently, and the pair is produced by photon in an external field.
4. Mixed mechanism(2): photon is radiated via the beamstrahlung mechanism, and pair is produced in the interaction of this photon with individual particles of oncoming beam, i.e. in interaction with potential fluctuations.
5. Incoherent electroproduction of pair.

In the actual case $\chi \ll 1$ mixed and incoherent mechanisms mostly contribute. We start with the mixed mechanism (2). In the case $\chi_m \ll 1$ the parameter κ Eq.(4.46) containing the energy of emitted photon is also small and the incoherent cross section of pair creation by a photon is weakly dependent on the photon energy. To logarithmic accuracy

$$\sigma_p = 28/9\alpha^3\lambda_c^2 \ln(\sigma_y/\lambda_c) (1 + 396\kappa^2/1225). \quad (4.47)$$

If the term $\propto \kappa^2$ being neglected, the pair creation probability is factorized (we discuss coaxial beams of identical configuration). The number of pairs created by this mechanism (per one initial electron) is

$$\begin{aligned} n_p^{(2)} &= \int_{-\infty}^{\infty} W_\gamma(\boldsymbol{\varrho}, t) dt \int_t^{\infty} 2\sigma_p n_\perp(\boldsymbol{\varrho}, t') dt' d^2\varrho \\ &= \frac{35}{9} \sqrt{\frac{\pi}{6}} N r \alpha^3 \lambda_c^2 \ln \frac{\sigma_y}{\lambda_c} \int \chi_0(\boldsymbol{\varrho}) n_\perp^2(\boldsymbol{\varrho}) d^2\varrho = \frac{35}{9} \sqrt{\frac{\pi}{6}} N r \chi_m \alpha^3 \frac{\lambda_c^2}{2\pi\sigma_x\sigma_y} \frac{4}{\pi} \\ &\times \int_0^{\infty} \exp(-3v^2 - 2w^2) [\operatorname{erf}^2(w) - \operatorname{erf}^2(iv)]^{1/2} dw dv \\ &= 0.1167\alpha^3 N r \chi_m \frac{\lambda_c^2}{\sigma_x\sigma_y} \ln \frac{\sigma_y}{\lambda_c}. \end{aligned} \quad (4.48)$$

So for the project TESLA parameters the total number of produced pairs by this mechanism is $N n_p^{(2)} \sim 1.4 \cdot 10^4$ per bunch in one collision.

Now we turn over to discussion of incoherent electroproduction of pairs when both intermediate photons are virtual. To within the logarithmic accuracy for any χ and κ one can use the method of equivalent photons

$$\frac{d\sigma_v}{d\omega} = n(\omega)\sigma_p(\omega), \quad (4.49)$$

where

$$n(\omega) = \frac{2\alpha}{\pi\omega} \ln \frac{\Delta}{q_m}, \quad \Delta = m(1 + \kappa)^{1/3},$$

$$q_m = m \frac{\omega}{\varepsilon} \left(1 + \frac{\varepsilon\chi}{\omega}\right)^{1/3} + \frac{1}{\sigma_y} \equiv q_F + q_\sigma. \quad (4.50)$$

Taking into account that the cross section of pair photoproduction is

$$\sigma_p(\omega) = \frac{28\alpha^3}{9m^2} \ln \frac{m}{q_m(\omega')}, \quad \omega' = \frac{m^2}{\omega} \quad (\kappa \ll 1); \quad \sigma_p \propto \kappa^{-2/3} \quad (\kappa \gg 1), \quad (4.51)$$

we obtain in the main logarithmic approximation for the cross section of the pair electroproduction

$$\sigma(2e \rightarrow 4e) = \frac{56\alpha^4}{9m^2} \int_{\omega_{min}}^{\omega_{max}} \ln \frac{m}{q_m(\omega)} \ln \frac{m}{q_m(\omega')} \frac{d\omega}{\omega}, \quad (4.52)$$

where $\omega_{max} = \varepsilon/(1 + \chi)$, $\omega_{min} = m^2/\omega_{max}$. If we put $\chi = 0$, $\sigma_y = \infty$ we obtain the standard Landau-Lifshitz cross section σ_{LL} (see e.g. [11], [8])

$$\sigma_{LL} = \frac{28\alpha^4}{27m^2} \ln^3 \gamma^2. \quad (4.53)$$

With regard for the bounded transverse dimensions of beam and influence of an external field the equivalent photon spectrum changes substantially. For $\chi \sim 1$ we have $q(\omega) = m(\omega/\varepsilon)^{2/3} + 1/\sigma_y$ and under condition $\gamma^{2/3}\lambda_c/\sigma_y \geq 1$ we find

$$\sigma_v = \frac{28\alpha^4}{3m^2} \ln \left(\gamma^{4/3} \frac{\lambda_c}{\sigma_y} \right) \ln^2 \frac{\sigma_y}{\lambda_c}. \quad (4.54)$$

For TESLA parameters $\gamma^{2/3}\lambda_c/\sigma_y \simeq 1$ then

$$\sigma_v = \frac{28\alpha^4}{81m^2} \ln^3 \gamma^2. \quad (4.55)$$

This cross section is three times smaller than standard σ_{LL} . For the project TESLA parameters the number of pairs produced by this mechanism is $n_v = L\sigma_v/2 \simeq 1.5 \cdot 10^4$ in one direction per bunch in one collision, $L = 1/(4\pi\sigma_x\sigma_y)$ is the geometrical luminosity per bunch. So the both discussed mechanisms give nearly the same contribution for this project. It should be noted that the above analysis was performed under assumption that the configuration of beams doesn't changed during collision, although in the TESLA project the disruption parameter $D_y > 1$.

So we see that the beam-size effect and an external field effects are very essential for pair creation mechanism also.

Acknowledgments

The authors are indebted to the Russian Foundation for Basic Research supported in part this research by Grants 00-02-18007, 03-02-16154.

We would like to thank S. Klein for many fruitful discussions.

A Appendix

Basic equations

The quasiclassical operator method developed by authors is adequate for consideration of the electromagnetic processes at high energy. The probability of the radiation process has a form (see [10], p.63, Eq.(2.27)); the method is given also in [11], for classical limit see [71]

$$dw = \frac{e^2}{(2\pi)^2} \frac{d^3k}{\omega} \int dt_2 \int dt_1 R^*(t_2)R(t_1) \exp \left[-\frac{i\varepsilon}{\varepsilon'} (kx(t_2) - kx(t_1)) \right], \quad (\text{A.1})$$

where $k = (\omega, \mathbf{k})$ is the 4-momentum of the radiated photon, $k^2 = 0$, $x(t) = (t, \mathbf{r}(t))$, t is the time, and $\mathbf{r}(t)$ is the particle location on a classical trajectory, $kx(t) = \omega t - \mathbf{k}\mathbf{r}(t)$, $\varepsilon' = \varepsilon - \omega$, let us remind that we employ units such that $\hbar = c = 1$. The matrix element $R(t)$ is defined by the structure of a current. For an electron (spin 1/2 particle) one has

$$\begin{aligned} R(t) &= \frac{m}{\sqrt{\varepsilon\varepsilon'}} \bar{u}_{s_f}(\mathbf{p}') \hat{e}^* u_{s_i}(\mathbf{p}) = \varphi_{s_f}^+ (A(t) + i\boldsymbol{\sigma}\mathbf{B}(t)) \varphi_{s_i}, \\ A(t) &= \frac{\mathbf{e}^* \mathbf{p}(t)}{2\sqrt{\varepsilon\varepsilon'}} \left[\sqrt{\frac{\varepsilon' + m}{\varepsilon + m}} + \sqrt{\frac{\varepsilon + m}{\varepsilon' + m}} \right] \simeq \frac{1}{2} \left(1 + \frac{\varepsilon}{\varepsilon'} \right) \mathbf{e}^* \boldsymbol{\vartheta}, \\ \mathbf{B}(t) &= \frac{1}{2\sqrt{\varepsilon\varepsilon'}} \left[\sqrt{\frac{\varepsilon' + m}{\varepsilon + m}} (\mathbf{e}^* \times \mathbf{p}(t)) - \sqrt{\frac{\varepsilon + m}{\varepsilon' + m}} (\mathbf{e}^* \times (\mathbf{p}(t) - \hbar\mathbf{k})) \right] \\ &\simeq \frac{\hbar\omega}{2\varepsilon'} \left(\mathbf{e}^* \times \left(\frac{\mathbf{n}}{\gamma} - \boldsymbol{\vartheta} \right) \right), \end{aligned} \quad (\text{A.2})$$

here \mathbf{p} , $\mathbf{p}' = \mathbf{p} - \mathbf{k}$ is the initial and final momentum of an electron, \mathbf{e} is the vector of the polarization of a photon (the Coulomb gauge is used), the four-component spinors u_{s_f} , u_{s_i} and the two-component spinors φ_{s_f} , φ_{s_i} describe

the initial (s_i) and final (s_f) polarization of the electron, $\mathbf{v}=\mathbf{v}(t)$ is the electron velocity, $\boldsymbol{\vartheta} = v^{-1}(\mathbf{v} - \mathbf{n}(\mathbf{n}\mathbf{v})) \simeq \mathbf{v}_\perp$, \mathbf{v}_\perp is the component of particle velocity perpendicular to the vector $\mathbf{n} = \mathbf{k}/|\mathbf{k}|$, $\gamma = \varepsilon/m$ is the Lorentz factor. The final expressions in (A.2) are given for radiation of ultrarelativistic electrons, they are written down with relativistic accuracy (terms $\sim 1/\gamma$ are neglected) and in the small angle approximation. If we are not interested in the initial and final particles polarization, then

$$R^*(t_2)R(t_1) \rightarrow \frac{1}{2\varepsilon'^2} \left[\frac{\omega^2}{\gamma^2} + (\varepsilon^2 + \varepsilon'^2) \boldsymbol{\vartheta}\boldsymbol{\vartheta}' \right] = \frac{1}{2} \mathcal{L}(\boldsymbol{\vartheta}', \boldsymbol{\vartheta}), \quad (\text{A.3})$$

where we have used the notation $\boldsymbol{\vartheta}' = \boldsymbol{\vartheta}(t_2)$, $\boldsymbol{\vartheta} = \boldsymbol{\vartheta}(t_1)$. For polarized initial electron we have

$$R^*(t_2)R(t_1) = \frac{\varepsilon}{2\varepsilon'\gamma^2} \left\{ \frac{\omega^2}{\varepsilon\varepsilon'} + \left(\frac{\varepsilon}{\varepsilon'} + \frac{\varepsilon'}{\varepsilon} \right) \mathbf{p}\mathbf{p}' + i\frac{\omega}{\varepsilon} ((\mathbf{p}' - \mathbf{p}) \times \mathbf{v})\boldsymbol{\zeta} \right\}, \quad (\text{A.4})$$

where $\boldsymbol{\zeta}$ is the vector describing the initial polarization of the electron (in its rest frame), $\mathbf{p} = \gamma\boldsymbol{\vartheta}(t_1)$ and $\mathbf{p}' = \gamma\boldsymbol{\vartheta}(t_2)$.

If the particle moves along a definite trajectory, then substituting the classical values $\mathbf{r}(t)$ and $\mathbf{v}(t)$ in (A.1)-(A.3), we obtain the desired probability for this process. When there is scattering, Eq.(A.1) must be averaged over all possible particle trajectories. This operation is performed with the aid of the distribution function, averaged over atomic positions in the scattering medium and satisfying the kinetic equation. We consider here general case with the external field (particle acceleration) taken into account. The emission probability per unit time is then (in this Appendix we follow the paper [9])

$$dW = \left\langle \frac{dw}{dt} \right\rangle = \frac{e^2}{(2\pi)^2} \frac{d^3k}{\omega} \text{Re} \int_0^\infty d\tau \exp\left(-i\frac{\varepsilon}{\varepsilon'}\omega\tau\right) \int d^3v d^3v' d^3r d^3r' \mathcal{L}(\boldsymbol{\vartheta}', \boldsymbol{\vartheta}) \\ \times F_i(\mathbf{r}, \mathbf{v}, t) F_f(\mathbf{r}', \mathbf{v}', \tau; \mathbf{r}, \mathbf{v}) \exp\left(-i\frac{\varepsilon}{\varepsilon'}\mathbf{k}(\mathbf{r}' - \mathbf{r})\right). \quad (\text{A.5})$$

The distribution function F in (A.5) satisfies the kinetic equation

$$\frac{\partial F(\mathbf{r}, \mathbf{v}, t)}{\partial t} + \mathbf{v} \frac{\partial F(\mathbf{r}, \mathbf{v}, t)}{\partial \mathbf{r}} + \mathbf{w} \frac{\partial F(\mathbf{r}, \mathbf{v}, t)}{\partial \mathbf{v}} \\ = n \int \sigma(\mathbf{v}, \mathbf{v}') [F(\mathbf{r}, \mathbf{v}', t) - F(\mathbf{r}, \mathbf{v}, t)] d^3v', \quad (\text{A.6})$$

where n is the number density of atoms in the medium, and $\sigma(\mathbf{v}, \mathbf{v}')$ is the scattering cross section. The normalization condition

$$\int d^3r \int d^3v F(\mathbf{r}, \mathbf{v}, t) = 1 \quad (\text{A.7})$$

should be also satisfied, as well as the initial condition for F_f :

$$F_f(\mathbf{r}', \mathbf{v}', 0; \mathbf{r}, \mathbf{v}) = \delta(\mathbf{r} - \mathbf{r}')\delta(\mathbf{v} - \mathbf{v}').$$

In Eq.(A.5), we integrate over $d^3r d^3(r - r')$, taking advantage of the fact that $F_f(\mathbf{r}', \mathbf{v}', \tau; \mathbf{r}, \mathbf{v})$ can only depend on the coordinate difference $\mathbf{r}' - \mathbf{r}$:

$$dW = \frac{e^2}{(2\pi)^2} \frac{d^3k}{\omega} \text{Re} \int_0^\infty d\tau \int d^3v d^3v' \mathcal{L}(\boldsymbol{\vartheta}', \boldsymbol{\vartheta}) F_i(\mathbf{v}, t) F_k(\mathbf{v}', \tau; \mathbf{v}), \quad (\text{A.8})$$

where

$$F_i(\mathbf{v}, t) = \int d^3r F_i(\mathbf{r}, \mathbf{v}, t)$$

$$F_k(\mathbf{v}', \tau; \mathbf{v}) = \exp\left(-i\frac{\varepsilon}{\varepsilon'}\omega\tau\right) \int d^3r' \exp\left(-i\frac{\varepsilon}{\varepsilon'}\mathbf{k}(\mathbf{r}' - \mathbf{r})\right) F_f(\mathbf{r}', \mathbf{v}', \tau; \mathbf{r}, \mathbf{v}) \quad (\text{A.9})$$

We can put

$$\begin{aligned} F_k(\mathbf{v}', \tau; \mathbf{v}) &= U(\boldsymbol{\vartheta}', \boldsymbol{\vartheta}, \tau) \delta(|\mathbf{v}'| - |\mathbf{v}|) \\ U(\boldsymbol{\vartheta}', \boldsymbol{\vartheta}, 0) &= \delta(\boldsymbol{\vartheta}' - \boldsymbol{\vartheta}), \end{aligned} \quad (\text{A.10})$$

if we take into account that in ultrarelativistic limit $\mathbf{w}\mathbf{v} \sim O(1/\gamma^3)$, $\mathbf{w} \simeq \mathbf{w}_\perp$, and the scattering cross section is

$$\sigma(\mathbf{v}, \mathbf{v}') = \delta(|\mathbf{v}'| - |\mathbf{v}|) \sigma(\boldsymbol{\vartheta}', \boldsymbol{\vartheta}). \quad (\text{A.11})$$

Making use of these results and Eq.(A.6) for F_f , we obtain the following equation for $U(\boldsymbol{\vartheta}', \boldsymbol{\vartheta}, \tau)$

$$\begin{aligned} \frac{\partial U}{\partial \tau} + i\frac{\omega\varepsilon}{2\varepsilon'} \left(\frac{1}{\gamma^2} + \boldsymbol{\vartheta}'^2 \right) U + \mathbf{w} \frac{\partial U}{\partial \boldsymbol{\vartheta}'} \\ = n \int d^2\vartheta'' \sigma(\boldsymbol{\vartheta}', \boldsymbol{\vartheta}'') [U(\boldsymbol{\vartheta}'', \boldsymbol{\vartheta}, \tau) - U(\boldsymbol{\vartheta}', \boldsymbol{\vartheta}, \tau)], \end{aligned} \quad (\text{A.12})$$

where for scattering in the screened Coulomb potential the cross section in the Born approximation is

$$\sigma(\boldsymbol{\vartheta}', \boldsymbol{\vartheta}) = \frac{4Z^2\alpha^2}{\varepsilon^2((\boldsymbol{\vartheta}' - \boldsymbol{\vartheta})^2 + \vartheta_1^2)^2}, \quad (\text{A.13})$$

here $\vartheta_1 = \frac{1}{\varepsilon a_s}$, a_s is the screening radius ($a_s = 0.81a_B Z^{-1/3}$, a_B is the Bohr radius). A similar equation for the $\boldsymbol{\vartheta}$ -dependence of U can be obtained by letting $\boldsymbol{\vartheta}' \rightarrow \boldsymbol{\vartheta}$ and $\mathbf{w} \rightarrow -\mathbf{w}$.

If the final state of the charged particle is of no interest, the probability (A.8) must be integrated over d^3v' . The resulting emission probability per unit time, normalized to a single particle moving at a speed \mathbf{v} is then

$$dW = \frac{e^2}{(2\pi)^2} \frac{d^3k}{\omega} \operatorname{Re} \int_0^\infty d\tau \exp\left(-i\frac{a\tau}{2}\right) \left[\frac{\omega^2}{\varepsilon'^2 \gamma^2} V_0(\boldsymbol{\vartheta}, \tau) + \left(1 + \frac{\varepsilon^2}{\varepsilon'^2}\right) \boldsymbol{\vartheta} \mathbf{V}(\boldsymbol{\vartheta}, \tau) \right], \quad (\text{A.14})$$

where $a = \frac{\omega m^2}{\varepsilon \varepsilon'}$, and $V_\mu = (V_0, \mathbf{V})$ satisfies the equation

$$\begin{aligned} \frac{\partial V_\mu}{\partial \tau} + i\frac{b}{2} \boldsymbol{\vartheta}^2 V_\mu - \mathbf{w} \frac{\partial V_\mu}{\partial \boldsymbol{\vartheta}} \\ = n \int d^2\vartheta' \sigma(\boldsymbol{\vartheta}, \boldsymbol{\vartheta}') [V_\mu(\boldsymbol{\vartheta}', \tau) - V_\mu(\boldsymbol{\vartheta}, \tau)], \end{aligned} \quad (\text{A.15})$$

here $b = \frac{\omega \varepsilon}{\varepsilon'}$. The initial conditions for V_μ are

$$V_0(\boldsymbol{\vartheta}, 0) = 1, \quad \mathbf{V}(\boldsymbol{\vartheta}, 0) = \boldsymbol{\vartheta}. \quad (\text{A.16})$$

If the scattering cross section $\sigma(\boldsymbol{\vartheta}, \boldsymbol{\vartheta}')$ depends solely on the angle difference $\boldsymbol{\vartheta} - \boldsymbol{\vartheta}'$, as Eq.(A.13), then Eq.(A.15) is most conveniently solved by Fourier transforming with respect to the variable $\boldsymbol{\vartheta}$:

$$\begin{aligned} \varphi_\mu(\mathbf{x}, \tau) &= \frac{1}{(2\pi)^2} \int d^2\vartheta \exp(i\boldsymbol{\vartheta} \mathbf{x}) V_\mu(\boldsymbol{\vartheta}, \tau), \\ V_\mu(\boldsymbol{\vartheta}, \tau) &= \int d^2x \exp(-i\boldsymbol{\vartheta} \mathbf{x}) \varphi_\mu(\mathbf{x}, \tau). \end{aligned} \quad (\text{A.17})$$

From Eq.(A.15), with the initial conditions (A.16), we have

$$\begin{aligned} \frac{\partial \varphi_\mu(\mathbf{x}, \tau)}{\partial \tau} - i\frac{b}{2} \Delta_x \varphi_\mu(\mathbf{x}, \tau) + i\mathbf{w} \mathbf{x} \varphi_\mu(\mathbf{x}, \tau) \\ = (2\pi)^2 n [\Sigma(\mathbf{x}) - \Sigma(0)] \varphi_\mu(\mathbf{x}, \tau), \quad \Sigma(\mathbf{x}) = \int d^2\vartheta \exp(i\boldsymbol{\vartheta} \mathbf{x}) \sigma(\boldsymbol{\vartheta}); \\ \varphi_0(\mathbf{x}, 0) = \delta(\mathbf{x}), \quad \boldsymbol{\varphi}(\mathbf{x}, 0) = -i\nabla \delta(\mathbf{x}) \end{aligned} \quad (\text{A.18})$$

If the angular distribution of the radiation is of no interest, Eq.(A.14) must be integrated over the photon emission angles $\boldsymbol{\vartheta}$. Bearing in mind that $d^3k =$

$\omega^2 d\omega d^2\vartheta$, and that

$$\begin{aligned} \frac{1}{(2\pi)^2} \int V_0(\boldsymbol{\vartheta}, \tau) d^2\vartheta &= \varphi_0(0, \tau), \\ \frac{1}{(2\pi)^2} \int \boldsymbol{\vartheta} \mathbf{V}(\boldsymbol{\vartheta}, \tau) d^2\vartheta &= -i \nabla \boldsymbol{\varphi}(\mathbf{x}, \tau)|_{\mathbf{x}=0}, \end{aligned} \quad (\text{A.19})$$

we obtain the following expression for the spectral distribution of emission probability per unit time

$$\frac{dW}{d\omega} = \alpha\omega \text{Re} \int_0^\infty d\tau \exp\left(-i\frac{a\tau}{2}\right) \left[\frac{\omega^2}{\varepsilon'^2 \gamma^2} \varphi_0(0, \tau) - i \left(1 + \frac{\varepsilon^2}{\varepsilon'^2}\right) \nabla \boldsymbol{\varphi}(0, \tau) \right]. \quad (\text{A.20})$$

The equation like (A.18) in the classical limit and with $\mathbf{w} = 0$ was discussed in [4], Appendix V.

For the cross section (A.13) we have for $\Sigma(\mathbf{x})$ (A.18)

$$\Sigma(x) = \frac{Z^2 \alpha^2}{\pi \varepsilon^2} \frac{x}{\vartheta_1} K_1(x\vartheta_1), \quad (\text{A.21})$$

where $K_1(x\vartheta_1)$ is the modified Bessel function. Bearing in mind that contributions to the cross section come from $x \sim \vartheta_{ef}^{-1} \ll \vartheta_1^{-1}$, and expanding $K_1(x\vartheta_1)$ as a power series in $x\vartheta_1$ we obtain the following equation for $\varphi_\mu(\mathbf{x}, \tau)$ from Eq.(A.18), to power-series accuracy:

$$\begin{aligned} \frac{\partial \varphi_\mu(\mathbf{x}, \tau)}{\partial \tau} - i \frac{b}{2} \Delta_x \varphi_\mu(\mathbf{x}, \tau) + i \mathbf{w} \mathbf{x} \varphi_\mu(\mathbf{x}, \tau) &= u(x) \\ u(x) &= \frac{2\pi n Z^2 \alpha^2}{\varepsilon^2} x^2 \left(\ln \frac{x\vartheta_1}{2} + C - \frac{1}{2} \right), \end{aligned} \quad (\text{A.22})$$

where $C = 0.577216\dots$ is the Euler constant.

The "potential" $u(x)$ is calculated in the Born approximation since Eq.(A.13) was used. The Coulomb correction to the potential $u(x)$ were calculated in Appendix A of [17]. The eikonal approximation was use which is valid for arbitrary value $Z\alpha$. Substituting this correction we have

$$u(x) = \frac{2\pi n Z^2 \alpha^2}{\varepsilon^2} x^2 \left(\ln \frac{x\vartheta_1}{2} + C - \frac{1}{2} + f(Z\alpha) \right), \quad (\text{A.23})$$

where the function $f(Z\alpha)$ is defined in Eq.(2.5). In absence of radiation and an external field ($\mathbf{b}=\mathbf{w}=0$) Eqs.(A.22) and (A.17) at the initial condition

$\varphi(\mathbf{x}, 0) = (2\pi)^{-2}$ give the solution of pure scattering problem (the initial condition for the distribution function $F(\boldsymbol{\vartheta}, t)$ is $F(\boldsymbol{\vartheta}, 0) = \delta(\boldsymbol{\vartheta})$):

$$\begin{aligned}\varphi(x, t) &= \frac{1}{(2\pi)^2} e^{u(x)t}, \\ F(\boldsymbol{\vartheta}, t) &= \frac{1}{(2\pi)^2} \int \exp(-i\boldsymbol{\vartheta}\mathbf{x} + u(x)t) d^2x \\ dw(\boldsymbol{\vartheta}, t) &= \left[\int_0^\infty J_0(\boldsymbol{\vartheta}x) e^{u(x)t} x dx \right] \boldsymbol{\vartheta} d\boldsymbol{\vartheta}\end{aligned}\tag{A.24}$$

For another form of solution see Eq.(3.25).

References

- [1] L. D. Landau and I. Ya. Pomeranchuk, Dokl.Akad.Nauk SSSR **92** (1953) 535, 735. See in English in *The Collected Papers of L. D. Landau*, Pergamon Press, 1965.
- [2] A. B. Migdal, Phys. Rev. **103** (1956) 1811.
- [3] A. B. Migdal, Sov. Phys. JETP **5** (1957) 527.
- [4] M. L. Ter-Mikaelian, *High Energy Electromagnetic Processes in Condensed Media*, John Wiley & Sons, 1972.
- [5] E. L. Feinberg and I. Ya. Pomeranchuk, Nuovo Cimento, Supplement to Vol. **3** (1956) 652.
- [6] V. M. Galitsky and I. I. Gurevich, Nuovo Cimento **32** (1964) 396.
- [7] V. N. Baier and V. M. Katkov, Sov. Phys. JETP, **26** (1968) 854; **28** (1969) 807.
- [8] V. N. Baier, V. M. Katkov and V. S. Fadin, *Radiation from Relativistic Electrons* (in Russian) Atomizdat, Moscow, 1973.
- [9] V. N. Baier, V. M. Katkov and V. M. Strakhovenko, Sov. Phys. JETP **67** (1988) 70.
- [10] V. N. Baier, V. M. Katkov and V. M. Strakhovenko, *Electromagnetic Processes at High Energies in Oriented Single Crystals*, World Scientific Publishing Co, Singapore, 1998.
- [11] V. B. Berestetskii, E. M. Lifshitz and L. P. Pitaevskii, *Quantum Electrodynamics* Pergamon Press, Oxford, 1982.
- [12] P. L. Anthony, R. Becker-Szendy, P. E. Bosted *et al*, Phys. Rev. Lett. **75** (1995) 1949.

- [13] P. L. Anthony, R. Becker-Szendy, P. E. Bosted *et al*, Phys. Rev. Lett. **76** (1996) 3550.
- [14] P. L. Anthony, R. Becker-Szendy, P. E. Bosted *et al*, Phys.Rev.**d56** (1997) 1373.
- [15] S. Klein, Rev. Mod. Phys. **71** (1999) 1501.
- [16] H. D. Hansen, U. I. Uggerhoj, C.C.Biino *et al*, Phys.Rev.Lett. **91** (2003) 014801.
- [17] V. N. Baier and V. M. Katkov, Phys.Rev. **D57** (1998) 3146.
- [18] V. N. Baier and V. M. Katkov, *Quantum Aspects of Beam Physics*, ed.P. Chen, World Scientific PC, Singapore, 1998, p.525.
- [19] V. N. Baier and V. M. Katkov, Phys.Rev. **D59** (1999) 056003.
- [20] V. N. Baier and V. M. Katkov, Phys.Rev. **D60** (1999) 076001.
- [21] V. N. Baier and V. M. Katkov, Phys.Rev. **D62** (2000) 036008.
- [22] R. Blencenbeckler and S. D. Drell, Phys.Rev. **D53** (1996) 6265.
- [23] B. G. Zakharov, Pis'ma v ZhETF **63** (1996) 906.
- [24] B. G. Zakharov, Pis'ma v ZhETF **64** (1996) 781.
- [25] R. Baier, Yu. L. Dokshitzer, A. H. Mueller, S. Peigne, and D. Schiff, Nucl. Phys. **B478** (1996) 577.
- [26] V. N. Baier and V. M. Katkov, Phys.Rev. **D63** (2001) 116008.
- [27] V. N. Baier, and V. M. Katkov, Sov. Phys. Dokl. **17** (1973) 1068.
- [28] V. M. Katkov, and V. M. Strakhovenko, Sov. J. Nucl.Phys. **25** (1977) 660.
- [29] J. Schwinger, Phys.Rev. **73** (1948) 416; **76** (1949) 790.
- [30] V. N. Baier, V. M. Katkov and V. M. Strakhovenko, Lett. Nuovo Cimento **15** (1976) 149; Sov. J. Nuc. Phys. **24** (1976) 197.
- [31] V. N. Baier, and V. M. Katkov, Phys.Lett. A 280 (2001) 275.
- [32] V. N. Baier, and V. M. Katkov, Phys.Lett. A 286 (2001) 299.
- [33] V. N. Baier, V. M. Katkov and V. M. Strakhovenko, Sov. Phys. Doklady **16** (1971) 230.
- [34] V. I. Ritus, Sov. Phys. JETP **30** (1970) 1181.
- [35] J. Schwinger, Phys.Rev. **75** (1949) 1912; **82** (1951) 664.
- [36] N. B. Narozhny, Zh. Eksp.Teor.Fiz., **55** (1968) 714.
- [37] A. I. Milstein and M. Schumacher, Phys. Rep.C243 (1994) 183.
- [38] M. Cheng and T. T. Wu, Phys.Rev. **182** (1969) 1873; D **2** (1970) 2444; D **5** (1972) 3077.

- [39] A. I. Milstein and V. M. Strakhovenko, Sov. Phys. JETP **58** (1983) 8.
- [40] R. N. Lee and A. I. Milstein, Phys.Lett. A 198 (1995) 217.
- [41] R. N. Lee, A. I. Milstein, and V. M. Strakhovenko, Jour. Exper. Theor. Phys. **90** (2000) 66.
- [42] V. M. Katkov and V. M. Strakhovenko, Jour. Exper. Theor. Phys. **92** (2001) 561.
- [43] V. N. Baier, V. M. Katkov, Phys.Rev. **D63** (2001) 116008.
- [44] H. A. Bethe, Phys.Rev. **89** (1953) 1256.
- [45] G. Molière, Z.Naturforsch.**2a** (1947) 133.
- [46] V. M. Katkov, and V. M. Strakhovenko, Sov. Phys. Dokl. **21** (1976) 658.
- [47] Y.-S. Tsai, Rev. Mod. Phys. **46** (1974), 815.
- [48] V. N. Baier, V. M. Katkov and V. M. Strakhovenko, Nucl. Phys. **B328** (1989) 387.
- [49] R. Blankenbecler, Phys.Rev **D55** (1997) 2441.
- [50] V. N. Baier, V. S. Fadin, V. A. Khoze and E.A. Kuraev, Phys. Rep. **78** (1981) 293.
- [51] I. I. Gol'dman, Sov. Phys. JETP **11** (1960) 1341.
- [52] F. F. Ternovskii, Sov. Phys. JETP **12** (1960) 123.
- [53] V. E. Pafomov, Sov. Phys. JETP **20** (1965) 253.
- [54] N. F. Shul'ga and S. P. Fomin, Sov. Phys. JETP **86** (1998) 32.
- [55] N. F. Shul'ga and S. P. Fomin, Nucl.Instr.and Meth. B **145** (1998) 73.
- [56] I. S. Gradshteyn and I. M. Ryzhik, *Table of Integrals, Series, and Products*, Academic Press, New York, 1965.
- [57] X. Artru, G. B. Yodh and G. Mennesier, Phys.Rev. **D12** (1975) 1289.
- [58] V. N. Baier and V. M. Katkov, Phys.Lett. A 252 (1999) 263.
- [59] N. F. Shul'ga and S. P. Fomin, JETP Lett. **63** (1996) 873.
- [60] L. D. Landau, J.Phys. USSR **8** (1944) 201.
- [61] R. Blankenbecler, Phys.Rev **D55** (1997) 190.
- [62] V. N. Baier and V. M. Katkov, Nucl. Instr. Meth. A 439 (2000) 189.
- [63] N. V. Laskin, A. S. Mazmanishvili, N. N. Nasonov, N. F. Shul'ga, Jour. Exper. Theor. Phys. **89** (1985) 763.
- [64] V. G. Zakharov, Phys. Atom. Nucl.**62** (1999) 1075.
- [65] M. Miezowitz, O. Stanisiz and W. Wolther, Nuovo Cimento **5** (1957) 513.
- [66] P. H. Fowler, D. H. Perkins and K. Pinkau, Phil.Mag. **4** (1959) 1030.

- [67] A. Varfolomeev, I. Gerasimova, I. I. Gurevitch et al., *Sov.Phys. JETP* **11** (1960) 23.
- [68] E. Lohrmann, *Phys.Rev* **122** (1961) 1908.
- [69] S. C. Strautsz et al., in *Proc.of the 22th Intl.Cosmic Ray Conf.*,Dublin, Ireland, V.4, p.233.
- [70] A. Varfolomeev, et al., *Sov.Phys. JETP* **42** (1976) 218.
- [71] L. D. Landau and E. M. Lifshitz, *Classical Theory of Fields* 4th English Ed., Pergamon Elmsford, New York, 1975.
- [72] A. E. Blinov, A. E. Bondar, Yu. I. Eidelman et al., *Preprint INP 82-15, Novosibirsk 1982*; *Phys.Lett.* **B113** (1982) 423.
- [73] V. N. Baier, V. M. Katkov, V. M. Strakhovenko, *Preprint INP 81-59, Novosibirsk 1981*; *Sov.J.Nucl.Phys.*, **36** (1982) 95.
- [74] A. I. Burov and Ya. S. Derbenev, *Preprint INP 82-07, Novosibirsk 1982*.
- [75] G. L. Kotkin, S. I. Polityko, and V. G. Serbo, *Yad.Fiz.*, **42** (1985) 692, 925.
G. L. Kotkin et al., *Z.Phys.*, **C39** (1988) 61.
- [76] V. N. Baier and V. M. Katkov, *Phys. Rev.* **D66** (2002) 053009.
- [77] K. Piotrkowski, *Z.Phys.* **C67** (1995) 577.
- [78] V. N. Baier, V. M. Katkov, and V. M. Strakhovenko, *Particle Accelerators*, **30** (1990) 43.
- [79] R. J. Noble, *Nucl.Instr.Meth.*, **A256** (1987) 427.
- [80] O. Napoly, *Proceedings of the 2001 Particle Accelerator Conference*, Chicago, (2001) p.402.
- [81] V. N. Baier, V. M. Katkov, and V. M. Strakhovenko, *Phys. Lett.* **A229** (1992) 429.
- [82] V. A. Bazylev, V. V. Golovoznin, and A. V. Demura, *Zhurn.Teor.i Eksp. Fiziki*, **92** (1987) 1921.
- [83] V. N. Baier, V. M. Katkov, V. M. Strakhovenko, *phys.stat.sol.(b)* **149** (1988) 403.
- [84] V. N. Baier and V. M. Katkov, *On coherent radiation in electron-positron colliders*, *Proceedings of Quantum Aspects of Beam Physics*, ed.P. Chen, World Scientific PC, Singapore, 2003 (in print).

V.N. Baier and V.M. Katkov

**Concept of formation length
in radiation theory**

В.Н. Байер, В.М. Катков

**Концепция длины формирования
в теории излучения**

Budker INP 2003-58

Ответственный за выпуск А.М. Кудрявцев
Работа поступила 10.09.2003 г.

Сдано в набор 18.09.2003 г.

Подписано в печать 19.09.2003 г.

Формат бумаги 60×90 1/16 Объем 8.2 печ.л., 6.6 уч.-изд.л.

Тираж 105 экз. Бесплатно. Заказ № 58

Обработано на IBM PC и отпечатано на
ротапринте ИЯФ им. Г.И. Будкера СО РАН
Новосибирск, 630090, пр. академика Лаврентьева, 11.